

CENTRIFUGE MODELLING OF DISCRETE PILE ROWS TO STABILISE SLOPES

By

Boung Shik Yoon

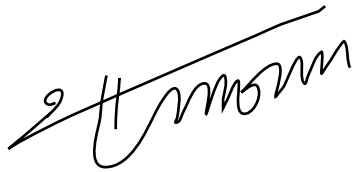
B.Sc, M.Sc.

**Thesis submitted to the University of Nottingham
for the degree of Doctor of Philosophy**

November 2008

DECLARATION

I declare that the work in this dissertation was carried out in accordance with the Regulations of the University of Nottingham. The work is original except indicated by references in the text and no part of this dissertation has been submitted for any other degree.

A handwritten signature in black ink, appearing to read 'Boungh Shik, Yoon', written over a horizontal line.

Boungh Shik, Yoon

ABSTRACT

Discrete pile rows are widely used for improving the stability of potentially unstable slopes, where columns of reinforced concrete are constructed in the ground to reinforce it and inhibit instability. The method becomes more cost effective with wider pile spacings, but simultaneously there is also increasing risk that the soil will flow through the gap between adjacent piles, rather than arching across it. The impact of pile spacing along the row, which is likely to have a significant effect on stability, is not clearly understood from a current design perspective. In this study the effects of pile spacing on passive interaction with the slope are investigated using a series of geotechnical centrifuge model tests which are interpreted with a proposed theoretical framework.

A total of 23 geotechnical centrifuge model tests were successfully carried out (Chapters 3 and 4):

- A plane strain model slope was subjected to up to 50 *g* centrifugal acceleration, with the upper layer of the slope tending to fail on an underlying predefined surface. The model piles were instrumented to measure bending moment, and hence the shear force and pressure on the piles resulting from interaction with the unstable layer were deduced using a curve-fitting technique. Cameras ‘on-board’ the centrifuge model allowed in-flight photogrammetry to be used to determine soil or pile displacement.
- Pile spacing (s/d) was varied, which determined limiting pile-soil interaction for the row, and variation of other geometrical parameters (l/h) for the slope controlled the total load on the pile row.
- A number of mechanisms of behaviour for the reinforced slope were identified ranging from a successfully stabilised slope to shallow and deeper slips passing

through the pile row, as well as slips which occurred upslope of the pile row and thus did not interact with it.

A theoretical framework was developed and used to interpret the results (Chapter 5):

- The centrifuge model test results have been successfully interpreted using the proposed analytical approach.
- The centrifuge test results confirm previous numerical modelling results, and hence a simple theory which can be used for calculation of the maximum stabilising force available from interaction of the pile row with the slope.

The work presented here also confirmed that another previous theoretical model, although quite widely used, is somewhat flawed. Comparison with a field study where stabilisation has been successful (to date) indicated consistency with the experimental results and associated interpretation.

AFFIRMATION

The following publications have been produced during the research for this thesis

Yoon, BS (2008). Centrifuge modelling of discrete piles used for slope stabilisation. *The Young European Arena of Research (YEAR) 2008 for Transport Research Arena (TRA)*, nominated as a finalist in a poster section

Yoon, BS & Ellis E.A. (2008). Centrifuge modelling of slope stabilisation using a discrete pile row. *Proceeding of 1st International Conference on Transportation Geotechnics*, Nottingham, UK, 2008. Taylor & Francis Group, London, ISBN 978-0-415-47590-7, pp. 109 – 114.

ACKNOWLEDGEMENTS AND DEDICATION

I wish to express my deepest gratitude to all those who have given great helps and advices during his research.

First and foremost I would like to show the greatest appreciation to Dr Ed Ellis who always provided excellent guidance and inspiration whenever need for performing my PhD research. He has arranged a regular meeting as well as made a room despite of his already busy schedule for meetings whenever I asked for. He has been more than just a superb supervisor – Not only has he motivated me to become a professional geotechnical engineer but also taught me how to sketch my future both in my career and in my life. Again I am sincerely thankful for the unique honour of working with him, and I also esteem his endless enthusiasm and endeavour for teach and research. Secondly I wish to acknowledge the supports provided by Prof. Hai-sui Yu. He has always made great efforts to give all NCG students (including me) good chances to extend their knowledge on Soil Mechanics.

The opportunity to work with Dr Ed Ellis and Prof. Hai-sui Yu has been the highlight of my professional career and personal experience in my life.

A special note of recognition and appreciation goes to all technicians of the School of Civil Engineering, in particular Craig Cox and Mike Langford, who provided the enthusiastic technical contributions in geotechnical centrifuge modelling.

I am also grateful to the School of Civil Engineering and the University of Nottingham for financial support that helped me concentrate on the research without financial problems during the course.

I would like to thank to Professor Heo Yol for his encouragement and to my friends and colleagues for their friendships and enjoyable discussions.

Finally, I wish to express his sincere gratitude and appreciation to his parents, my wife (Ju-hee) and my daughter (Ye-jin) for their love and support. I am forever grateful for the many moments that we enjoyed together in Nottingham.

LIST OF SYMBOLS AND ABBREVIATIONS

English letters

a_1, a_2	polynomial multipliers in the passive zone
b	width of upslope block into page
b_0, b_1, b_2	polynomial multipliers in the active zone
d	pile diameter
e_{\max}, e_{\min}	maximum and minimum void ratio of soil
g	Earth gravity
h	thickness of slip from the surface to the slip plane
l	length of upslope block
l/h	geometric parameter
n	the number of piles across the width b
m	the rate of pluviation
p	pressure in a pile
p_p	equivalent pressure on a pile
$p_{p,ult}$	ultimate equivalent pressure on the pile
p_r	equivalent average pressure per unit width for the pile row
	$p_r = p_p (d / s) = P_p / s$
r_u	pore pressure coefficient
s	spacing across the pile row
s/d	pile spacing (centre to centre)
$(s / d)_{crit}$	critical pile spacing
t	thickness of a sand layer deposited by a single pass of the hopper
u	pile deflection with depth
v_s	travel velocity of hopper during pouring

z_a	depth (in the passive zone) measured from the head of the pile
z_b	depth (in the active zone) measured from the tip of the pile
A	$= (1 - \alpha) \sin \beta$ where, $\alpha = F_\mu / F_d$
A_{\max}	maximum value of A
B_{mob}	normalised lateral interaction stress (= lateral interaction stress on pile / nominal vertical stress)
B_{\max}	normalised maximum lateral interaction stress (= maximum lateral interaction stress on pile / nominal vertical stress)
C_u	uniformity of coefficient
C_z	coefficient of curvature
D_{10}, D_{30}	particle size corresponding to 10% and 30% of particle size distribution
D_{50}	average particle size
EI	flexural stiffness of a pile
F_μ	resisting force
F_d	driving force
G	shear modulus of soil
G_s	specific gravity
I_D	relative density of sand
K_a	active earth pressure coefficient (= $(1 - \sin \phi') / (1 + \sin \phi')$)
K_p	passive earth pressure coefficient (= $1 / K_a$)
K_s	coefficient of earth pressure on sides
M	moment
M_{int}	the bending moment measured at the pre-defined slip interface
N	scaling factor or gravity level

N_s, T_s	normal and shear forces on the front and back sides in the model
N_b, T_b	normal and shear forces on the base in the model
P	force acting on the pile per unit length along the axis
P_{ult}	net ultimate lateral soil load per unit length of pile
S	shear force in a pile
S_p	stabilising interaction force on pile (normal load to a pile) equivalent to the shear force at the sliding interface
$S_{p,int}$	the total stabilising interaction force on an instrumented pile
W	the weight of the upslope block above the pile row ($W = lhb\gamma$)

Greek letters

α	$= F_\mu / F_d$
β	slope angle
δ_s	upslope displacement
δ_p	pile head displacement
δ_r	relative pile-soil displacement
ΔF	improvement in the factor of safety
ϕ'	'Mohr-Coulomb' friction angle
ϕ'_{mob}	mobilised angle of shearing ($= \sin^{-1}(t / s')$)
γ	the unit weight of the soil
γ_d	dry density of soil
γ_w	water density
θ	gradient (rotation)
μ_s, μ_b	coefficient of friction on sides and base
ν	Poisson's ratio

ρ	dry density of soil in model (g / mm ³)
$\rho_{s,max}, \rho_{s,min}$	maximum and minimum dry densities of soil
σ'_v	effective vertical stress in the model
σ'_{v0}	the nominal vertical effective stress in the soil for a given depth
ψ	dilation angle of soil

Abbreviations

PIV	Particle Image Velocimetry
BMT	Bending Moment Transducer
DAS	Data Acquisition System
LB	Leighton Buzzard sand
AAE	Average Absolute Error
RMSE	Root Mean Square Error
FoS	Factor of Safety

CONTENTS

Declaration.....	ii
Affirmation	v
Acknowledgements and dedication	vi
Abstract.....	iii
List of symbols and abbreviations	vii
Contents	xi
List of Figures	xv
List of Tables	xxi
CHAPTER 1 INTRODUCTION	1
1.1 Research Background	1
1.2 Aim and Objectives.....	4
1.3 Layout of the Thesis.....	5
CHAPTER 2 LITERATURE REVIEW	6
2.1 Introduction.....	6
2.1.1 General aspects of analysis/ design.....	6
2.1.2 Structure	8
2.2 Lateral pile-soil interaction	9
2.2.1 Elastic Response (isolated pile)	9
2.2.2 Ultimate Capacity (isolated pile and pile row)	11
2.2.3 Full response (combined elastic and ultimate response).....	14
2.3 Limit equilibrium methods.....	18
2.3.1 Slip circle methods.....	18

2.4 More complex analytical methods	22
2.5 Other references	24
2.6 Review of critical factors	27
2.6.1 Pile location in slope	27
2.6.2 Pile spacing	32
2.6.3 Effect of pile/soil interface roughness	35
2.6.4 Effect of soil dilation	36
2.7 Summary	37
 CHAPTER 3 CENTRIFUGE MODELLING: METHODOLOGY	38
3.1 Introduction	38
3.1.1 Centrifuge modelling: principles and scaling laws	38
3.1.2 Structure	40
3.2 Test programme	41
3.3 NCG Geotechnical Centrifuge Facilities	45
3.3.1 NCG Geotechnical centrifuge	45
3.3.2 In-flight digital image processing	47
3.3.3 Plane strain box	50
3.3.4 Sand hoppers	51
3.4 Test material: Leighton Buzzard sand	54
3.4.1 Engineering behaviour of granular soils	54
3.4.2 Test soil property	54
3.5 Centrifuge test model	57
3.5.1 Model slope	57
3.5.3 Model pile	62
3.6 Modelling considerations	66
3.6.1 Boundary effects	66

3.6.2 Particle size effects.....	69
3.6.3 Stress error	70
3.7 Test procedure.....	72
3.8 Summary	74
 CHAPTER 4 CENTRIFUGE MODELLING: TEST DATA	75
4.1 Introduction.....	75
4.1.1 Note on data presentation.....	75
4.1.2 Structure of the chapter	77
4.2 Ground and pile movement data	78
4.2.1 Displacements in the cross sectional plane	78
4.2.2 Movement of the slope face	86
4.2.3 Ground deformation characteristics	95
4.2.4 Pile head displacements	99
4.2.5 Relative pile-soil displacement	102
4.3 Pile moment data.....	104
4.3.1 Variation of moment with time	104
4.3.2 Moment, shear force, and pressure profiles with depth	106
4.3.3 Derived and idealised pile displacements with depth	114
4.4 Summary	116
 CHAPTER 5 CENTRIFUGE MODELLING: INTERPRETATION AND COMPARISON	117
5.1 Introduction.....	117
5.2 Theoretical framework for a piled slope	117
5.2.1 Problem definition	118

5.2.2 Stabilising (shear) force	121
5.2.3 Pile row interaction	123
5.3 Interpretation and comparison	125
5.3.1 Interpretation of test data	125
5.3.2 Variation of A and B with g-level in each test	127
5.3.3 Variation of A and B_{mob} with (s/d)	130
5.3.4 Relationship between pile row interaction, (s/d) and (l/h)	136
5.4 Comparison with previous works	141
5.4.1 Ito and Matsui (1975).....	142
5.4.2 Chen and Martin (2002); Ang (2005); Durrani (2006)	145
5.4.3 Davies et al. (2003)	149
5.5 Summary	154
CHAPTER 6 CONCLUSIONS	157
6.1 Work reported in the thesis	157
6.1.1 Centrifuge model tests	157
6.1.2 Analytical model	159
6.2 Implications for design	159
6.3 recommendations for future work.....	161
APPENDIX	163
A. Derivation of pile displacement profile with depth.....	163
REFERENCES	166

LIST OF FIGURES

CHAPTER 1

Figure 1.1 - Slope stabilisation using a discrete bored pile wall: (a) Contribution to slope stability, and (b) Passive pile-soil-pile interaction	3
--	---

CHAPTER 2

Figure 2.1 - Fundamental analysis of pile-soil interaction: (a) Assumed circular boundary conditions, and (b) Assumed plane strain section	10
Figure 2.2 - An Idealised piled slope system (after Ito and Matsui, 1975)	13
Figure 2.3 - ‘Constant overburden’ approach to modelling pile-soil-pile interaction (after Durrani et al., 2006)	15
Figure 2.4 - Conceptual models of an isolated pile and a continuous wall	16
Figure 2.5 - Ultimate equivalent pressures on a pile row and theoretical limits versus normalised pile spacing (after Durrani, 2006): (a) Equivalent pressure of a pile at ‘ultimate’ condition, and (b) Equivalent average pressure ‘along’ the pile row	17
Figure 2.6 - Limit equilibrium analyses for a potentially unstable slope stabilised with pile	19
Figure 2.7 - Idealised pile-slope system (after Wang and Yen, 1974)	20
Figure 2.8 - Arching development and effect (after Adachi et al., 1987)	24
Figure 2.9 - Comparison of the optimal pile location in stabilising a slope: (a) Optimal location of the pile for a typical slip for comparison, (b) Optimal location of the pile for a deep seated failure slip in cohesive soils (after Lee et al., 1995), and (c) Optimal location of the pile for a log spiral slip (after Ausilio et al., 2003)	29

Figure 2.10 - Depth of slip measured at crest, midslope, and toe of a slope for a typical slip	30
Figure 2.11 - Effects of pile spacing on the stability of a stabilised slope with the piles: (a) Improvement ratio versus (s/d) (after Lee et al., 1995), (b) Factor of safety versus (s/d), and (c) Improvement in FoS versus (s/d) (after Durrani, 2007)	33
Figure 2.12 - Effect of interface roughness on ultimate equivalent pressure on the pile	35
Figure 2.13 - Effects of soil dilatancy on ultimate resistance and passive interaction ...	36

CHAPTER 3

Figure 3.1 - Stress distributions for prototype and centrifuge model (after Schofield, 1980)	39
Figure 3.2 - Configuration of slope model with a row of piles: (a) Front view, and (b) Plan view	43
Figure 3.3 - Centrifuge testing programme	44
Figure 3.4 - NCG centrifuge components	46
Figure 3.5 - Example of PIV analysis used in a test: (a) Initial test mesh, of size 75×75 pixels, (b) Final test mesh and (c) Control point positions, and (d) Contour plot at $5g$	49
Figure 3.6 - Plane strain box components	50
Figure 3.7 - Sand hoppers: (a) Spot type hopper, and (b) Line type hopper	51
Figure 3.8 - Variation of relative density with thickness of layer for each pass of the hopper	53

Figure 3.9 - Stress analysis of a conventional triaxial test: (a) Mohr circle of effective stress for a triaxial test, and (b) Derived internal friction angles at peak and at critical state	56
Figure 3.10 - Schematic arrangement of the test model assuming plane strain conditions	57
Figure 3.11 - Arrangement of the model construction components	58
Figure 3.12 - Test model construction procedures: (a) Stable granular material, (b) Interface installation, (c) Control points and Latex installation, (d) Model pile installation, (e) Model without the upper soil layer, (f) Upper soil layer construction, (g) Upper soil layer without texture, and (h) Complete upper soil layer with texture	60
Figure 3.13 - Instrumentation of the model pile	63
Figure 3.14 - Friction angle of interface between soil and pile	65
Figure 3.15 - Cross-section of side boundary lubrication at the edge of the plane strain section	67
Figure 3.16 - Comparison of friction at lubricated and non-lubricated interfaces: (a) Modified shear box test, (b) Lubricated boundary interface, and (c) Non-lubricated boundary interface	68
Figure 3.17 - Model dimensions for stress error calculation	70
Figure 3.18 - Vertical stress distributions with depth in the centrifuge model at 50 g and corresponding prototype	71
Figure 3.19 - Complete arrangement of a test package in the centrifuge: (a) Arrangement of test, and (b) Complete test package on the centrifuge swing	73

CHAPTER 4

Figure 4.1	- General notation and conventions for position, displacement and loading: (a) Coordinate system and displacements, and (b) Positive sign conventions for bending moment, shear force, and pressure	76
Figure 4.2	- Selection of representative examples (BSY12a and BSY15a)	77
Figure 4.3	- Example of the cross sectional plane view for BSY12a $((s/d) = 2.5, (l/h) = 4.0)$	81
Figure 4.4	- Contours of downslope movement (mm at model scale) for BSY12a $((s/d) = 2.5, (l/h) = 4.0)$	82
Figure 4.5	- Examples of the cross sectional plane view for BSY15a $((s/d) = 5.9, (l/h) = 1.5)$	84
Figure 4.6	- Contours of downslope movement (mm at model scale) for BSY15a $((s/d) = 5.9, (l/h) = 1.5)$	85
Figure 4.7	- View of the slope face for BSY12a $((s/d) = 2.5, (l/h) = 4.0)$	87
Figure 4.8	- Contour plots of downslope movement (mm, model scale) on the slope face for BSY12a $((s/d) = 2.5, (l/h) = 4.0)$	88
Figure 4.9	- Upslope and downslope displacement (δ) normalised by pile diameter (d) showing variation with g-level for BSY12a $((s/d) = 2.5, (l/h) = 4.0)$	89
Figure 4.10	- View of the slope face for BSY15a $((s/d) = 5.9, (l/h) = 1.5)$	90
Figure 4.11	- Contours of upslope movement (mm, model scale) on the slope face for BSY15a $((s/d) = 5.9, (l/h) = 1.5)$	91
Figure 4.12	- Shallow surface failure	92
Figure 4.13	- Upslope displacement (δ_u) normalised by pile diameter (d) showing variation with g-level for BSY12a and 15a	93
Figure 4.14	- Upslope displacement (δ_u) normalised by pile diameter (d) showing variation with g-level for all tests	94

Figure 4.15 - Typical characteristics of passive yielding behaviours	95
Figure 4.16 - Investigation of arching development between the piles for BSY12a	97
Figure 4.17 - Flow action between the piles for BSY15d ($(l/h) = 2.5$, $(s/d) = 8.9$)	98
Figure 4.18 - Pile head displacements with g -level for all tests	100
Figure 4.19 - 'Normalisation' of pile displacement with g -level for all tests	101
Figure 4.20 - General definition of relative pile-soil displacement	102
Figure 4.21 - Relative pile-soil displacement with g -level	103
Figure 4.22 - Variation of bending moment for BMT 6 (at the interface elevation) with time	105
Figure 4.23 - Bending moment, shear force, and lateral pressure acting on the pile	108
Figure 4.24 - Moment, shear force, and pressure profiles for BSY12a $((s/d) = 2.5$, $(l/h) = 4.0$)	112
Figure 4.25 - Moment, shear force, and pressure profiles for BSY15a $((s/d) = 5.9$, $(l/h) = 1.5$)	113
Figure 4.26 - Derived and idealised pile displacement profiles with depth (BSY12a at 30 g)	115

CHAPTER 5

Figure 5.1 - Idealisation of a piled slope problem for semi-infinite slope	118
Figure 5.2 - Concepts of limiting interaction capacity for a pile in a row: (a) Isolated pile, and (b) Continuous wall	124
Figure 5.3 - Variation of A with g -level for all tests	128
Figure 5.4 - Variation of B_{mob} with g -level for all tests	129
Figure 5.5 - Variation of A with various (s/d) for a given (l/h)	133

Figure 5.6 - Variation of B_{mob} with (s/d) for a given (l/h)	135
Figure 5.7 - Concept of the pile row interaction in terms of A and B_{mob}	137
Figure 5.8 - Concept of the pile row interaction in terms of (l/h) and (s/d)	137
Figure 5.9 - Comparison of test results with the theoretical lines for relative displacement	138
Figure 5.10 - Variation of B_{mob} with relative soil-pile displacement at 50 g showing results from all tests	140
Figure 5.11 - Comparison of ultimate equivalent pressure on pile (B_{mob}) with (s/d) for purely frictional soil ($\phi' = 32^\circ$)	144
Figure 5.12 - Boundary conditions of 2d and 3d numerical models used: (a) Plane strain model (after Chen and Martin, 2002), and (b) Three-dimensional horizontal slice model (after Ang, 2005)	147
Figure 5.13 - Ultimate equivalent pressures on a pile and on a pile row with theoretical limits: (a) Ultimate equivalent pile pressure (equivalent to B_{mob}), and (b) Equivalent average pressure along the pile row	148
Figure 5.14 - Geomorphological mapping and schematic layout: (a) Geomorphological map, (b) Schematic layout of cross-sectional plane section, and (c) Stabilising force versus improved factor of safety	152
Figure 5.15 - Comparison of B_{mob} with the ‘factored’ and ‘unfactored’ theoretical limits	153

APPENDIX

Figure A.1 - General definitions and conventions for pile rotation and displacement	163
---	-----

LIST OF TABLES

CHAPTER 2

Table 2.1	- Summary of references and optimal locations	31
-----------	---	----

CHAPTER 3

Table 3.1	- Centrifuge model scaling relationships	39
Table 3.2	- Centrifuge testing programme	44
Table 3.3	- Centrifuge specification	46
Table 3.4	- Technical specification of the digital still camera in a test	47
Table 3.5	- Properties of Fraction E Leighton Buzzard sand	54
Table 3.6	- Summary of unstable layer and stable material	61

CHAPTER 4

Table 4.1	- Curve fitting functions used for deriving moment, shear force, pressure profiles	109
-----------	--	-----

CHAPTER 5

Table 5.1	- Analysis specification for comparison	146
Table 5.2	- Geotechnical material properties	149

CHAPTER 1

INTRODUCTION

1.1 Research background

Severe instability of slopes involves economic and safety implications for infrastructure such as roads or railways, damage to other assets located on or adjacent to the potentially unstable slopes, and potentially even loss of human life. In particular, a significant proportion of UK transport infrastructure such as embankments or cutting slopes for motorways or railways may be at risk, due to their age, or from widening projects (Perry et al., 2003a and b). Climate change with potentially wetter winters and drier summers would pose a further threat.

A variety of remediation techniques for stabilising a potentially unstable slope exist, for instance

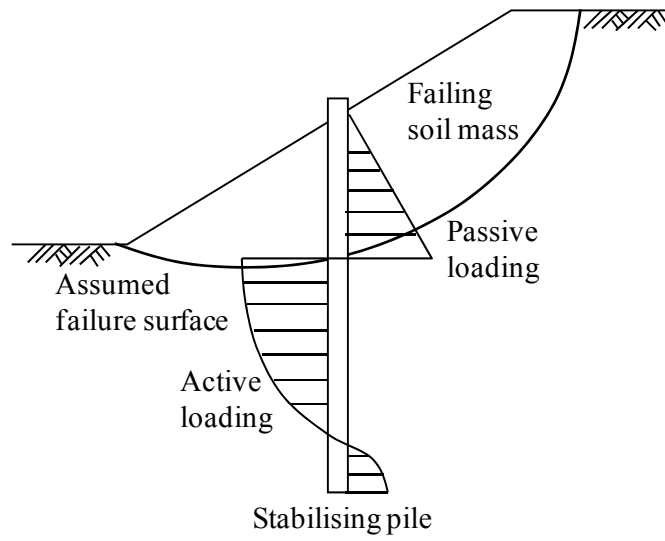
- (1) alteration of the slope geometry to a more stable profile,
- (2) installation of drainage to reduce pore water pressure,
- (3) insertion of reinforcing inclusions (e.g. retaining walls, piles or geosynthetics)
- (4) ground improvement (e.g. grouting or lime mixtures).

The technique of using a single or multiple rows of discrete piles to stabilise potentially unstable natural or man-made slopes is widely used both in the UK and abroad. The solution is generally permanent and cost effective, and piles can be situated near the transport infrastructure (e.g. road or railway line) to provide direct protection to the asset.

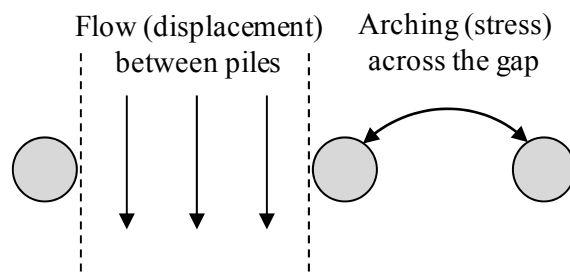
As shown in Figure 1.1(a) the stabilising piles are installed to penetrate through a sliding soil mass into stable soil below the slip. Each pile provides horizontal ‘passive’ restraint to the potentially unstable soil mass, transferring this load down the pile to the underlying stable ground, where it ‘actively’ resists the load. This results in shear force and bending moments in the piles, which must have sufficient structural capacity to withstand the loading. Note that the use of ‘active’ and ‘passive’ in this context does not correspond to earth pressures on a retaining wall. ‘Passive’ implies that the soil moves relative to the pile and ‘active’ that the piles moves relative to the soil.

However, the impact of important design factors related to effective performance of the pile row (e.g. spacing between piles) are not fully understood. The cost effectiveness of the technique increases as wider pile spacing is used, but simultaneously there is increasing danger that the soil will ‘flow’ through the gap between piles, rather than arching across it (Figure 1.1(b) in which arching is a load-transfer mechanism by which stresses from the yielding parts of the soil mass (potentially unstable soil) are redistributed to the adjoining non-yielding regions (ultimately the stabilising piles in this case), and hence there is an improvement in stability of the slope. Arching effects are much greater in sands than in silts or clays and are greater in dense sands than in loose sands). These uncertainties potentially lead to conservative and uneconomical design.

The present study focuses on the stabilisation of an inherently unstable slope having a pre-existing translational slip. This approach allows the pile row interaction and ultimate resistance for the unstable slope for any frictional soils (e.g. drained behaviour of clay, although the frictional angle would be lower) to be examined without further complication regarding the nature of instability through the depth of the slope.



(a) Contribution to slope stability



(b) Passive pile-soil-pile interaction

Figure 1.1 - Slope stabilisation using a discrete bored pile wall

1.2 Aim and objectives

The general aim of the research is to investigate the behaviour of a piled slope (e.g. pile row interaction), to give an appraisal on the suitability of a row of discrete piles to stabilise the slope, and to give fundamental guidance on its design.

The objectives can be specified as:

- to conduct a series of centrifuge model tests on a piled slope
- to examine behaviour of the model by comprehensive analysis of the test data
- to propose a theoretical framework to facilitate interpretation of the results
- to compare the interpreted centrifuge test data with previous work.

1.3 Layout of the thesis

Chapter 2 summarises previous studies on the behaviour of piles for slope stabilisation, ranging from the conventional design method (limit equilibrium approach) to more complex methods (analytical, empirical and numerical approaches). A review of critical factors affecting passive interaction is also presented.

Chapter 3 describes the experimental methodology used for centrifuge modelling of a slope stabilised by a row of piles. The experimental testing programme is first presented, and the NCG Geotechnical centrifuge facilities such as the centrifuge, model container, model components and digital image processing techniques are introduced.

Chapter 4 presents an overview of typical centrifuge test data, focusing on profiles of ground and pile movements (based on image analysis), and pile moment, shear force and pressure profiles. Preliminary discussion of test results is presented.

Chapter 5 introduces the proposed theoretical framework for interpretation of the results. The framework is used to present centrifuge test data from all 23 tests, and the results are compared with selected previous work presented in the literature.

Chapter 6 gives conclusions and suggestions for further work.

CHAPTER 2

LITERATURE REVIEW

2.1 Introduction

2.1.1 General aspects of analysis/ design

Most design of piled stabilisation of slopes includes the following aspects (with some iteration):

1. Evaluation of the total horizontal (or shear) force needed to increase the factor of safety of the slope by the desired amount
2. Evaluation of the maximum stabilising force available from piles interaction with potentially unstable material, and comparison with (1)
3. Consideration of other aspects such as
 - 3a. Other slips which do not interact with the piles (e.g. shallow slips upslope or downslope, or beneath the pile toes)
 - 3b. Whether the piles have sufficient active capacity in the underlying stable soil.

This may also require a check on pile displacement, which will be governed mainly by active response – however since the calculation is inherently based on an enhanced factor of safety for the slope displacements may not be considered meaningful.
 - 3c. Structural design of the piles, based on shear forces and (particularly) bending moments derived from the passive and active pressure distributions.

(1) is normally based on routine slope stability analysis (e.g. method of slices), including the effect of a horizontal line load representing the total passive restraint from the piles. (3a) is based purely on slope stability analysis. Since this thesis primarily considers stabilisation of the slope, established methods of analysis for slope stability will not be considered in detail.

(2) and (3b) are related topics, but since (2) has most direct impact on slope stability it will be the main focus of this thesis. Since (3c) concerns structural design, it will not be considered in any detail.

The design will need to consider the following characteristics of the piles:

- the position of the piles in the slope (e.g. near the crest, midslope, or toe)
- the diameter (d) and spacing (s), as well as other structural characteristics
- the length

Practicalities of construction will also impact on these aspects.

The position of the piles in the slope will have some impact on (1) and (2) above, and thus is likely to be decided at an early stage, mainly based on practicalities of construction and (3a) (slips occurring upslope or downslope of the piles). Section 2.6 below summarises existing information in the literature regarding the effectiveness of various locations.

The spacing ratio (s/d) will have a large impact on (2), and this will be the main focus of the thesis. The pile diameter and type of pile (structural capacity and flexural stiffness) are mainly related to (3c) and (3b) respectively. The length of the piles is governed by (3a) (slips passing below the toe of the piles), and (3b).

Some authors refer to ‘coupling’ of (1) and (2) above. Generally speaking, the most straightforward methods consider the various aspects independently (uncoupled), whereas more complex methods (e.g. 3-d finite element analysis) may claim to completely integrate (couple) all aspects. However, such approaches are unlikely to be used in routine design.

2.1.2 Structure

It is difficult to categorise all references into well-defined groups. However, in an effort to structure this the chapter is divided as follows:

- 2.2 Lateral pile-soil interaction (both active and passive)
- 2.3 Limit equilibrium methods
- 2.4 More complex analytical methods
- 2.5 Other references (e.g. lab and field studies)
- 2.6 Review of critical factors
- 2.7 Summary

2.2 Lateral pile-soil interaction

Linear elastic and fully plastic (ultimate) responses are initially considered for an ‘isolated’ pile and piles in a row. It is assumed that the ground surface is horizontal (not sloping). Finally, full response is considered for a row of piles.

2.2.1 Elastic Response (isolated pile)

Baguelin et al. (1977) derived an analytical solution for the lateral reaction of a rigid circular section (representing the cross section of the pile) displaced through an elastic medium (representing the soil) with a distant circular boundary about its centre (Figure 2.1(a)). A plane strain section normal to the axis of the pile was considered (Figure 2.1(b)). The following solution, based on relative pile-soil displacement in terms of basic elastic soil parameters, was derived:

$$\frac{p}{G} = 16\pi(1-\nu) \left\{ 2(3-4\nu) \ln\left(\frac{D}{d}\right) - \frac{2}{(3-4\nu)} \right\}^{-1} \left(\frac{\delta}{d}\right) \quad (2.1)$$

where

- p = P/d = equivalent pressure acting on the pile section
- P = force acting on the pile per unit length along the axis
- d = pile diameter
- δ = relative pile displacement
- G = shear modulus for the elastic medium (soil)
- ν = Poisson’s ratio of the elastic medium (soil)
- D = diameter of circle defining the rigid boundary

The value of ν can be varied for consideration of drained or undrained loading and soil properties whereas the value of G is not varied. The value of (D/d) is somewhat arbitrary in practice, although it must be finite for there to be any resistance to the movement. It is now known that using a more realistic high stiffness at small strain would reduce this dependency on far-field effects. A value of 30 has been used by previous researchers to consider an ‘isolated’ pile (i.e. one which is not significantly affected by any neighbouring piles) in conjunction with the linear elastic response.

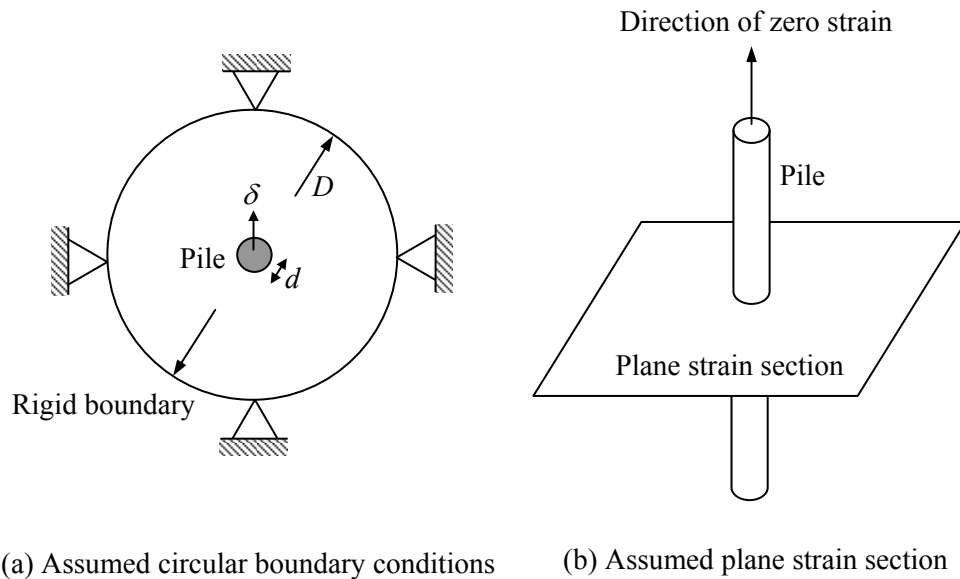


Figure 2.1 - Fundamental analysis of pile-soil interaction

2.2.2 Ultimate Capacity (isolated pile and pile row)

Single (isolated) pile

For granular soils, Broms (1964) suggested an equation deduced from active lateral load tests on a single pile. It was assumed that ultimate lateral force per unit length is equivalent to three times the passive earth pressure at all depths.

$$P_{ult} = 3K_p \sigma'_v d \quad (2.2)$$

where,

P_{ult} = net ultimate lateral soil load per unit length of pile

K_p = passive earth pressure coefficient equivalent to $(1 + \sin \phi')/(1 - \sin \phi')$

σ'_v = vertical effective stress

d = pile diameter

Fleming et al. (1994) proposed an empirical equation based on centrifuge test data for a laterally loaded pile (Barton, 1982) to predict the ultimate lateral load of a single pile. It was considered that P_{ult} increases in proportion to the square of K_p , giving

$$P_{ult} = K_p^2 \sigma'_v d \quad (2.3)$$

Other authors have proposed variation in proportion to K_p^3 , and hence Equation (2.3) can be used as an ‘intermediate’ form of various approaches. Additionally it gives results which are numerically quite similar to Equation (2.2) for practical values of K_p . Numerical modelling by Durrani (2006) has also shown this value to be broadly appropriate for limiting interaction (although potentially slightly high).

Pile row

The theory proposed by Ito and Matsui (1975) has been used in a number of publications for the purpose of calculating the ultimate lateral pressure due to passive pile loading. It was developed on the basis of a mechanism of plastic deformation of the soil ‘squeezing’ between adjacent piles. Referring to Figure 2.2, a row of piles with diameter (d) at centre-to-centre spacing (D_1) was considered (the ‘clear’ spacing between piles is $D_2 = D_1 - d$). The equivalent lateral pressure acting on a pile ($p = P/d$) for granular soils is calculated by Equation (2.4).

$$p = \frac{\gamma z}{N_\phi d} \left\{ A \exp \left[\frac{D_1 - D_2}{D_2} N_\phi \tan \phi \tan \left(\frac{\pi}{8} + \frac{\phi}{4} \right) \right] - D_2 \right\} \quad (2.4)$$

where

$$A = D_1 \left(\frac{D_1}{D_2} \right)^b$$

$$b = N_\phi^{1/2} \tan \phi + N_\phi - 1$$

$$N_\phi = K_p = \tan^2 \left(\frac{\pi}{4} + \frac{\phi}{2} \right)$$

$$\gamma = \text{the unit weight of the soil}$$

$$\phi = \text{the friction angle of the soil}$$

$$z = \text{depth within the moving layer of soil}$$

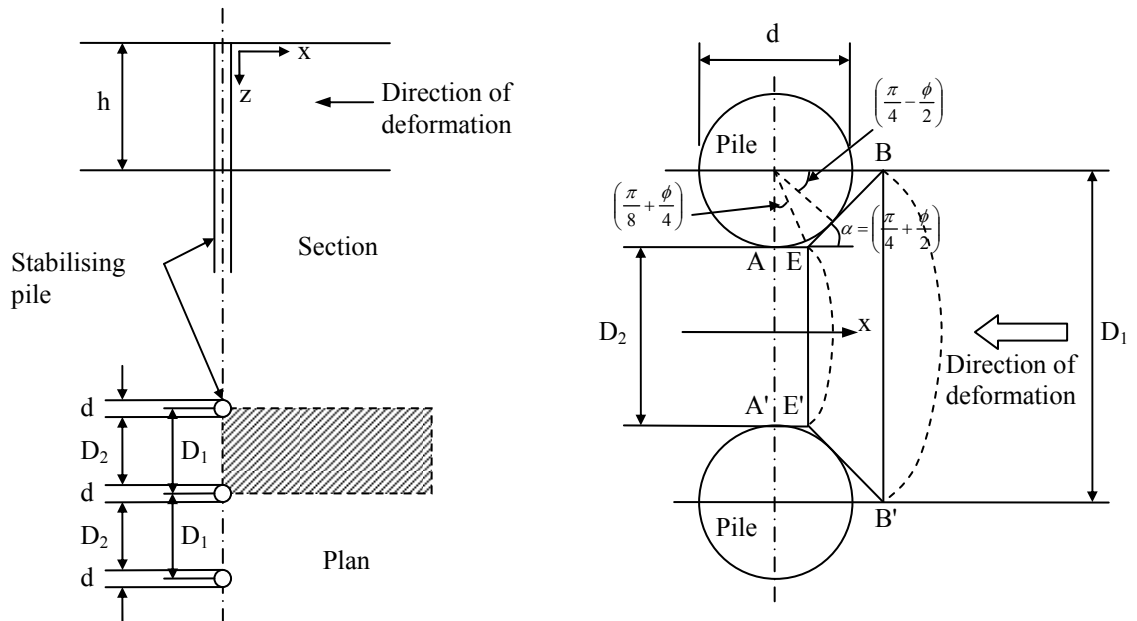


Figure 2.2 - An Idealised piled slope system (after Ito and Matsui, 1975)

The calculated lateral pressure on the pile(s) tends toward infinity as the pile spacing becomes a 'contiguous wall' ($D_2 \rightarrow 0$), whilst the lateral pressure approaches zero at very wide spacings (an 'isolated single pile'). Both these extremes of behaviour are clearly unrealistic for passive interaction in a slope. Nevertheless, it has been proposed that the method is valid for a restricted range of 'intermediate' pile spacings (e.g. De Beer and Carpentier, 1976).

2.2.3 Full response (combined elastic and ultimate response)

Liang and Zheng (2002) investigated the soil arching mechanism for ‘drilled shafts’ (piles) used for slope stabilisation using finite element analysis (PLAXIS). It was reported that the arching effect reduced as the ratio exceeded three times the pile diameter. Adjacent piles do no longer interact when the pile spacing is equal to or larger than eight times of the pile diameter.

Chen and Martin (2002) studied the load-transfer mechanism of stabilising piles using plane strain numerical analyses (FLAC), focusing on arching development between adjacent piles. It was reported that tendency of arching becomes stronger as pile spacing get closer whereas it is likely to be diminished at higher (s/d) in the range 4 to 6. It was also noted that the load transfer onto the piles is primarily caused by redistribution of the stresses upslope of the piles with rotation of the principal stress directions.

Durrani et al. (2006) studied pile-soil interaction arising from relative lateral pile-soil movement, taking account of arching along a pile row in a horizontal section. A translating pile was used on the basis that there is no fundamental difference between moving a pile relative to static remote boundaries, and moving remote boundaries relative to a static pile (e.g. Figure 2.1). (Consideration of a pile row rather than an isolated pile means that boundaries normal to a line along the row are not remote). The situation was analysed using a 3-dimensional ‘constant overburden analysis’ (Figure 2.3). This was proposed as an alternative to a plane-strain analysis, with the stress applied at the upper surface of the section representing the weight of overlying material. It was found that for a purely frictional soil strength this gave more rational results than a plane-strain section which had previously been used by other authors, although the ‘thickness’ of the 3-d section could influence the results (Durrani et al., 2006).

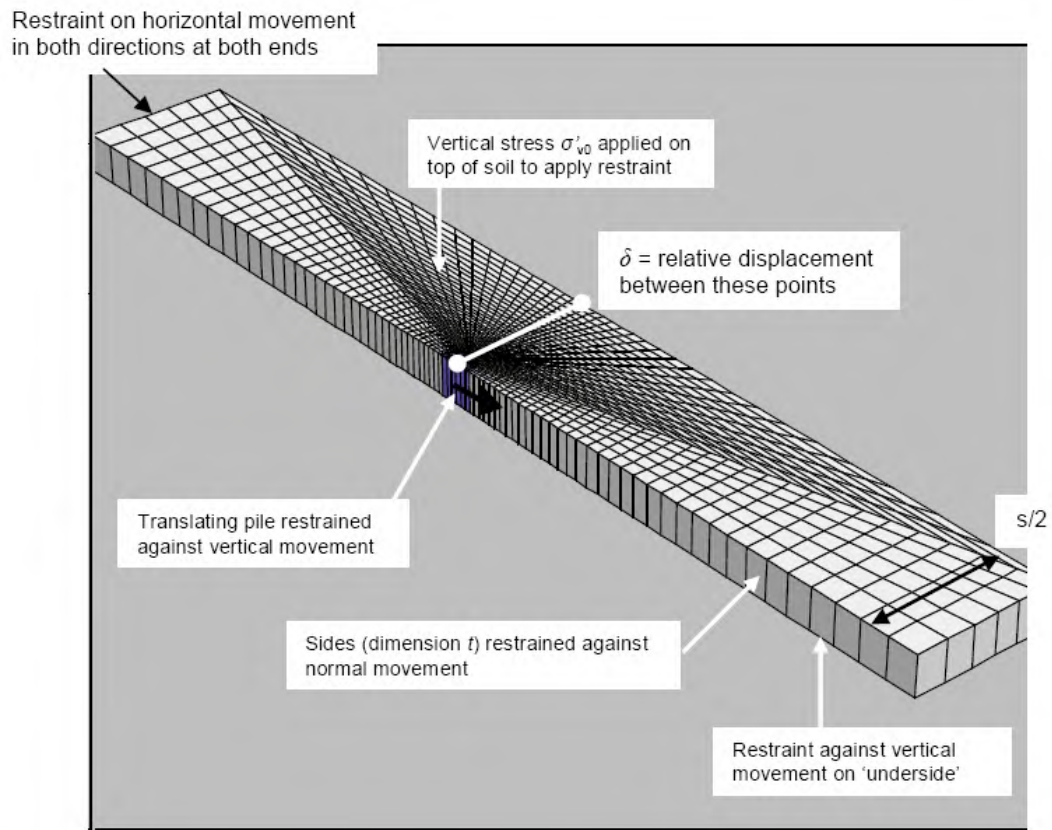


Figure 2.3 - ‘Constant overburden’ approach to modelling pile-soil-pile interaction (after Durrani et al., 2006)

Figure 2.4 shows conceptual models for the behaviour of

- (1) an ‘isolated pile’
- (2) a ‘continuous wall’

with corresponding earth pressures in the soil which is passively loading the pile or row, as proposed by Durrani et al. (2006). The limits are based on Equation 2.3 and active and passive limits for a retaining wall in level ground respectively.

Figure 2.5(a) shows the equivalent pressure on a pile at ‘ultimate’ conditions, ($p_{p,ult}$, where relative pile-soil movement was sufficient to give a maximum interaction pressure),

normalised by the ‘constant overburden’ stress (Figure 2.3). Variation with normalised pile spacing along the row is shown (s = centre-to-centre pile spacing, d = pile diameter).

Equations derived from the conceptual models are also shown (see Chapter 5), and it can be seen that the data conform quite well to the conceptual models, with behaviour changing from a continuous wall to an isolated pile as spacing increases. Durrani et al. (2006) proposed that the intersection of the lines was an approximate limit on arching between adjacent piles to give an equivalent wall.

Figure 2.5(b) shows an equivalent pressure ‘along’ the pile row, $p_r = p_p (d/s)$, which is more relevant to slope stability analysis in a vertical plane strain section. It is now apparent that as pile spacing increases the ultimate pressure which the row can offer to resist soil movement reduces, as would be expected.

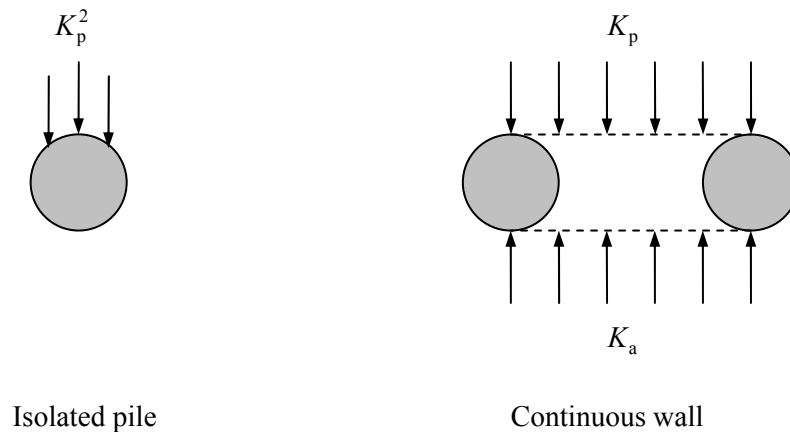
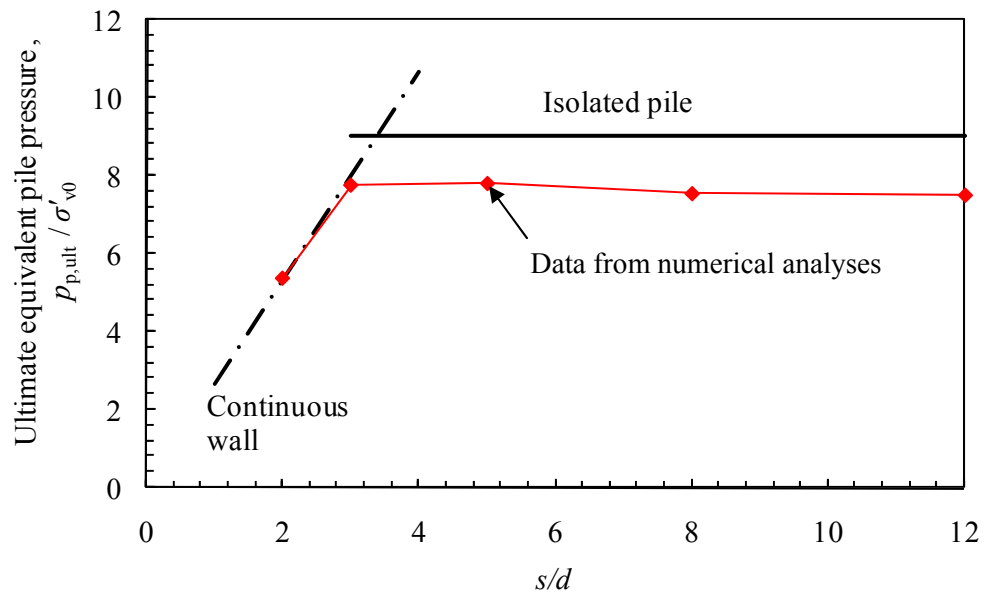
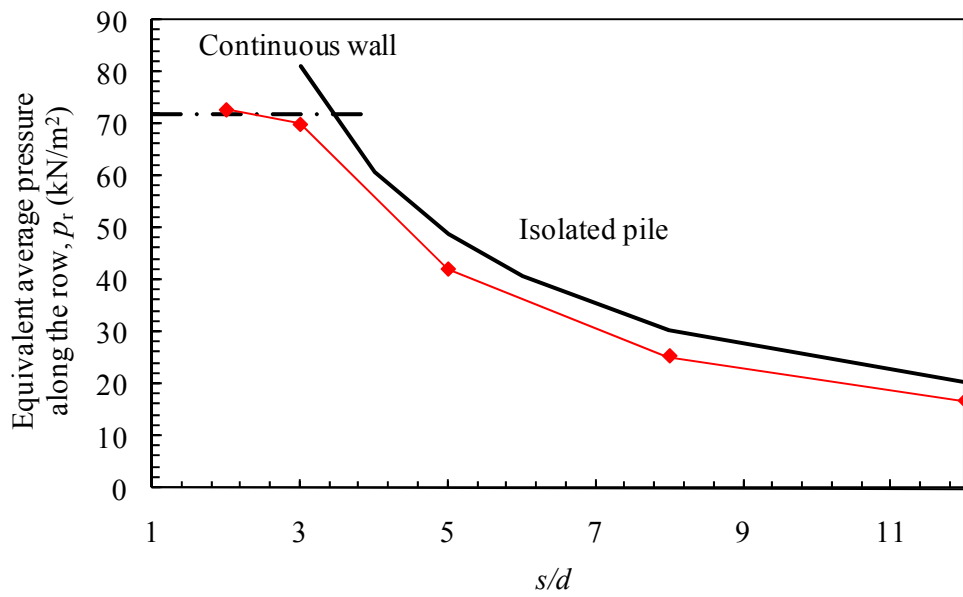


Figure 2.4 - Conceptual models of an isolated pile and a continuous wall



(a) Equivalent pressure for a pile at 'ultimate' condition



(b) Equivalent average pressure 'along' the pile row

Figure 2.5 - Ultimate equivalent pressures on a pile row and theoretical limits versus normalised pile spacing (after Durrani, 2006)

2.3 Limit equilibrium methods

Limit equilibrium analyses are widely used in the analysis of stability of earth structures with or without reinforcing members. They account for the static equilibrium condition of forces and/or moments developed on potential failure surfaces in the soil. An average factor of safety along the failure surface is generally calculated by comparing the required shear strength to maintain a condition of static limit equilibrium with the available shear strength of the soil.

2.3.1 Slip circle methods

In a slope reinforced with discrete piles a horizontal shear force resulting from soil-structure interaction is generally assumed to act where the piles intersect with a potential failure slip (Figure 2.6). The presence of the reinforcing piles in an unstable slope can make a major contribution to overall stability of the slope by providing an additional resisting force against sliding.

Slip circle methods for slope stability (normally based on the method of slices) are most frequently used in design, incorporating the interaction force as a horizontal line load (which acts on the slip surface which is critical prior to stabilisation). Commercial software packages for slope stability e.g. SLOPE/W easily allow this approach.

A number of authors (e.g. Lee et al, 1995; Hassiotis et al, 1997; Ausilio et al 2001) have inherently modified slip circle methods to incorporate the effect of passive interaction above the slip surface (for instance using Ito & Matsui's limiting pressure). It is shown (e.g. by Hassiotis et al, 1997) that inherently considering the stabilising force modifies the critical slip, and Durrani (2007) demonstrated that logically the critical slip becomes slightly deeper

for a given stabilising force. However, for routine design any modification of the slip which is critical prior to stabilisation is normally ignored.

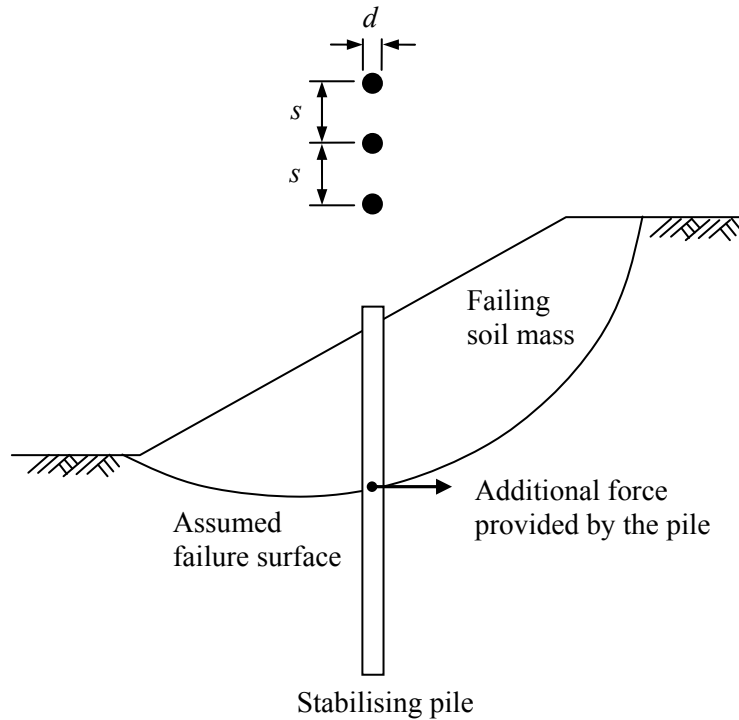


Figure 2.6 - Limit equilibrium analyses for a potentially unstable slope stabilised with piles

Wang and Yen (1974) assumed that the ‘yielding’ (unstable) layer failed along a potential failure plane parallel to the slope, and that a row of stabilising piles was embedded in a firm underlying base (Figure 2.7). The behaviour of the soil was assumed to be rigid-plastic. The solution proposed two relative spacings ($m = B/h$), where B is the clear spacing between the piles and h is the thickness of the unstable layer:

- (1) optimum spacing (m_m) at which soil arching is likely to be most effective
- (2) critical spacing (m_{cr}) beyond which the piles are unlikely to provide any stabilisation.

However, three limitations of the theory are apparent:

1. The pile row would behave as a ‘continuous wall’ at narrow spacing. This was not the ‘most effective’ spacing since arching may be developed even at a wider spacing.
2. The infinite slope assumption might be an ‘oversimplification’ of a complex three-dimensional problem, most particularly with regard to the upslope and downslope directions. Additionally, the length of the shear zones (a-a') upslope of the piles is required to be used in the analysis. Assuming the full upslope length of the slope can give unrealistic results (Hayward et al., 2000), whilst assumptions for a reduced length will be arbitrary.
3. The pile diameter was not considered in arching development since only equilibrium of the soil between the piles was considered.

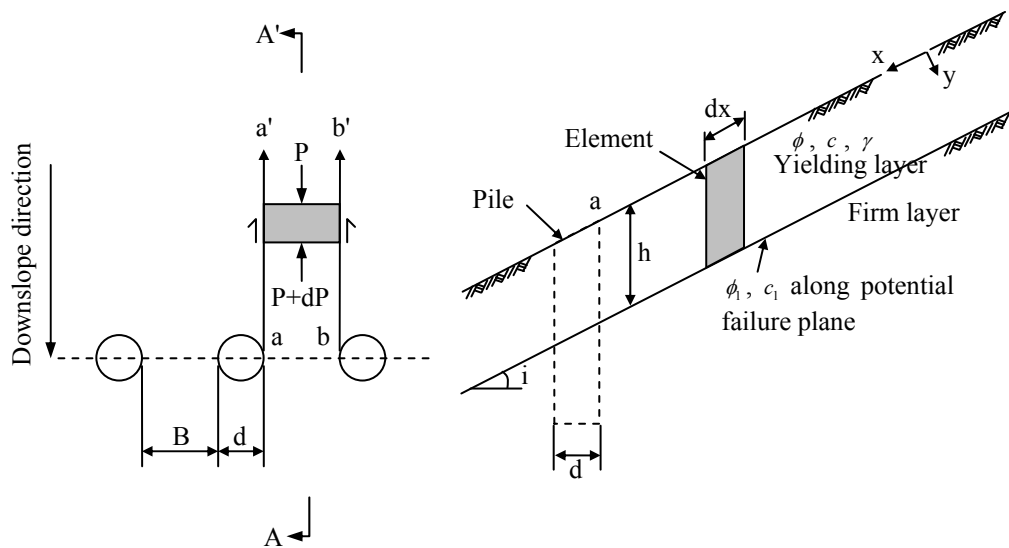


Figure 2.7 - Idealised pile-slope system (after Wang and Yen, 1974)

Viggiani (1981) proposed practical solutions to determine the maximum shear force provided by the pile on the slip surface and the bending moments acting on the pile for the different failure modes that may occur in practice. The solutions only considered the ultimate state of purely cohesive soils and the cohesion of the unstable and stable soils were assumed to be constant with depth. The pile-soil interaction in relation to spacings along the pile row was not reflected in the solutions.

Some of the conclusions from these references are considered in Section 2.6.

2.4 More complex analytical methods

Chen and Poulos (1997) and Poulos (1999) developed methods for computing lateral pile response based on a specified free-field soil movement profile using a simplified boundary element analysis or finite difference analysis. The pile was modelled as a simple elastic beam and the soil as an elastic continuum. It was concluded that a reasonable prediction was only made when the ratio of soil movement to pile diameter is smaller than about 10%. Lateral responses rely upon a ‘free field’ soil displacement for the unstable soil (in the absence of piles) as an input to the analysis, and thus are likely to have limited applicability in practice.

Jeong et al. (2003) described a simplified numerical approach for analysing the lateral response of piles in a row. Group interaction factors (representing the effect of pile-soil-pile interaction) were determined by comparing the maximum bending moment of a pile group with that of a single pile for a given free-field soil movement in finite element analysis (ABAQUS). Bishop’s simplified method was used to determine the factor of safety of a slope without piles and the critical failure surface. The non-linear characteristics of the pile-soil interaction were modelled by a hyperbolic load transfer curve. The ultimate lateral soil pressure for a pile in a row was calculated by multiplying the ultimate pressure for a single pile by the group interaction factor. A computer programme (RSSP) was developed to perform a series of sequences of the proposed pile-slope stability analysis.

A number of attempts have been made to identify the impact of various design factors influencing pile-soil interaction in a piled slope based on numerical approaches (e.g. finite element, finite difference). Examples include Cai and Ugai (2000), Carder and Easton (2001), Won et al. (2005), Ang (2005) and Durrani et al. (2006). The soil behaviour is generally assumed to be characterised by an elasto-plastic Mohr-Coulomb failure criterion.

The factor of safety of the pile stabilised slope is usually calculated by the strength reduction technique (in which the soil shear strength is gradually reduced until the analysis indicates failure).

‘Coupling’ of the pile-soil-pile interaction along the row with slope stability is inherently incorporated in 3-d analyses, or normal and shear ‘coupling springs’ are used in plane strain analyses. In principle such approaches (particularly 3-d analysis) offer more realistic outcomes than less sophisticated methods. However, the strength reduction technique is required to instigate failure, and the result may not be completely representative of actual failures instigated by other effects, and the suitability of constitutive models is always of some concern in numerical modelling. Some of the authors compared the results of numerical analyses with equivalent modified Bishop analyses.

Some of the conclusions in these references are considered in Section 2.6.

2.5 Other references

Bosscher and Gray (1986) performed reduced-scale model tests in order to investigate the effect of soil arching in a sandy slope that was restrained by a series of ‘fixed gates’ and ‘swing gates’. The width of the swing gate is analogous to the open spacing between piles. It was observed that the effect of arching becomes less effective as the swing gate width increases.

Adachi et al. (1989) attempted to investigate arching phenomenon by examining the deformation pattern of soil particles (e.g. particle A, B, and C in Figure 2.8) in a series of model tests using trapdoors. Particles B and C within the arching zone of soil were not influenced by arching development, as opposed to soil particle A which was. The lateral pressure is superimposed along the developed arch between the piles and transferred to the piles. The loads acting on the piles increased with an increase of the pile spacing. However, the pile behaved like a single pile at $(s/d) > 8$ (indicating disappearance of any arching effect).

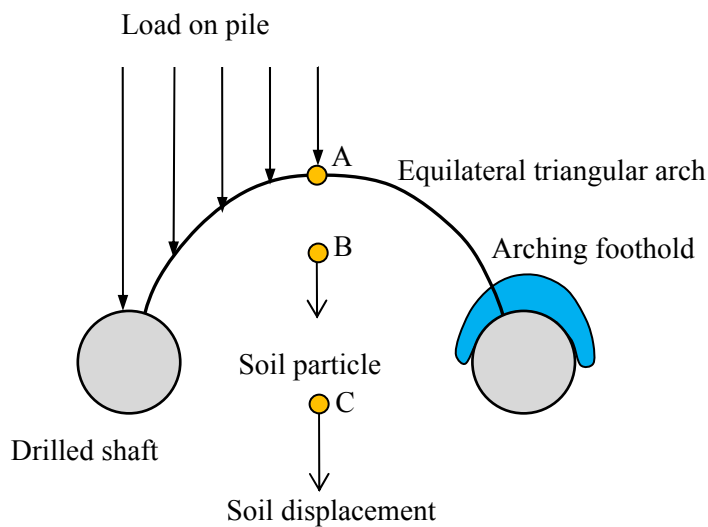


Figure 2.8 - Arching development and effect (after Adachi et al., 1987)

Poulos et al. (1995) and Chen et al. (1997) conducted laboratory model tests on single piles and pile groups embedded in calcareous sand and subjected to lateral soil movement. The group effects of the piles were estimated using a dimensionless group factor (the ratio of ultimate soil pressures for a pile in the group to a single isolated pile). It was reported that the group effects were diminished when the spacing between the piles exceeded 8 times the pile diameter.

Hayward et al. (2000) reported a sequence of centrifuge tests on a model cut slope in clay without or with discrete piles spaced at 3.2, 4.2, and 6.3 diameters. It was concluded that at a spacing of 3.2 and 4.2 diameters deep seated failure was prevented, but not at a spacing of 6.3 or the unreinforced slope. The limiting lateral pressure on the piles steadily increased as the pile spacing became larger. A pile spacing of $4d$ appeared to be critical for preventing the slope failure in this case.

The centrifuge test results were compared with other methods for predicting the limiting lateral pressure. The limiting lateral pressure profile at 6 diameter spacings for a given depth showed good agreement with the method proposed by Fleming et al. (1994) but the method proposed by Broms (1964) gave an overestimate. Theoretical methods proposed by Ito and Matsui (1975) and Wang and Yen (1974) did not give agreement in many respects (e.g. the relationship of limiting pressure distributions versus pile spacing), indicating that they may not be suitable for use in analysis.

Carder and Temporal (2000) presented a comprehensive review of the use of spaced piles to stabilise embankment and cutting slopes. The report reviewed case histories, construction techniques where soil flow and arching occur, and earlier design methods for stabilising piles.

Boeckmann (2006) conducted a series of large scale model tests to study load transfer in micropiles used to stabilise a sandy slope. Spacing ratios of 5, 10, 15, and 30 diameters were considered. It was reported that there was a slight tendency for increase in the limiting lateral pressures with increasing reinforcement spacing ratio. Piles whose head was restrained against lateral movement showed the greatest limiting pressure as expected.

Thompson and White (2006) performed large scale lateral load tests to verify the use of drilled and grouted slender piles subject to uniform lateral soil movement. From the results slender piles may become more cost effective than large diameter piles for particular slope failure conditions (e.g. shallow failure), considering the mobilised bending moment relative to maximum bending capacity of the pile. However an increasing danger of structural failure of the pile and requirement for more piles compared to larger diameter piles should also be taken into account.

Smethurst and Powrie (2007) presented bending behaviour of discrete piles used to stabilise a railway embankment at Hildenborough, Kent, UK. The site is underlain by the Weald Clay to a depth of about 250 m. Piles installed at a spacing of 4 diameters were considered, and the behaviour over four years after pile installation was monitored. In the short term there was a significant change in bending moment measured in the piles whilst the longer-term bending behaviour showed a relatively small subsequent variation. Analysis of the piles using a simple elastic analysis (using soil displacement measured at the midpoint between piles, based on the program ALP) was conducted, and showed a reasonable match to the bending moment and pile displacement measured.

2.6 Review of critical factors

Information available from the above references for aspects of analysis of a slope stabilised by a discrete pile wall are summarised as follows:

- pile row location in the slope
- pile spacing along the row
- effect of the pile-soil interface roughness
- effect of soil dilation

2.6.1 Pile location in slope

Figure 2.9 shows the effect of location (where the pile is most effective in stabilising a slope) proposed in various references (given in Table 2.1). Here L_x is the horizontal distance from the toe of the slope to the pile position and L is the horizontal distance from the slope toe to the crest. Hence for piles at the toe $L_x/L = 0$ and when the crest is reached $L_x/L = 1$.

For a typical slip (Figure 2.9(a)) the largest improvement is achieved when the piles are placed at midslope or near the crest. This is because the depth of the slip below the slope surface (indicating the depth and hence maximum magnitude of passive interaction) is similar at the midslope and nearer the crest, but much lower near the toe (Figure 2.10).

However, Lee et al. (1995) argued that for a purely cohesive soil whose strength does not increase with depth the critical slip tends to become very deep, even passing beneath the pile tips. The optimal position then becomes at the crest or the toe of the slope because this failure type readily occurs if the embedded depth of the piles is not sufficient (Figure 2.9(b)) in which the improvement ratio ($N_{ps} = F_p/F_s$) is the ratio of the improved factor of safety of the slope with piles (F_p), to the initial factor of safety of the slope without piles (F_s).

However, this finding is specific to analysis using undrained soil strength which does not increase with depth.

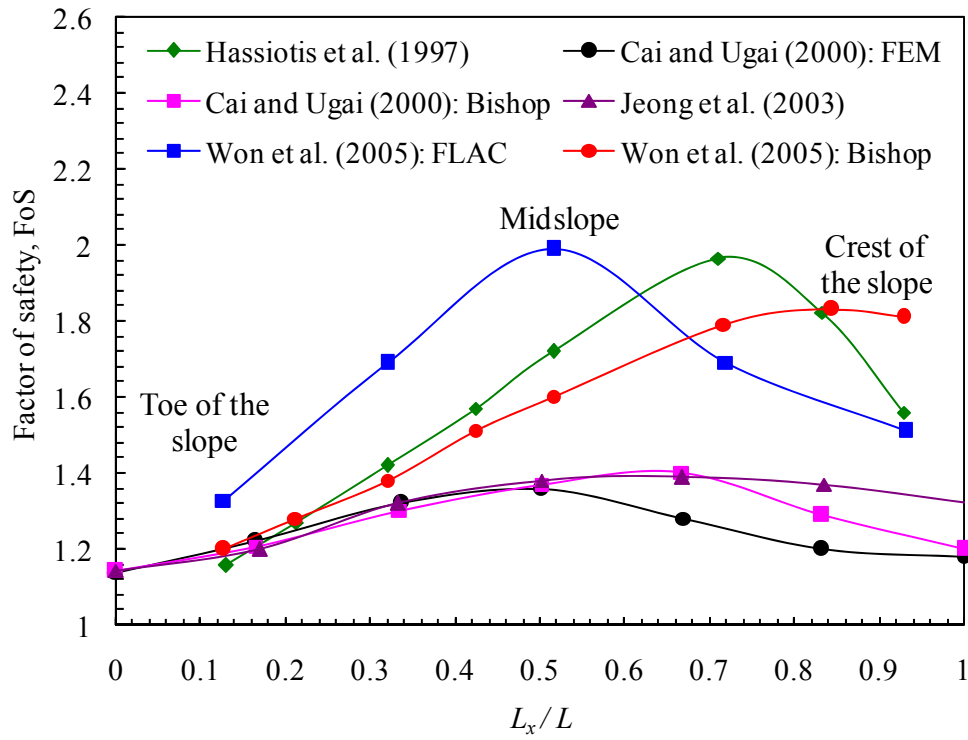
Ausilio et al. (2001) also argued that the critical slip can show increasing tendency to extend below the base of the slope if a log-spiral curve is used. For this case, the optimal location of the pile in the slope was then proposed to be between the midslope and toe. However, the probability of an upslope slip is then increased (Figure 2.9(c) in which K is the stabilising force normalised by $(\gamma H^2/2)$ and η is the improvement ratio in the factor of safety).

Durrani (2007) emphasised two important features of behaviour:

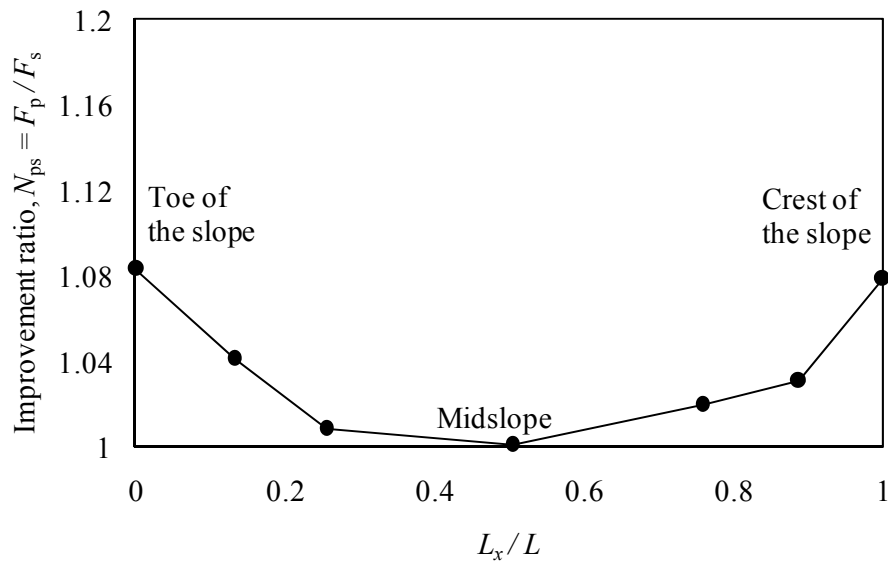
- (1) When the piles are near the toe of the slope the depth of interaction (and hence maximum interaction force) is small, or even zero for a slip occurring upslope of the pile row.
- (2) When the piles are near the crest, although the depth of interaction is quite large less passive loading was generated, presumably because the mass of soil which is ‘above’ the piles was small.

It is thus plausible that piles at the crest or toe are generally not as effective in stabilising the slope as at the midslope for a typical slip. These generic observations do not take any account of the practicality of constructing piles at various locations in the slope, or the location of infrastructure at the crest or toe of the slope. However, both these factors will also be of considerable importance in choice of location for actual design scenarios.

Summary of the references considered herein is given in Table 2.1.

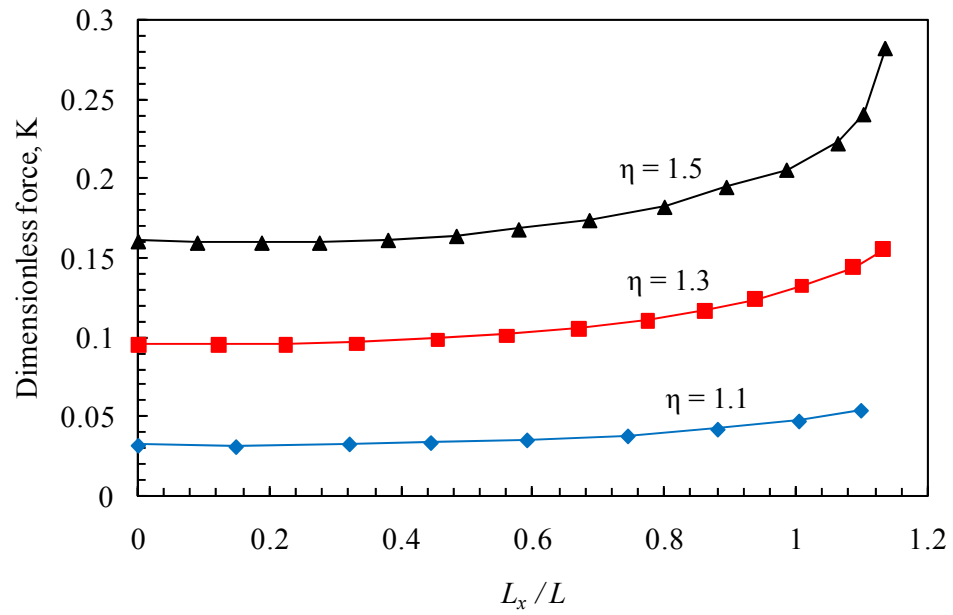


(a) Optimal location of the pile for a typical rotational slip for comparison



(b) Optimal location of the pile for a deep seated failure slip in cohesive soils

(after Lee et al., 1995)



(c) Optimal location of the pile for a log spiral slip (after Ausilio et al., 2003)

Figure 2.9 - Comparison of the optimal pile location in stabilising a slope

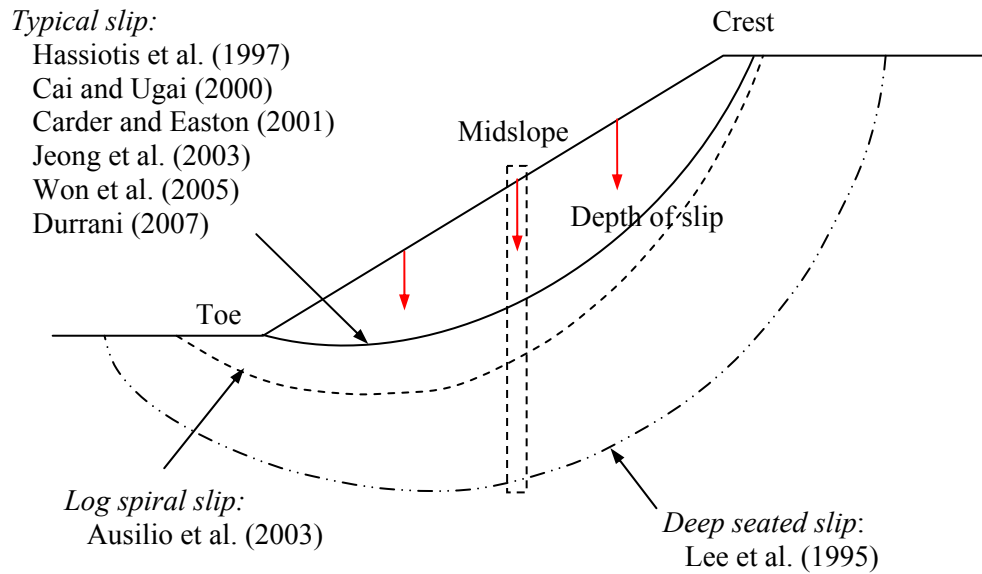


Figure 2.10 - Depth of slip measured at crest, midslope, and toe of a slope for a typical slip

Table 2.1 - Summary of references and optimal locations

References	Method	Failure slip type	Coupled / Uncoupled	Optimum location
Lee et al. (1995)	Limit equilibrium (for slope stability) Modified boundary element (for pile response prediction)	Deep seated failure slip (even passing beneath of the pile tip)	Uncoupled	Crest and toe of a slope
Hassiotis et al. (1998)	Limit equilibrium (for slope stability) Ito and Matsui's (for ultimate pile pressure prediction)	Typical failure slip	Coupled	Near the crest of a slope
Cai and Ugai (2000)	3d finite element	Typical failure slip	Coupled (inherently)	Midslope
	Modified Bishop's	Typical failure slip	Uncoupled	Between midslope and the crest
Ausilio et al. (2001)	Limit analysis based on the upper- and lower bound theorems of plasticity	Log-spiral curve type failure slip	Coupled	Between midslope and the toe
Carder and Easton (2001)	3d finite element	Typical failure slip	Coupled (inherently)	Between midslope and the crest
Jeong et al. (2003)	Bishop's simplified (for slope stability) Finite element (for determining group interaction factors required to calculate the ultimate pressure) Numerical (for pile response prediction)	Typical failure slip	Uncoupled	Between midslope and the crest
Won et al. (2005)	FLAC 3D	Typical failure slip	Coupled (inherently)	Midslope
	Modified Bishop's (incorporated with Ito and Matsui's solution for ultimate interaction pressure)	Typical failure slip	Uncoupled	Near the crest of a slope
Durrani (2007)	FLAC 3D (3d constant overburden)	Typical failure slip	Coupled (inherently)	Midslope

2.6.2 Pile spacing

Pile spacing has a significant impact on two important issues:

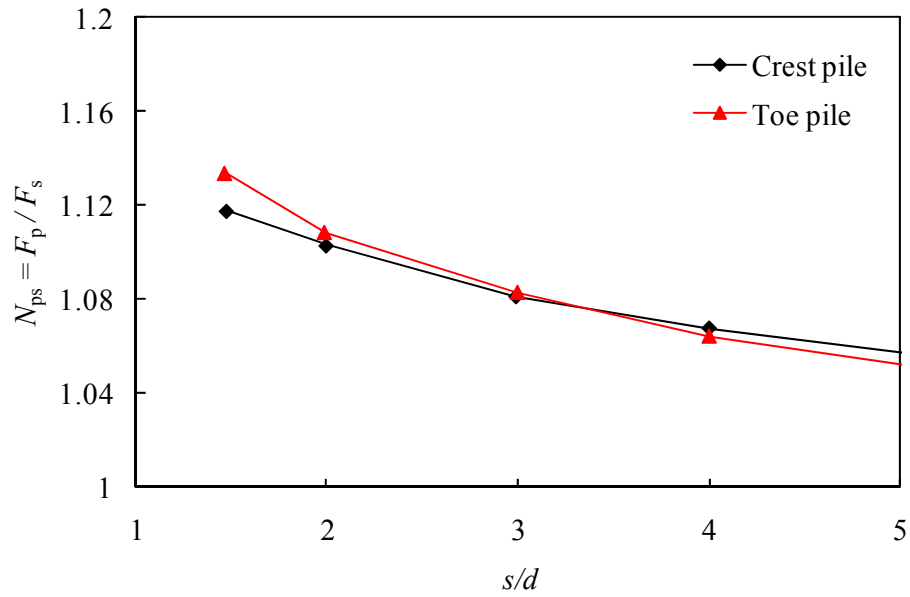
- (1) the improvement in stability of a slope reinforced with piles (considered herein)
- (2) passive interaction with respect to development of arching (also previously considered in Section 2.2.3).

The relationship of the safety factor (FoS) or the improvement ratio ($N_{ps} = F_p/F_s$) of the slope with the normalised spacing (s/d) shows that the stability significantly decreases with an increase of pile spacing (Figure 2.11(a)). This observation seems clearly reasonable – arching between piles becomes more effective as the pile spacing decreases whereas the tendency for flow between the piles increases at wider spacing (and hence there is the reduction in stability).

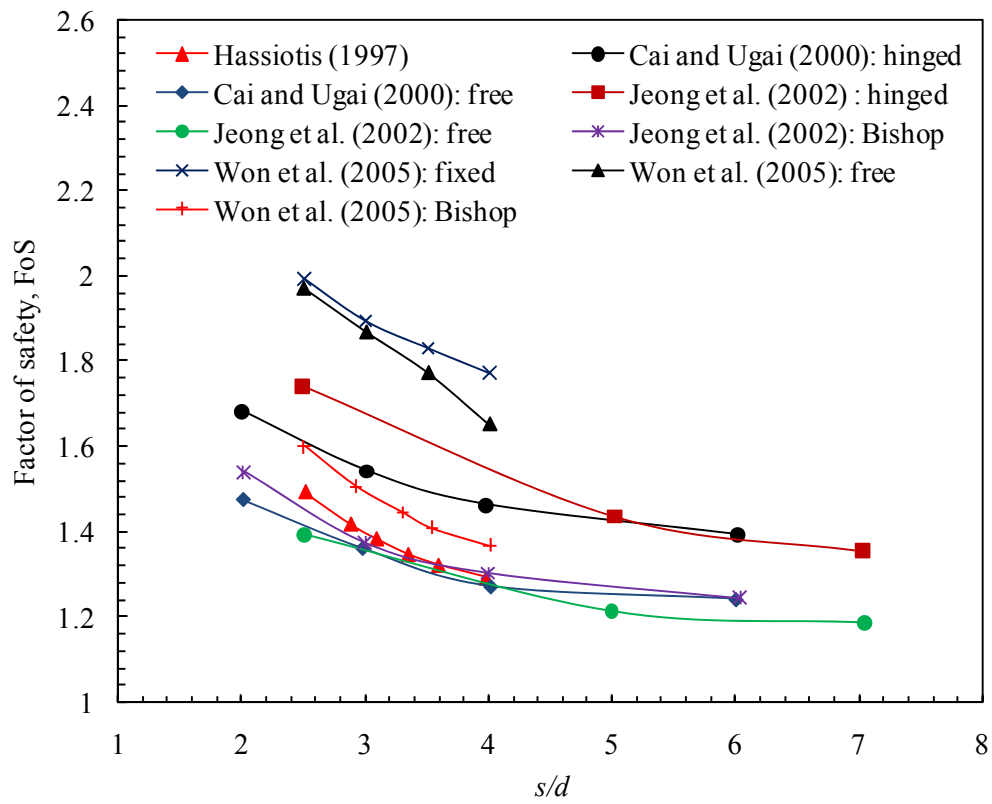
Figure 2.11(b) also indicates that the pile head condition can influence the factor of safety of the slope, with a pile which is ‘hinged’ (restrained against horizontal movement at the head) being more effective than a pile which is ‘free’ (unrestrained) at the head. The piles considered by Cai & Ugai are tubular, with quite low bending stiffness. Thus the pile displacement exceeds the soil displacement near the soil surface, giving active rather than passive loading at the head of the pile. This effect is rather unusual in the context of piles which are stabilising the slope and reduces the total passive resistance which the flexible piles offer to a potential slip when horizontal movement is allowed at the head.

Figure 2.11(c) (Durrani, 2007) shows a solid black line for comparison with results from a series of 3-d ‘constant overburden’ FLAC analyses. The origins of this model of behaviour are described in Section 5.2.3. Beyond a critical pile spacing (which is postulated to mark the upper limit of spacing for arching to occur) the improvement in FoS (ΔF) shown by the

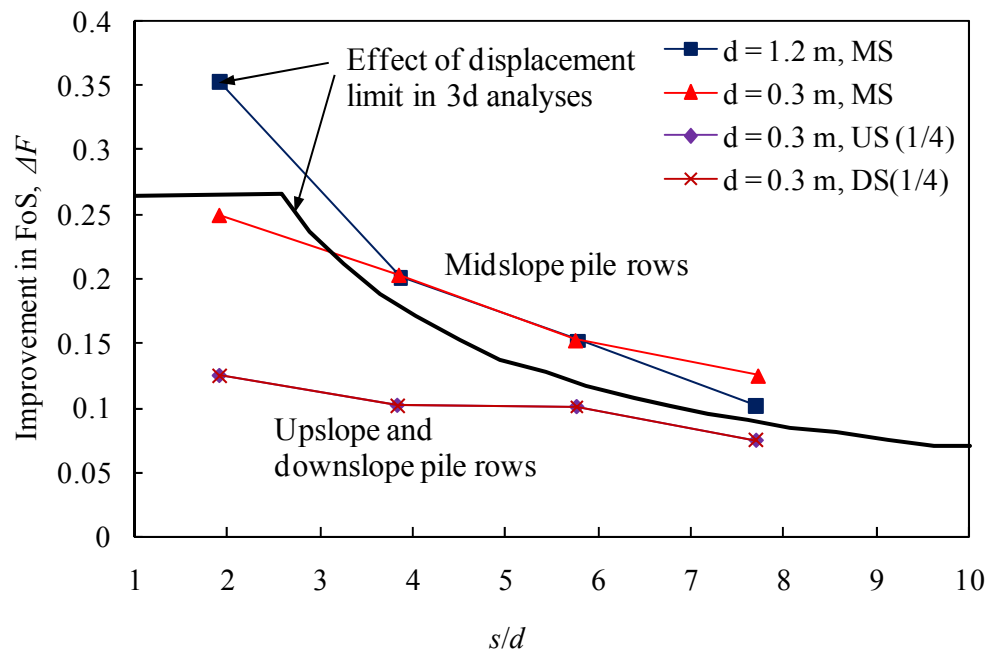
solid black line reduces as $(1/s)$, and it can be seen that the results show reasonable agreement with this trend, hence broadly quantifying this effect.



(a) Improvement ratio versus s/d (after Lee et al., 1995)



(b) Factor of safety versus s/d



(c) Improvement in FoS versus s/d (after Durrani, 2007)

Figure 2.11 - Effects of pile spacing on the stability of a stabilised slope with the piles

2.6.3 Effect of pile/soil interface roughness

The effect of pile/soil interface roughness on the ultimate capacity of a pile has been investigated for a pile spacing of 4 or 5 diameters by Chen and Martin (2002), and Durrani (2007). The internal friction angle of the granular soil considered was $\phi' = 30^\circ$. The ultimate equivalent pressure on the pile is plotted showing variation with the friction angle of the interface (Figure 2.12). The results show that there is some increase in the ultimate pressure up to 10° but very little effect thereafter. This is probably attributable to the dominance of difference in normal stresses on the ‘front’ and ‘back’ of the piles rather than actual shear stress at the interface. The results presented by Chen and Martin (2002) are inherently lower since they are based on a plane strain analysis rather than the ‘constant overburden’ approach used by Durrani.

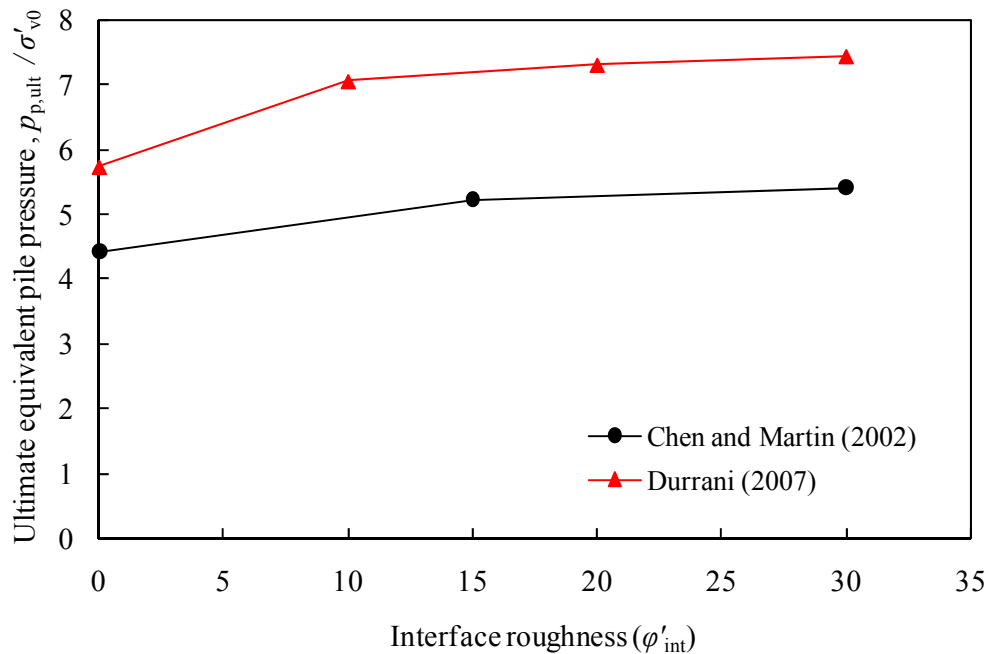


Figure 2.12 - Effect of interface roughness on ultimate equivalent pressure on the pile

2.6.4 Effect of soil dilation

Figure 2.13 shows variation of the ultimate resistance with different dilation angles for $(s/d) = 3, 4$, and 5 ; again showing data from Chen and Martin (2002), and Durrani (2007). The ultimate resistance is likely to be less affected for a closely spaced pile ($(s/d) = 3$ in the analyses by Durrani), when the pile row behaves as a ‘wall’. On the other hand, the higher dilation angle causes some increase of the ultimate resistance for more widely spaced piles, which seems reasonable since tendency for volumetric strain will increase the constraint on soil ‘squeezing’ through the gap between the piles.

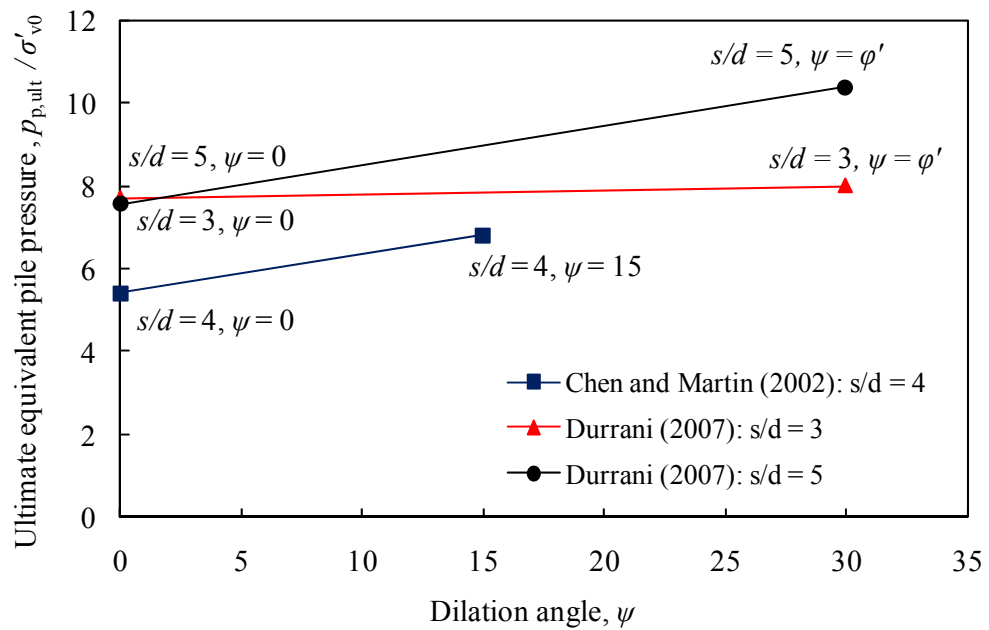


Figure 2.13 - Effects of soil dilatancy on ultimate resistance and passive interaction

2.7 Summary

A number of studies of stabilisation of a slope using piles have been introduced:

- limit equilibrium methods (Section 2.3)
- analytical and/or numerical methods (Section 2.4)
- model or field tests (Section 2.5)

Some of the references have provided a reasonable appraisal of lateral pile-soil interaction (involving linear elastic and ultimate responses). Many of the design methods presented have also attempted to provide geotechnical engineers with a generally acceptable prediction of lateral behaviour of the piles in practical design, but there are still some uncertainties regarding the impact of critical design factors.

From general observation of critical factors available from the references, the following conclusions have been drawn:

- The piles are generally most effective somewhere near the mid-height (or crest) of the slope. However, practical constraints of construction and location of infrastructure also impact significantly on this aspect of design.
- Arching between piles in a row becomes more effective as the pile spacing decreases whereas the tendency for flow between the piles increases at wider spacing. Beyond a critical pile spacing (which is postulated to indicate the upper limit of spacing for arching to occur), the effect of the piles tends to reduce as $(1/s)$ at wider spacings.
- Pile/soil interface roughness and soil dilation appear to have relatively little effect on ultimate resistance.

CHAPTER 3

CENTRIFUGE MODELLING: METHODOLOGY

3.1 Introduction

3.1.1 Centrifuge modelling: principles and scaling laws

It is widely recognised that reduced scale physical models do not replicate the corresponding stress regime of a full-scale geotechnical situation. This is a significant problem since the mechanical behaviour of soil is highly dependent on the magnitude of the current confining stress (and stress history). Geotechnical centrifuge modelling overcomes this problem and is the most efficient and robust tool in laboratory simulation for practice and research.

The principle of centrifuge modelling is that the particular full-scale stress regime can be approximately replicated by increasing centrifugal acceleration to N times Earth's gravity in an $1/N^{\text{th}}$ scale model. This approach works because (for the same soil density) the self-weight increases by a factor N whilst the length scale is reduced by the same factor so that $\sigma_v = \gamma z$ is correct. Figure 3.1 presents the stress regime in a centrifuge model compared to that of the equivalent 'prototype' (a version of the model which is N times larger).

The scale factors relevant to common geotechnical applications of the centrifuge are given in Table 3.1. Further details on centrifuge modelling can be found in Schofield (1980) and Taylor (1995). Errors associated with the inertial stress field are considered in Section 3.6.3.

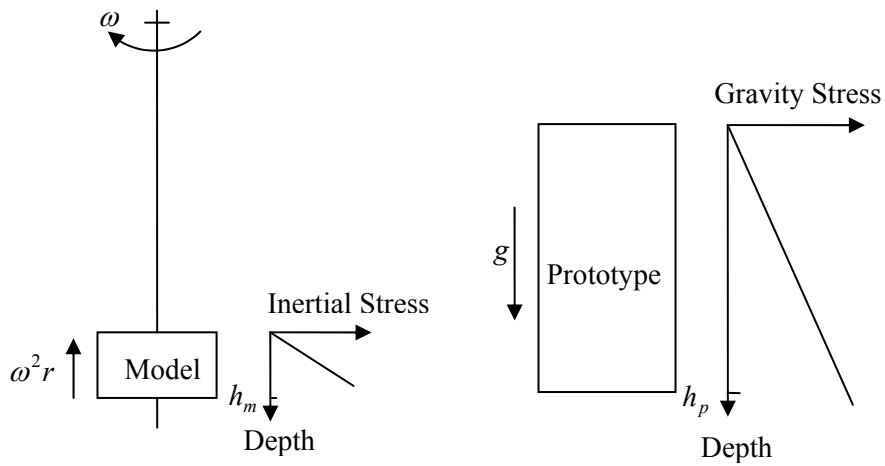


Figure 3.1 - Stress distributions for prototype and centrifuge model (after Schofield, 1980)

Table 3.1 - Centrifuge model scaling relationships

Quantity	Units	Scaling factor (prototype / model)
Acceleration	m/s^2	$1/N$
Density	kg/m^3	1
Unit weight	N/m^3	$1/N$
Linear dimension	m	N
Area	m^2	N^2
Volume	m^3	N^3
Stress	N/m^2	1
Strain	Dimensionless	1
Force	N	N^2
Force / unit width	N/m	N
Bending moment	Nm	N^3
Bending moment / unit width	Nm/m	N^2
Flexural stiffness	Nm^2	N^4
Flexural stiffness / unit width	Nm^2/m	N^3
Void ratio	Dimensionless	1
Particle friction	Dimensionless	1

3.1.2 Structure

The Chapter is split into sub-sections as follows:

- 3.2 Centrifuge test programme
- 3.3 NCG Geotechnical Centrifuge facilities
- 3.4 Test material (e.g. engineering properties of the test sand)
- 3.5 Centrifuge test model (e.g. test model and model pile)
- 3.6 Modelling considerations
- 3.7 Test procedure
- 3.8 Summary

3.2 Test programme

The centrifuge model was designed to represent an unstable slope in a purely frictional (granular) soil, inclined at 30° to the horizontal (Figure 3.2). The slope was comprised of a ‘sliding’ (unstable) layer and ‘stable’ underlying material, separated by a prescribed failure surface. The predefined failure surface was a translational slip plane parallel to the slope surface at 70 mm depth at model scale. The model piles were installed in a row at discrete intervals across the slope. The model was assumed to be plane strain (except the pile row, this will be discussed in Section 3.5.1).

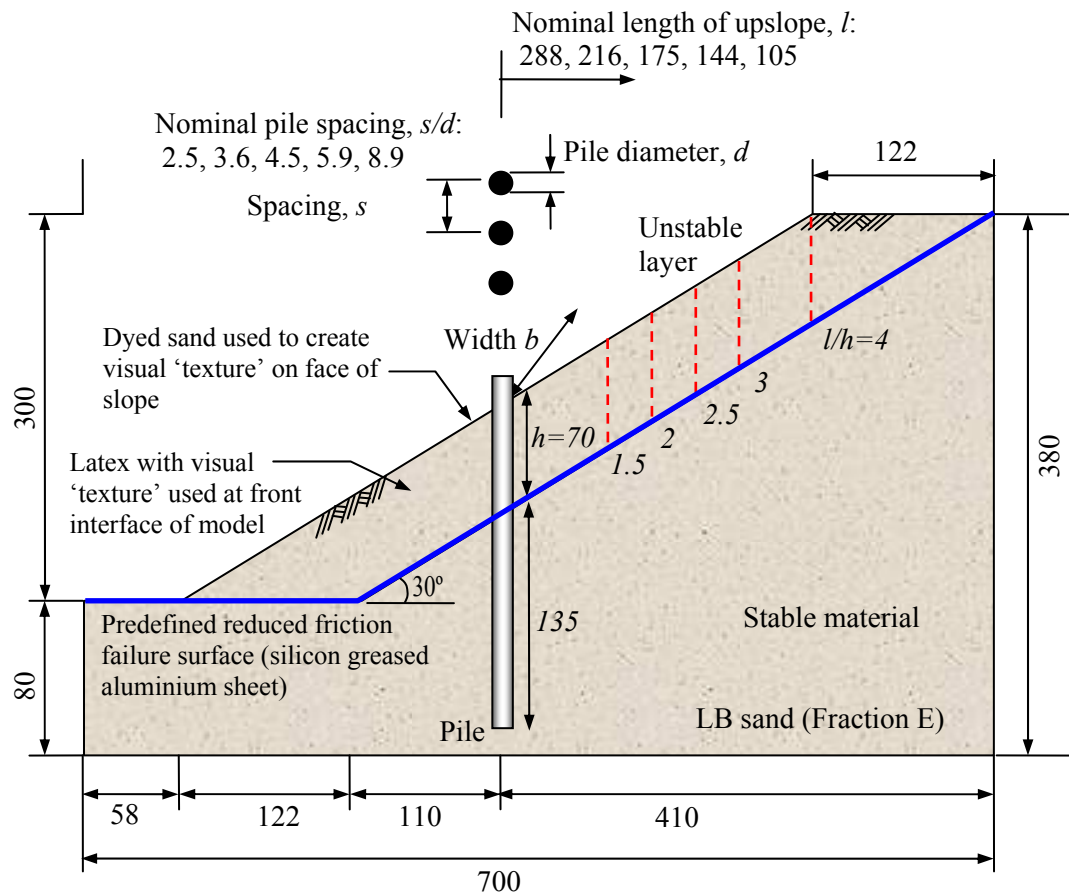
The model is somewhat idealised. The failure interface separating the unstable and stable material has a very low sliding resistance (see Section 3.6.1), increasing the tendency for the upper portion of the slope to cause passive loading on the piles over a known depth, so that this aspect of behaviour could be studied in detail. The model is intended to generically study this mechanism rather than to represent a specific prototype. It is also worth noting that design procedures often do not exactly represent real life, and thus idealised generic approaches such as this can be at least as valuable in informing design as more ‘realistic’ (and hence specific) studies. Likewise, sand has been used, but this is intended to represent any frictional soil (e.g. drained behaviour of clay, although the friction angle would be lower).

Selection of the variables was based on combination of the following factors affecting the pile-soil-pile interaction (Figure 3.2):

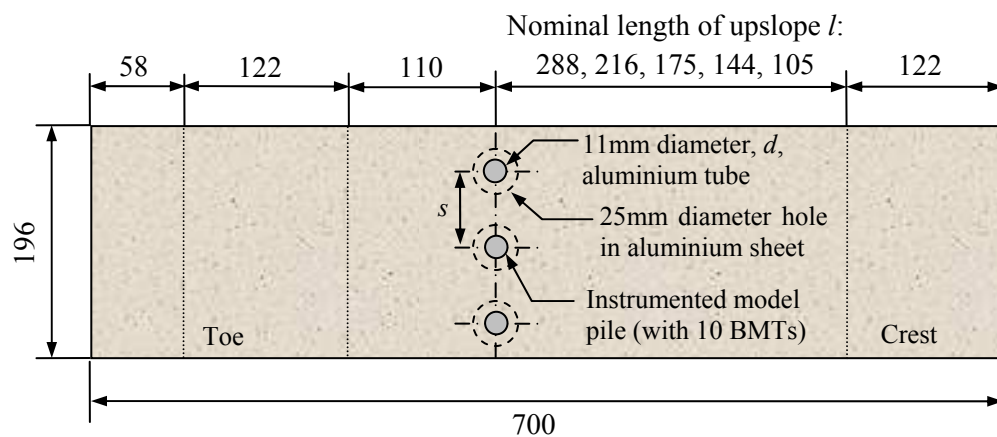
- (1) the ratio of the upslope length to the thickness of sliding soil ground (l/h) which essentially controlled the total load on the pile row
- (2) the normalised centre to centre pile spacing along the row (s/d) which is a significant factor in determining limiting pile-soil interaction for the row.

Both (1) and (2) (the load on the piles and the limiting capacity) increase nominally in proportion to g -level. Thus models were subjected to a variety of g -levels (in the range 10 to 50), which is unconventional. The aim was to explore the underlying principles controlling behaviour rather than consider a specific prototype. The range of g -levels used did however give soil behaviour considerably more representative of full-scale behaviour (in general) than a 1- g model. At the maximum acceleration of 50g the 70 mm thick unstable layer corresponded to 3.5 m.

Initial tests were undertaken to refine the modelling approach. The general arrangement and components are illustrated in Figure 3.2. Table 3.2 and Figure 3.3 show the tests forming the final data set reported here.



(a) Front view



(b) Plan view

Figure 3.2 - Configuration of slope model with a row of piles

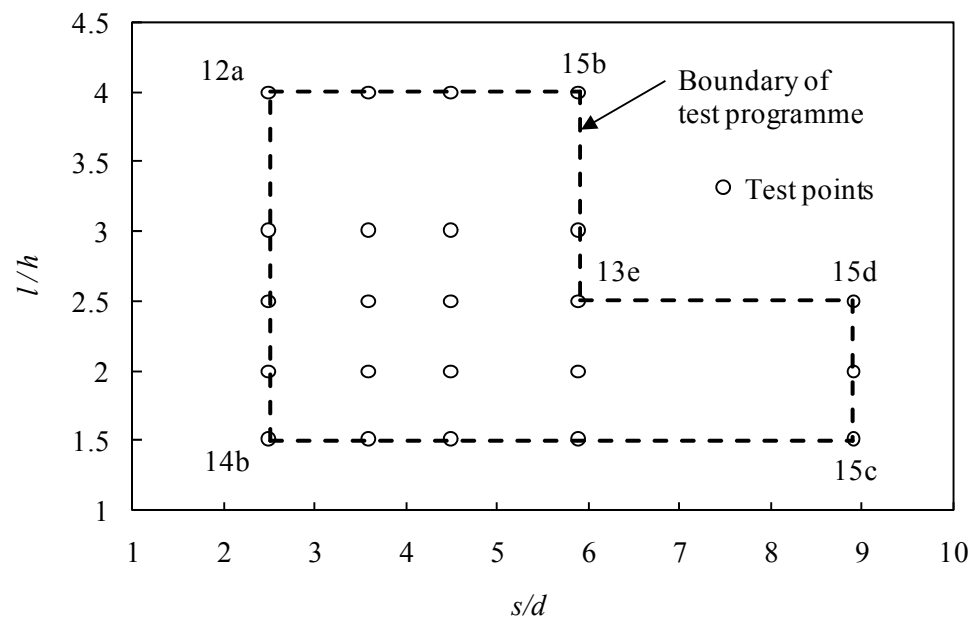


Figure 3.3 - Centrifuge testing programme

Table 3.2 - Centrifuge testing programme

l/h	s/d				
	2.5	3.6	4.5	5.9	8.9
4	12a	11a	13d	15b	-
3	12b	15f	13b	13f	-
2.5	14a	14c	13c	13e	15d
2	12c	12d	13a	14g	11c
1.5	14b	14d	15e	15a	15c

Note that boundary values of test programme were designed to cover the general ranges of pile spacing from critical spacing (3 to 4 s/d proposed by Hayward et al. (2000) and Durrani et al. (2006)) to the spacing at which the piles do not interact with the slope (8 s/d proposed by Liang and Zheng (2002)).

3.3 NCG geotechnical centrifuge facilities

3.3.1 NCG geotechnical centrifuge

The Nottingham Centre for Geomechanics (NCG) geotechnical centrifuge is a typical medium-size beam centrifuge with 2.0 m platform radius and a payload capacity of 500 kg at 1.7 m nominal radius up to 100 g. The centrifuge mainly consists of the following components:

- (1) a main body with rotating arms,
- (2) a swinging platform (cradle),
- (3) counterweight (fixed mass, adjustable position), supplemented by an in-flight automatic balancing system
- (4) electric motor
- (5) Data Acquisition System (DAS) cabinets for data transmission
- (6) slip rings for transmission of electrical signals and power, and fibre optic rotary joint for transmission of data

Specification of the NCG geotechnical centrifuge and the components are given in Table 3.3 and Figure 3.4. Specific discussion of NCG centrifuge and DAS can be found in Ellis et al. (2006).

Table 3.3 - Centrifuge specification

Performance criteria	Specification
Manufacturer	Thomas Broadbent & Sons
Radius to platform in flight	2.0 m
Max. size of payload	0.8 m wide (vertical in flight) 0.6 m wide (circumferential in flight) 0.9 m high (radius in flight)
Max. platform payload	500 kg at nominal radius of 1.7 m up to 100g
Max. acceleration	150g at nominal radius of 1.7m
In-flight balancing	+/- 50 kgm
Motor	75 kW 3 phase induction motor

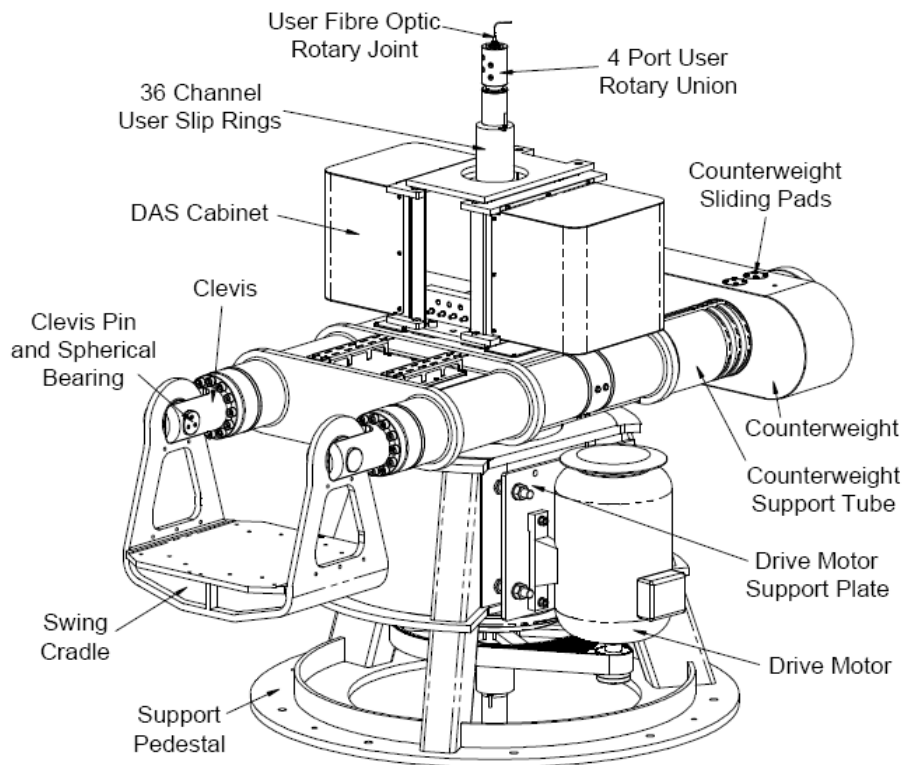


Figure 3.4 - NCG centrifuge components

3.3.2 In-flight digital image processing

Technical specification

Two digital cameras capable of recording low resolution video and high resolution digital still images were mounted on the centrifuge swinging platform and the model package. The technical specification of the digital cameras, and relevant settings used in the tests are described in Table 3.4. The cameras were controlled in real-time from a PC in the centrifuge control room using a direct USB connection via the slip rings.

Table 3.4 - Technical specification of the digital still camera in a test

Performance criteria	Specification
Camera Model Name	Canon PowerShot S70
Dimensions	114 × 57 × 39 mm
Resolution	3072 × 2304 pixels (7.1 megapixels)
Lens	5.8 – 20.7 mm
Focal length	8.6 mm (range: 28 – 100 mm)
Movie clips	640 × 480 pixels
Shooting mode	Aperture- priority AE
Shutter speed	1.0 sec (as required to give correct exposure)
Av (Aperture value)	8.0 (chosen to give ‘robust’ focus at g)
Light metering	Spot (centre or linked to focusing frame)
Exposure compensation	+ 2/3
Sensitivity (ISO Speed)	ISO 50
AF mode	Single AF
Drive mode	Single-frame shooting
Other features	PC-controlled shooting via USB

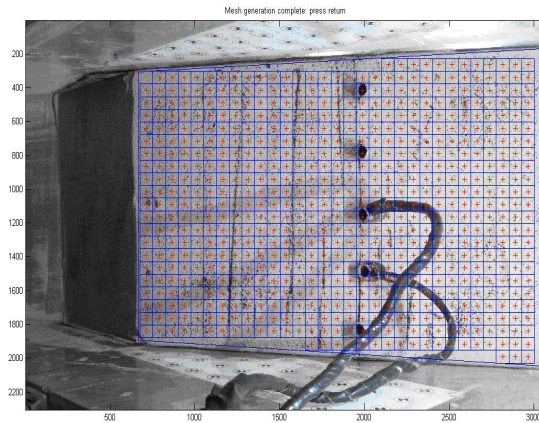
Artificial visual ‘textures’ consisting of latex sprayed with dots or dyed sand were used on the front face of the test model and on the exposed slope surface respectively. A sequence of digital images of these textures was used to infer ground movements using a digital image processing method based on particle image velocimetry (PIV). The theoretical background and details of this technique were discussed by White et al. (2003).

PIV analysis procedure

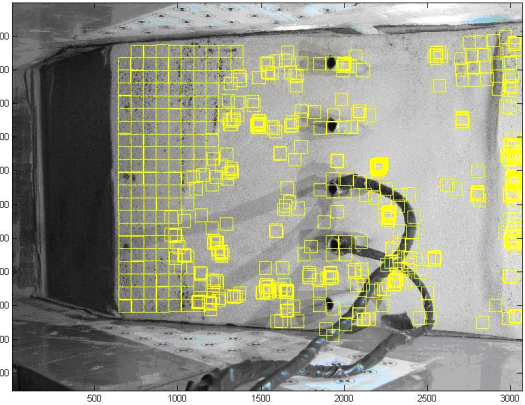
Digital image processing based on PIV was carried out by the following steps:

1. A sequence of digital images was taken during a test.
2. A mesh of test ‘patches’, of size 75×75 pixels, was generated in the first image to be analysed (Figure 3.5(a)).
3. A ‘template launch file’ which includes the images to be analysed, analysis parameters to use, and location of the initial mesh of patches was set up.
4. GeoPIV (programmed in Matlab, and supplied by White et al), tracked the displacement of test patches for each consecutive image pair and created text files, see Figure 3.5(b). Texture has been lost over quite a large area of the slope face at the end of the test due to shallow slope movement. However, more patches could be tracked earlier in the test, and the upper portion of the slope and the piles can still be tracked at the end.
5. Unnecessary ‘wild’ (erratic or erroneous) displacement vectors were eliminated.
6. Control point positions (known locations in object space) were defined on the first image (Figure 3.5(c)).
7. Step (2) – (5) was repeated.
8. Position and movements of the camera during a test were determined using Euler’s angle formula, focal length, and reference point locations.
9. The programme converted the displacement vectors in image space (pixel coordinates) into object space (XYZ coordinates)

10. Contour plots of the displacement vectors between successive images were generated and average values of the vectors were displayed (Figure 3.5(d)).



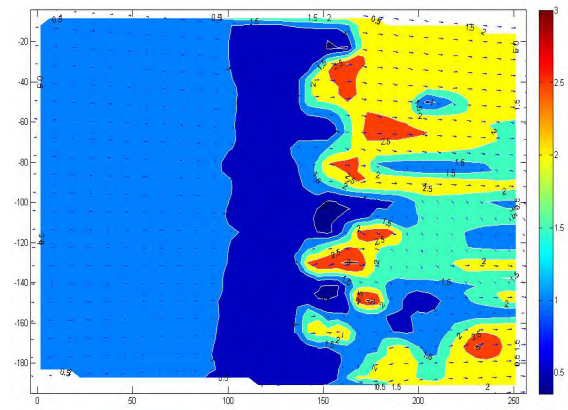
(a) Initial test mesh, of size 75×75 pixels



(b) Final test mesh



(c) Control point positions



(d) Contour plot at 5g

Figure 3.5 - Example of PIV analysis used in a test

3.3.3 Plane strain box

The model container (internal dimensions: 400 mm high \times 200 mm wide \times 700 mm long) is designed to simulate earth structures under plane strain conditions (Figure 3.6). The box has two end walls and flat base, a back face, and front window. The back face (40 mm thick) and two vertical side-walls (50 mm thick) of the box are made of aluminium plate with high stiffness to prevent significant lateral deformation due to earth pressure at high centrifugal acceleration. The front window is perspex 80 mm thick and allows observation of ground displacements and failure mechanisms occurring in the soil adjacent to the window.

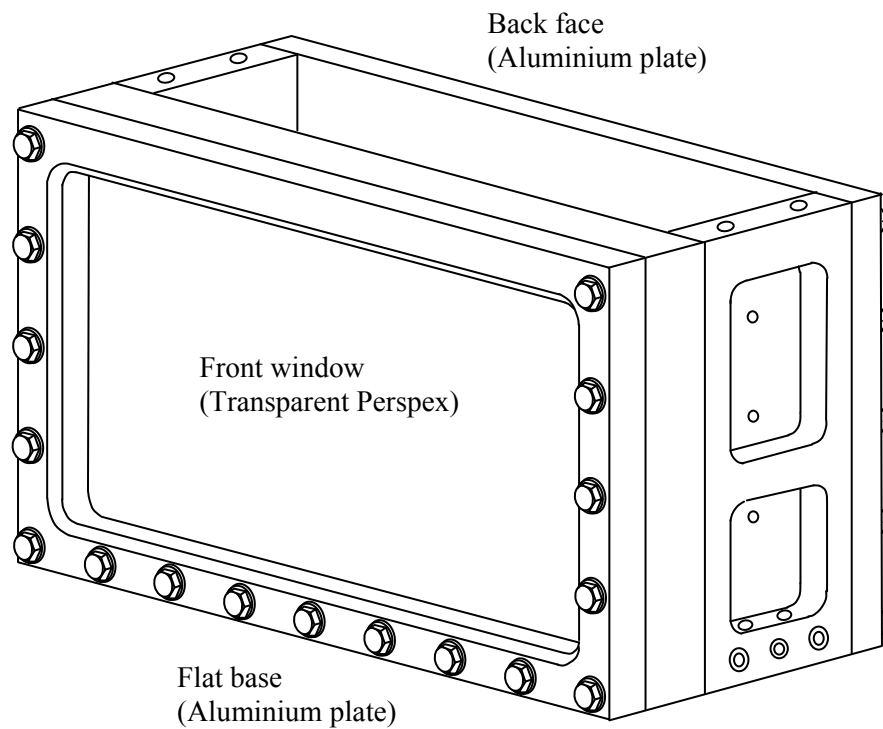


Figure 3.6 - Plane strain box components

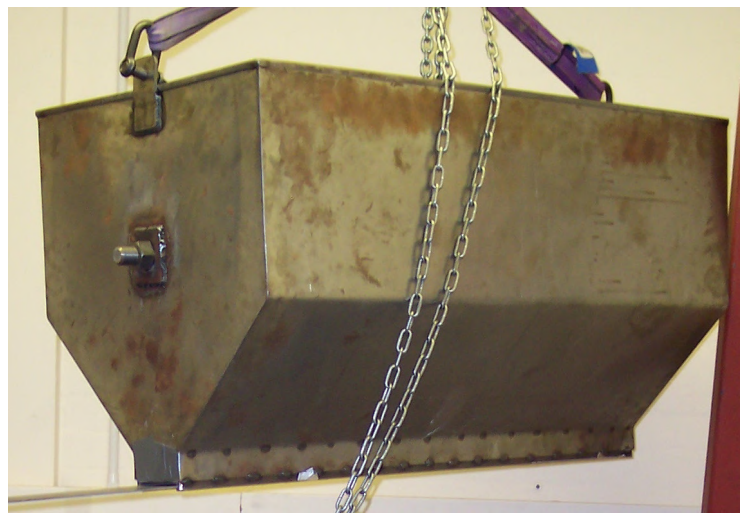
3.3.4 Sand hoppers

Spot/Line types hoppers

Two types of sand pouring hoppers ('spot' and 'line'), have been developed to construct centrifuge models at Nottingham (Figure 3.7). The apparatus enables the model soil to be constructed in a uniform and repeatable manner by means of air pluviation. A range of densities can be achieved by varying the rate and height of pluviation. The major advantages of the technique (compared to other methods such as tamping or pouring) are higher dry density, no particle crushing, less effect of segregation, and better repeatability. The technique has been verified by Takemura (1998) through cooperative experimental work undertaken in several centrifuge institutes. It was reported that almost identical dry densities of sand were achieved by spot and line type hoppers.



(a) Spot type hopper



(b) Line type hopper

Figure 3.7 - Sand hoppers

Factors controlling dry density

Factors which influence the density of air-pluviated samples are as follows:

- (1) the rate of pluviation (m , mass/time), which is controlled by the size and number of holes at the hopper outlet
- (2) travel speed of hopper (v_s) during pouring
- (3) height of free fall from the hopper to the surface which the soil particles ultimately land on

It is generally accepted that the density of the resulting model soil reduces as m increases. Increasing h increases density up to the point where the particles reach their terminal velocity during free-fall.

The thickness of a sand layer deposited by a single ‘pass’ of the hopper, t , has been derived by Equation (3.1). This value can be normalised by dividing by the mean particle size d_{50} of the soil.

$$t = \frac{m}{\rho v_s b} \quad (3.1)$$

where,

- t = thickness of layer (mm)
- m = pouring rate (g/sec)
- ρ = dry density of soil in model (g/ mm³)
- b = width of deposition for hopper pass (normal to direction of travel) (mm)
- v_s = travel velocity of hopper (mm/sec)

The relationship between the normalised thickness of a layer (t/d_{50}) and the achievable relative density ($(e_{\max} - e)/(e_{\max} - e_{\min})$) as derived in preliminary tests is shown in Figure 3.8.

The relative density becomes greater as the thickness of the layer decreases, showing a good

consistency for all data. This can be logically attributed to the argument that each layer is compacted by the impact of the subsequent layer, and it is accepted that thin layers are more readily compacted. The data (except for some of Test 5) was attained at drop height of 0.5 m for different pouring rates (m) and/or travel velocity of hopper (v_s). Some of the data (in Test 5) shows drop height of 1.0 m, which was sufficiently high that there was no increase in density for increased drop height.

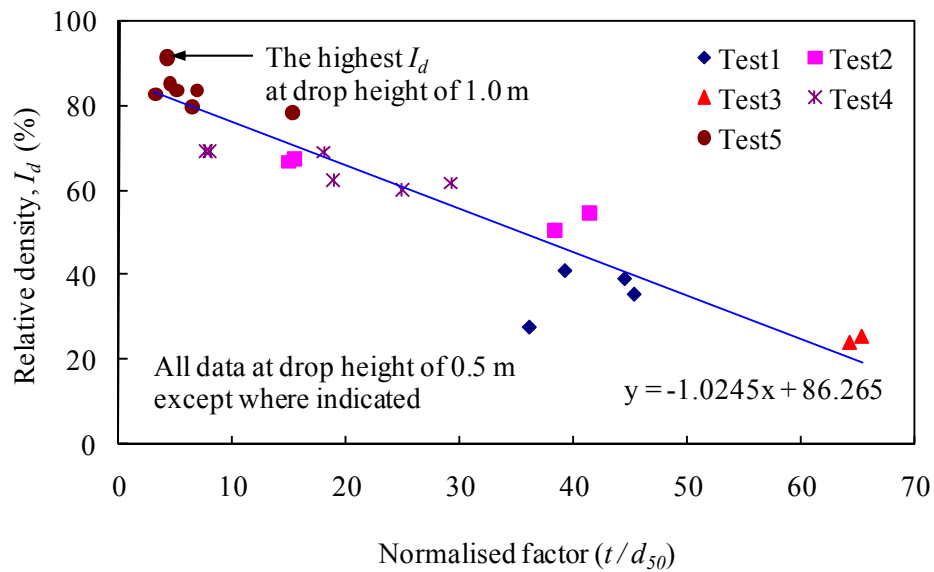


Figure 3.8 - Variation of relative density with thickness of layer for each pass of the hopper.

3.4 Test material: Leighton Buzzard sand

3.4.1 Engineering behaviour of granular soils

For granular soils which are not cemented, the strength is often assumed to be entirely frictional, with zero cohesion intercept. However, the failure envelope of peak strength for a dense soil usually has some curvature at low mean effective stress due to the transient effect of dilation which enhances strength. This feature can have significant implications in a reduced scale model, where confining stresses are small and hence the peak strength of the soil is unrepresentatively high – the use of centrifuge testing to overcome this has been discussed above.

3.4.2 Test soil property

Standard classification, particle density and limiting density tests were undertaken according to BS1377. Details of triaxial testing to determine the strength parameters are given below. Results are shown in Table 3.5.

Table 3.5 - Properties of Fraction E Leighton Buzzard sand

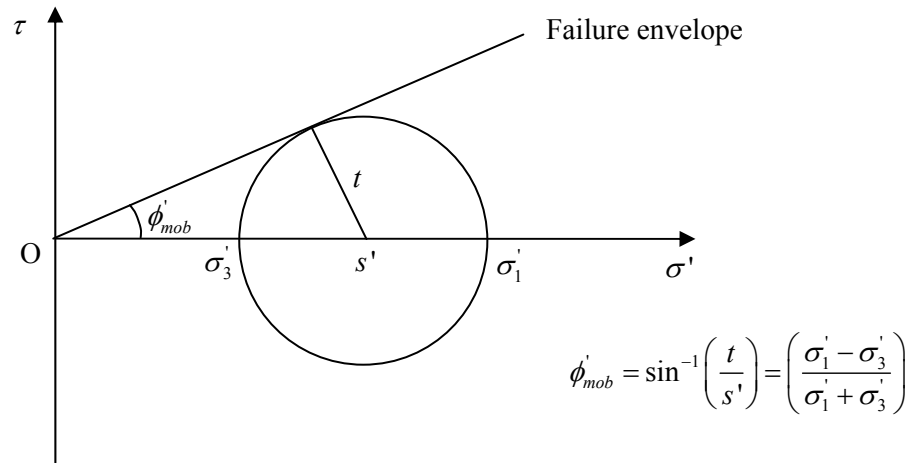
D_{10} (mm)	D_{30} (mm)	D_{50} (mm)	C_u	C_z	G_s
0.091	0.105	0.12	1.43	0.93	2.65
$\rho_{s,max}$ (kN/m ³)	$\rho_{s,min}$ (kN/m ³)	e_{min}	e_{max}	ϕ'_{peak} (°)	ϕ'_{crit} (°)
16.27	13.26	0.629	1.004	41	32

Interface properties relevant to the model are reported in Section 3.6.1.

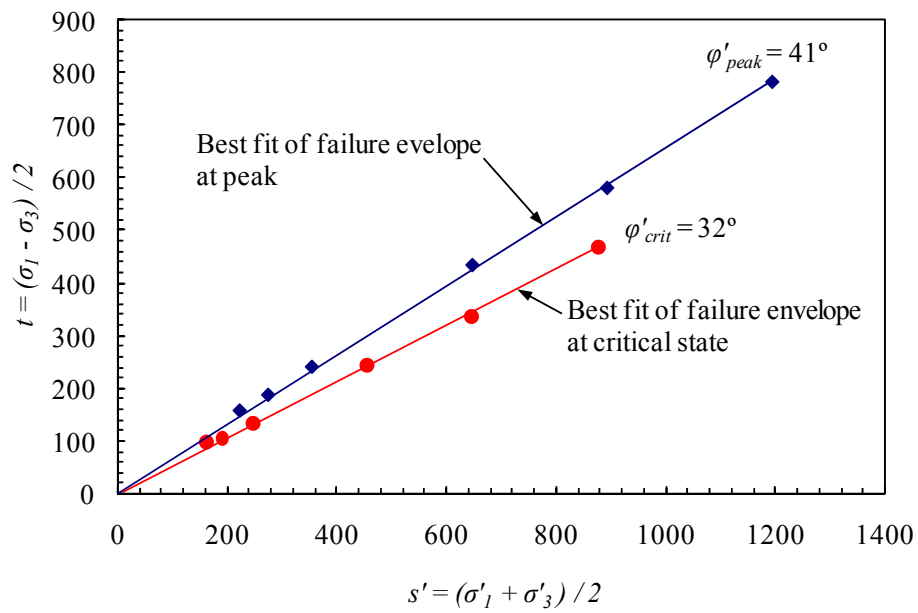
A series of drained triaxial tests on LB sand ($e = 0.69$, $I_d = 0.84$) were conducted to determine the shear strength of the test soil. The procedure is outlined below:

1. 38mm diameter test specimens were prepared by the dry tamping method in three sub-layers.
2. The test specimen was saturated under a back pressure of 300 kPa for 2 hours. The pore pressure coefficient (B) was measured and checked as being at least 95 %.
3. The fully saturated specimen was isotropically consolidated at a given mean effective pressure of 50, 80, 100, 200, 300 and 400 kN/m².
4. The sample was sheared under drained condition at a rate of 0.3 mm/min corresponding to 0.4 %/min, recording relevant data.

In the following stress analysis of a triaxial test, the sand is assumed to be a purely frictional material with a corresponding failure criterion. The state of stress is represented by drawing a series of Mohr circles on a $(\sigma' : \tau)$ plot. A mobilised angle of shearing ϕ'_{mob} corresponds to a mobilised stress ratio (τ / σ') during shearing. This is defined by a tangent to the Mohr circle which passes through the origin and expressed as $\phi'_{mob} = \sin^{-1}(t / s')$ where $t = (\sigma'_1 - \sigma'_3) / 2$ and $s' = (\sigma'_1 + \sigma'_3) / 2$ (Figure 3.9(a)). Taking the peak (maximum) and critical state ratio (τ / σ') during shearing for each test, the peak and critical state angles of shearing resistance were determined as $\phi'_{peak} = 41^\circ$ and $\phi'_{crit} = 32^\circ$ (Figure 3.9(b)).



(a) Mohr circle of effective stress for a triaxial test



(b) Derived internal friction angles at peak and at critical state

Figure 3.9 - Stress analysis of a conventional triaxial test

3.5 Centrifuge test model

3.5.1 Model slope

Plane strain section

The centrifuge model was designed to simulate the load transfer mechanism arising from passive interaction on a long row of discrete piles. The plane strain boundaries are required to be lines of symmetry along the row, and hence were at a location equivalent to the midpoint between piles in a row extending to either side of the box (Figure 3.10).

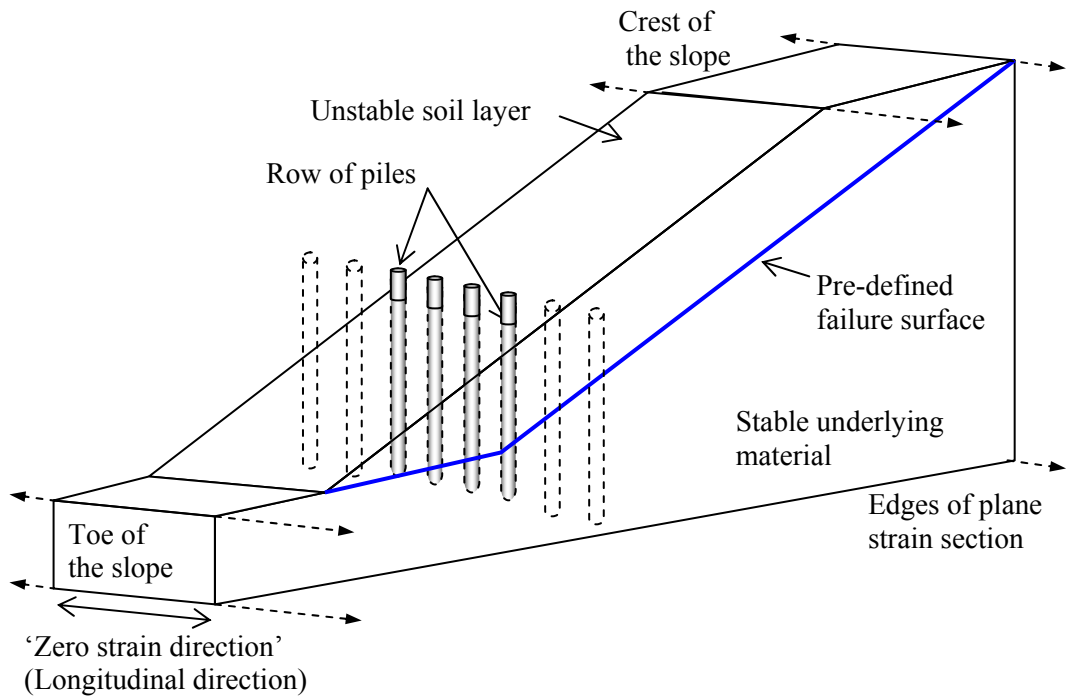


Figure 3.10 - Schematic arrangement of the test model assuming plane strain conditions

The model soil was Leighton Buzzard sand (Fraction E) pluviated through air from a line hopper. The sand is of consistent quality, and has been used extensively for geotechnical centrifuge testing in the UK. The small particle size was chosen mainly to ensure that

particle size did not have any adverse effect on interaction or interface behaviour with the piles (this will be discussed in Section 3.6.2).

An artificial interface made of 2.5mm thick aluminium sheet (on the bottom) and latex sheet (on the top) separated by silicon based grease were used to give a pre-defined failure surface at a depth of 70 mm (at model scale). Adoption of a low friction interface allowed the soil above the artificial failure surface to generate significant load on the pile row so that ‘ultimate’ interaction conditions could be observed. 25mm diameter holes in the sheet at the pile locations allowed the piles to pass through the interface and to move relative to it.

Construction technique

Components required for model construction are illustrated in Figure 3.11. The plane strain box was positioned under the line hopper inclined at an angle of approximately 30° to the horizontal. The drop height was approximately 1m at which terminal velocity was probably reached.

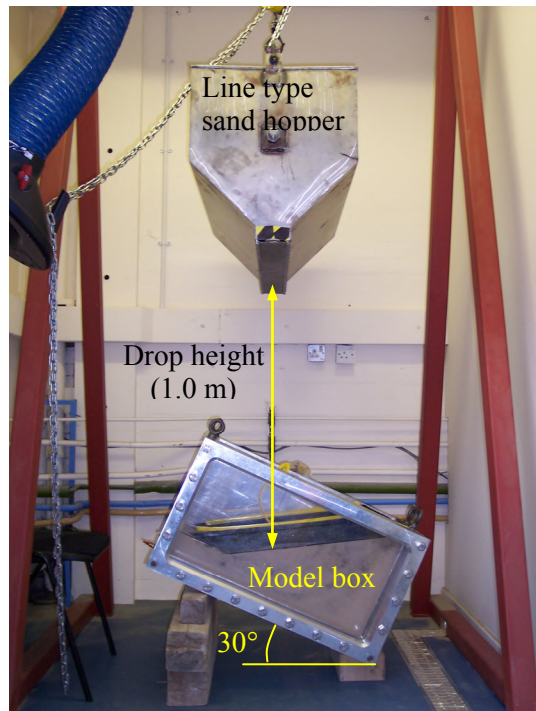
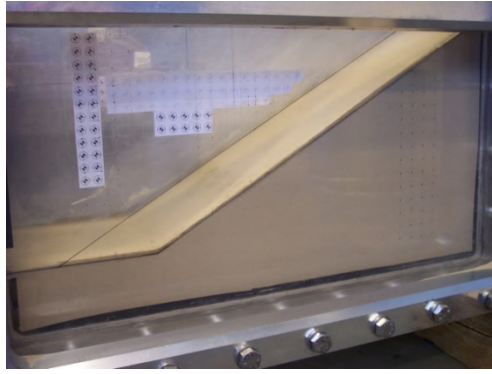


Figure 3.11 - Arrangement of the model construction components

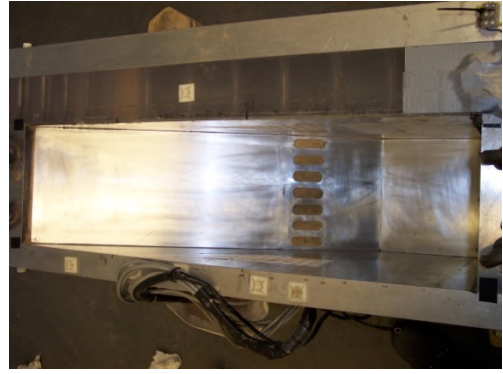
Details of model construction are summarised as following:

1. The stable underlying soil (Figure 3.12(a)) was constructed by air pluviation of sand to a required depth from a constant drop height. The hopper was moved at approximately constant velocity by swinging it from the gantry.
2. The exact profile of the underlying soil was ‘finished’ by hand to give the required shape and the ‘failure interface’ was inserted on the underlying soil (Figure 3.12(b)).
3. Latex sheet which had been spray painted to provide visual ‘texture’ (for PIV) was applied to the front window above the slip plane (Figure 3.12(c)), and similar plain latex sheet was applied to the back face of the box (see section 3.6.1). The silicone grease used to lubricate this interface acts to hold the latex on the vertical face during model construction.
4. Model piles were embedded into the underlying (stable) soil by pushing through the holes in the failure surface interface (Figures 3.12(d) and (e)).
5. The unstable soil layer was then pluviated onto the interface with pouring rate $m = 16$ g/sec and travel velocity of hopper $v_s = 260$ mm/s for width $b = 198$ mm. The finished slope was trimmed to the desired geometry (Figures 3.12(f) and (g)).
6. Dyed sand was sprinkled over the slope surface to provide PIV texture (Figure 3.12(h)).

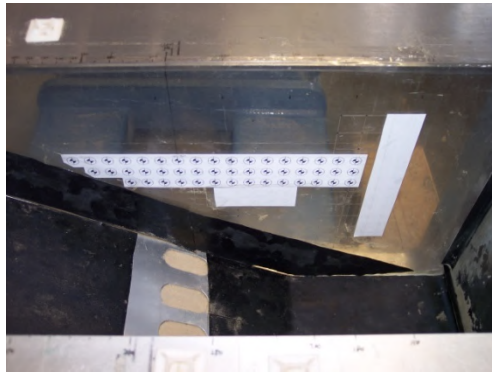
The relative density (I_D) and the void ratio (e) of the unstable layer and the stable material, as calculated in each test from the dry density of the resulting models using $G_s = 2.64$, $e_{\max} = 1.004$, and $e_{\min} = 0.629$ are summarised in Table 3.6. It can be seen that the relative density was consistently in the range 70 to 80 %.



(a) Stable granular material



(b) Interface installation



(c) Control points and Latex installation



(d) Model pile installation



(e) Model without the upper soil layer



(f) Upper soil layer construction



(g) Upper soil layer without texture



(h) Complete upper soil layer with texture

Figure 3.12 - Test model construction procedures

Table 3.6 - Summary of unstable layer and stable material

Test	Unstable layer			Stable material		
	γ_d (kN/m ³)	e	I_D (%)	γ_d (kN/m ³)	e	I_D (%)
BSY11A	15.42	0.72	76	15.38	0.72	75
BSY11C	15.38	0.72	75	15.38	0.72	75
BSY12A	15.50	0.71	78	15.33	0.73	73
BSY12B	15.33	0.73	73	15.33	0.73	73
BSY12C	15.38	0.72	75	15.33	0.73	73
BSY12D	15.38	0.72	75	15.33	0.73	73
BSY13A	15.38	0.72	75	15.41	0.72	76
BSY13B	15.50	0.71	78	15.41	0.72	76
BSY13C	15.53	0.71	79	15.41	0.72	76
BSY13D	15.55	0.70	80	15.50	0.71	78
BSY13E	15.53	0.71	79	15.50	0.71	78
BSY13F	15.50	0.71	78	15.50	0.71	78
BSY14A	15.36	0.73	74	15.41	0.72	76
BSY14B	15.26	0.74	71	15.41	0.72	76
BSY14C	15.31	0.73	73	15.41	0.72	76
BSY14D	15.26	0.74	71	15.31	0.73	73
BSY14G	15.41	0.72	76	15.31	0.73	73
BSY15A	15.26	0.74	71	15.36	0.73	74
BSY15B	15.55	0.70	80	15.36	0.73	74
BSY15C	15.26	0.74	71	15.36	0.73	74
BSY15D	15.31	0.73	73	15.53	0.71	79
BSY15E	15.26	0.74	71	15.53	0.71	79
BSY15F	15.50	0.71	78	15.53	0.71	79

3.5.3 Model pile

Specification

The model piles were made from 9.53mm outer diameter aluminium tube with 0.914mm wall thickness (3/8" 20 SWG). Allowing for 'heat shrink' later applied to the exterior of the pile the outer diameter was approximately 11 mm. Their embedded length was 205 mm.

The tube has second moment of inertia 226 mm^4 . Taking the Young's Modulus of aluminium as 70 kN/mm^2 this gives a flexural stiffness of $16 \text{ MNmm}^2 = 16 \text{ Nm}^2$. Taking an 'intermediate' g-level for the tests of 30g, the corresponding prototype diameter and flexural stiffness are 330 mm and 13 MNm^2 respectively. For a solid prototype pile this implies a Young's Modulus of approximately 20 GN/m^2 – an appropriate value for a cracked concrete section. The pile diameter is also reasonable since 300 or 450 mm diameter piles would routinely be used for slope stabilisation.

Pile instrumentation

One of the model piles was instrumented to measure bending moment at 10 locations through its depth using fully active strain gauge bridges. The gauges were attached to the exterior of the aluminium tube, and the 0.3mm thick wires also ran up the pile surface. The positions of the Bending Moment Transducers (BMTs) on the pile are shown in Figure 3.13. The pile length in the upper sliding layer was 70 mm, with a length of 135 mm in the lower stable material, making the total embedded length 205 mm.

The external instrumentation was protected (against damage during installation and testing) by epoxy coating and a plastic ‘heat shrink’, which increased the outer diameter of the pile to approximately 11 mm. The remaining (uninstrumented) model piles were also coated with heat shrink so that their diameter and surface properties were consistent with the instrumented pile.

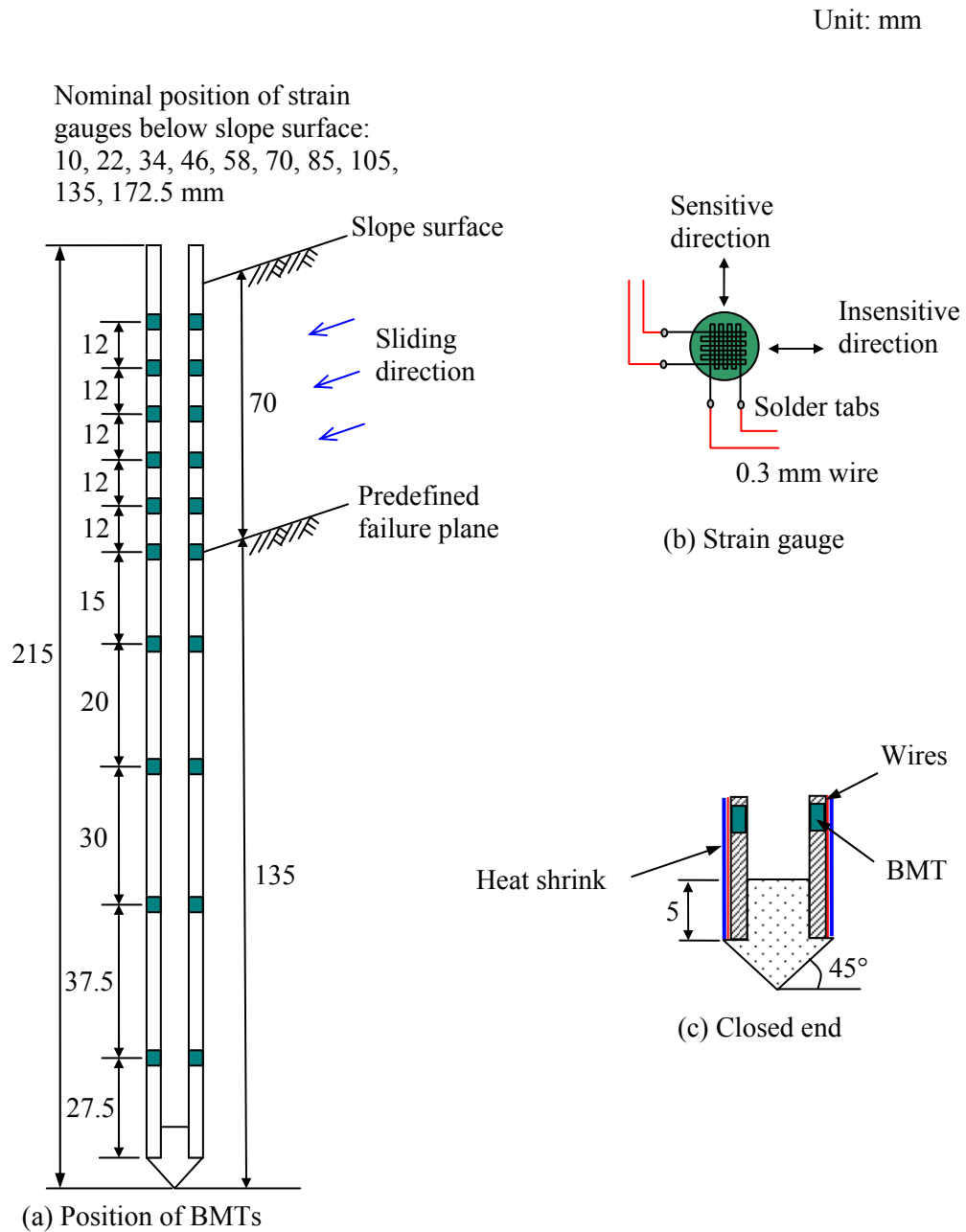


Figure 3.13 - Instrumentation of the model pile

BMTs calibration

The instrumented pile BMTs were calibrated using identical signal conditioning to that used during the test. 10V excitation was supplied to the BMTs and the magnitude of small signals produced was amplified using a gain of 250 in the signal conditioning. The top end of the pile was fixed using a clamping block. Small increments of load up to 2.5 kg were applied at the tip of the pile to cause a known bending moment at each transducer location. Calibration gave linear voltage output in response to applied bending moment, and hence the calibration coefficients for specific transducers were derived.

Pile installation

Ideally, model piles should be installed during centrifuge flight by duplicating a field construction process to give a similar stress regime around the pile. However, this is often impractical. Furthermore, a number of researchers have demonstrated that the effects of installation methods and acceleration level at the time of installation for a laterally loaded pile are less significant than for an axially loaded pile (Craig, 1984; Dyson and Randolph, 1998).

Thus the model piles were initially inserted (driven) into the stable material, and sand was pluviated around them in the sliding layer at 1 g prior to testing. Spacing between the piles for each test was carefully measured at the top and near the slip surface to ensure it was correct.

Pile roughness

As described above, the pile outer diameter consisted of plastic shrink wrap. Pile roughness can have some effect on lateral interaction with the soil (Lyndon and Pearson, 1988; Chen and Martin, 2002), tending to make it ‘stiffer’. However, Durrani (2006) showed (based on

numerical modelling) that provided the interface friction angle is greater than about $0.3 \phi'$ there was not significant effect on the ultimate interaction capacity (which consists mainly of ‘bearing’ on the piles rather than sliding at the interface). Interface friction tests between the shrink wrap and sand (Figure 3.14) indicated that the roughness was comparable to values for actual piles: precast concrete pile ($0.8 - 1.0 \phi'$) and rough steel ($0.7 - 0.9 \phi'$) as recommended by Kulhawy et al. (1991). Here the interface friction is about $0.75 \phi'$.

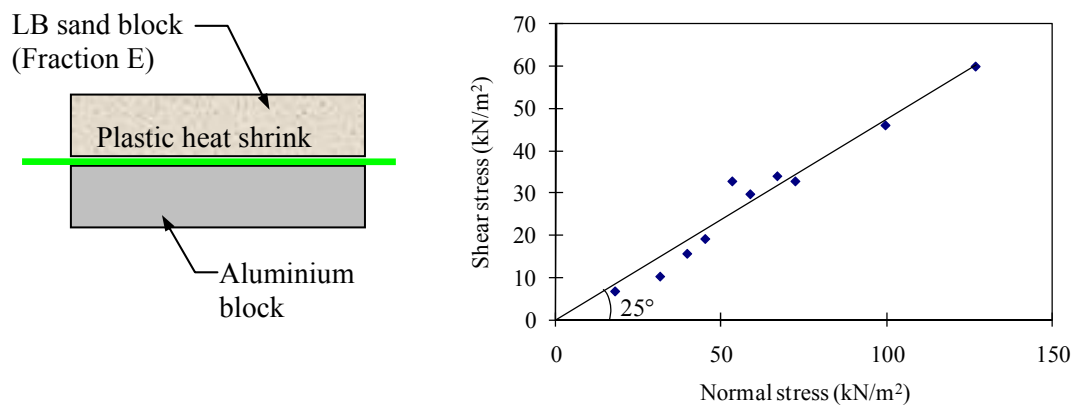


Figure 3.14 - Friction angle of interface between soil and pile

3.6 Modelling considerations

3.6.1 Boundary effects

The fundamental assumption of plane strain conditions in centrifuge modelling in principle requires that there is no friction at the side boundaries (normal to the zero strain direction). In practice this requires that the friction should be reduced to a practical minimum which does not have significant effect on the overall response of the model.

Both the unstable layer above the failure surface interface and the stable material below have contact with the side boundaries of the model container. Since there would be significant movement of the unstable layer it was important that side friction was minimal here. However, since the stable material would undergo relatively little movement, and have considerably less effect on the model in general there was no particular concern regarding this interface, and no particular precaution was taken to minimise friction here.

However, a latex sheet interface was used to minimise interface friction for the unstable layer. The latex sheet is directly in contact with the soil and is used to separate it from a layer of grease trapped between the latex and the inside of the model container (Figure 3.15). This technique is routinely used in centrifuge testing (Taylor, 1995).

The latex sheet used in the study was sufficiently flexible (having a stiffness of approximately 1.0 kN/m width) that it would not restrict differential movement of the sand, which in any case would have tended to move ‘uniformly’ above the failure interface. However there was likely to be differential movement ‘upslope’ and ‘downslope’ of the pile row so two separate sheets were used on each face, overlapping but not joined at the pile row location.

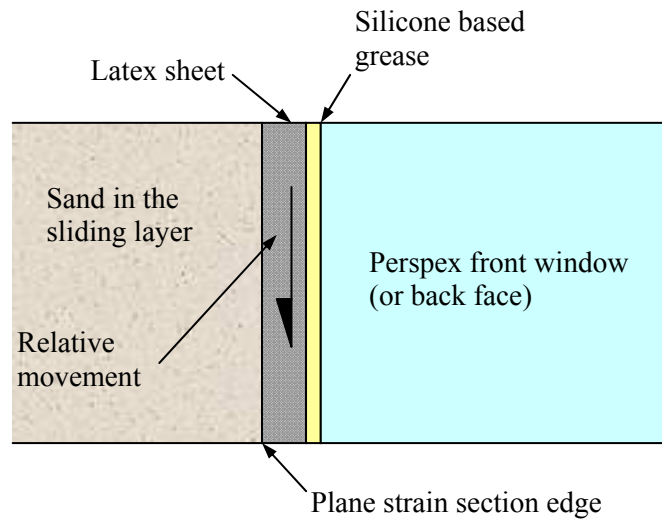


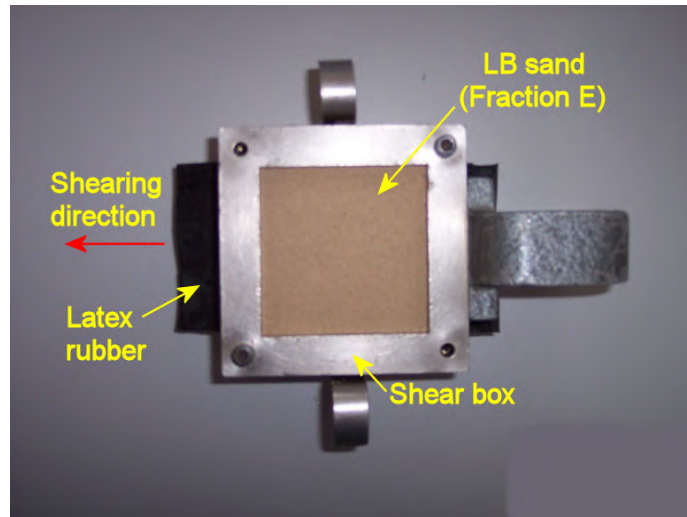
Figure 3.15 - Cross-section of side boundary lubrication at the edge of the plane strain section

A set of modified shear box tests were undertaken to investigate the friction at interfaces:

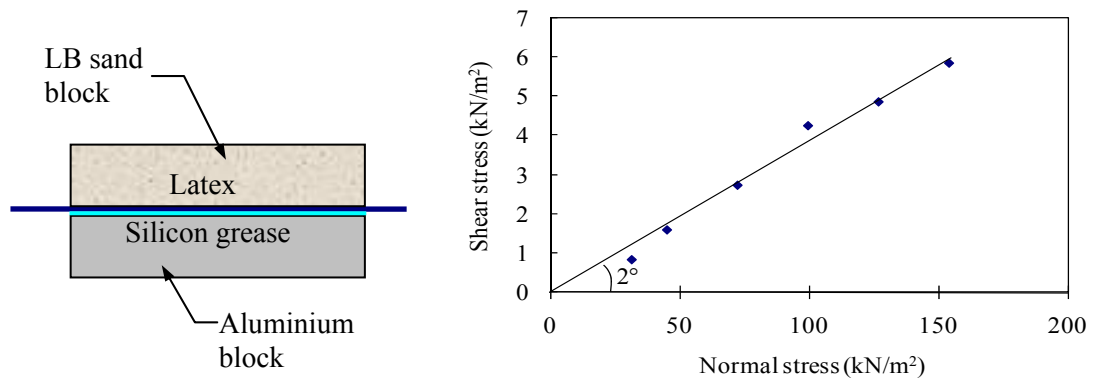
- (1) the silicone-greased latex panel/aluminium interface
- (2) a sand/aluminium interface.

The test configuration and test results are presented in Figure 3.16 (using relative density of 82 %). The results showed that the silicone-greased interface offered only 2° frictional resistance compared with up to 26° for sand/aluminium interface.

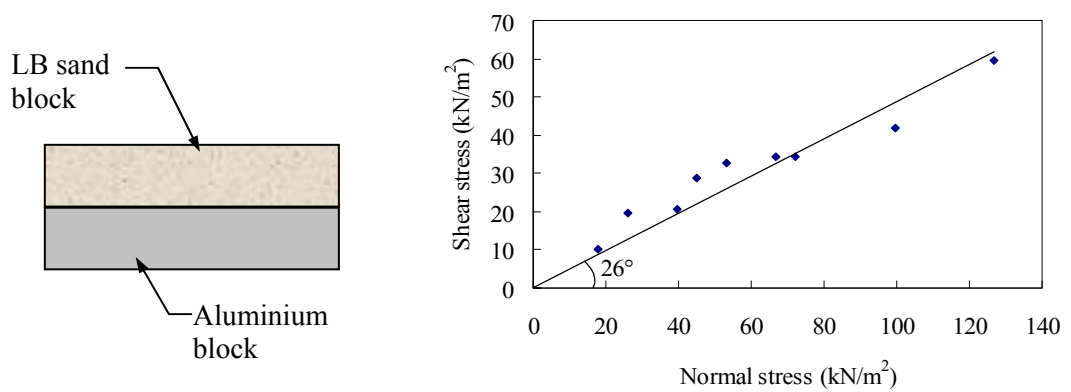
The greased latex/ aluminium interface with high stiffness was also used at the base of the unstable ground (the failure interface). The rationale for such an approach was described in Section 3.2.



(a) Modified shear box test



(b) Lubricated boundary interface



(c) Non-lubricated boundary interface

Figure 3.16 - Comparison of friction at lubricated and non-lubricated interfaces

3.6.2 Particle size effects

According to the centrifuge scaling laws, it could be argued that the typical particle size should be N times smaller in the model than in the prototype. However, it is generally accepted that the size of soil particles are not reduced in this way. It is more normal to ensure that the particles are small enough (compared to the other model components) that individual particle will not affect the continuum behaviour.

Garnier and Konig (1988) proposed that the diameter of a pile must be more than 100 times the average particle size to minimise any effect on shaft interface behaviour. In a similar study Foray et al. (1998) concluded that the model pile diameter should exceed 200 times the average grain size.

However, as noted in Section 3.5.3 lateral pile-soil interaction is more dependent on ‘bearing’ mechanisms than interface behaviour. Equivalent guidance for bearing at the end of a penetrometer (Gui & Bolton, 1998) requires a pile diameter only 20 times larger than the particle size.

The diameter of the pile and the smallest pile spacing ($= 2.5d$) used in the centrifuge tests was 90 times and 225 times larger than the d_{50} size of the sand respectively and thus it is considered extremely unlikely that there would have been any significant impact on behaviour.

3.6.3 Stress error

It is generally assumed that the gravitational acceleration field is uniform and parallel to a unique ‘vertical’ direction for structures on the earth. However, the inertial gravitational acceleration field in a centrifuge deviates slightly from this. It is therefore necessary to assess the corresponding error for given model dimensions.

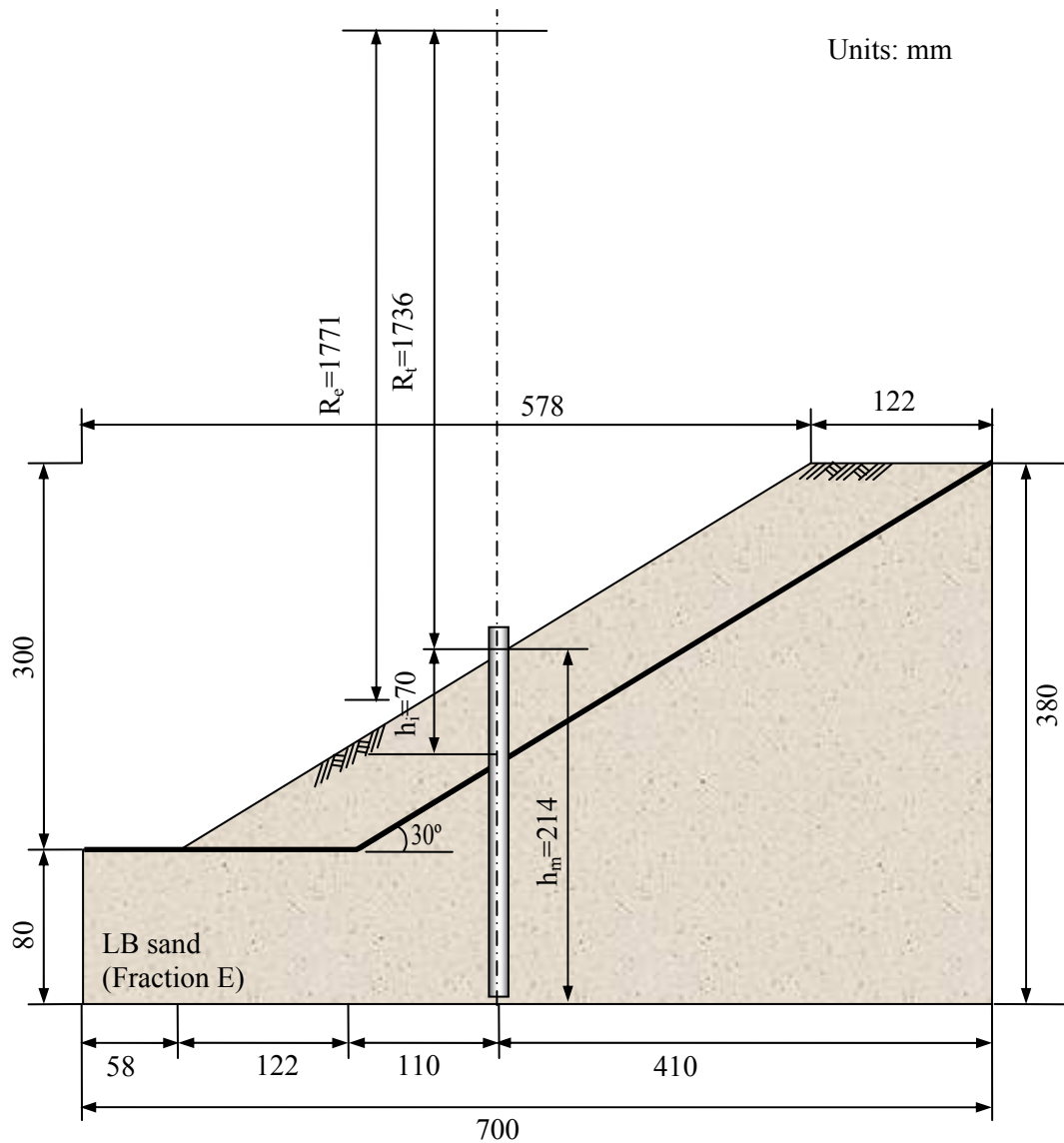


Figure 3.17 - Model dimensions for stress error calculation

Figure 3.17 shows specific dimensions for this study at the location of the pile row. The inertial acceleration increases proportionally with radius (depth) in a centrifuge model. Thus the profile of vertical stress with depth is slightly curved as shown in Figure 3.18 (for a soil density of 1552 kg/m^3 , and rotational speed of 16.6 rad/s corresponding to 50 g at a radius of 1.77 m). At the point of maximum under-stress the error compared to the ideal linear prototype distribution is 1% . At the failure plane the stress is correct, and at the base of the model the maximum over-stress is 4% - however, behaviour at smaller depths is of considerably more interest. The percentage errors are tolerably small (and independent of g -level).

The second error of the inertial field is that it always acts in a radial direction, and thus is inclined to the ‘vertical’ sides of the box. The maximum inclination in these tests is approximately 10° at the sides, but reducing to zero at the centre of the model (where the most critical model components are situated).

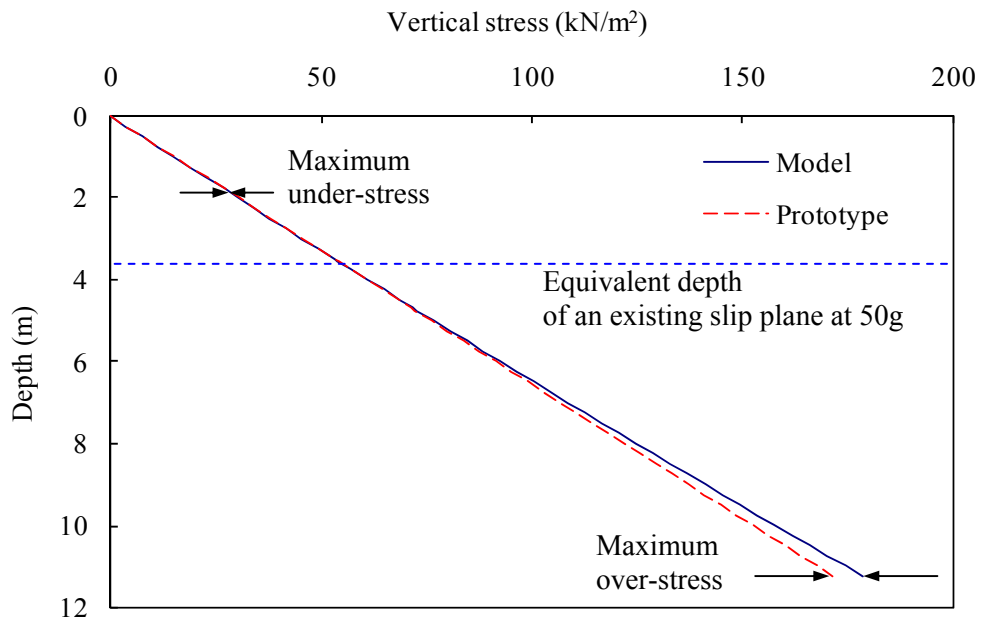
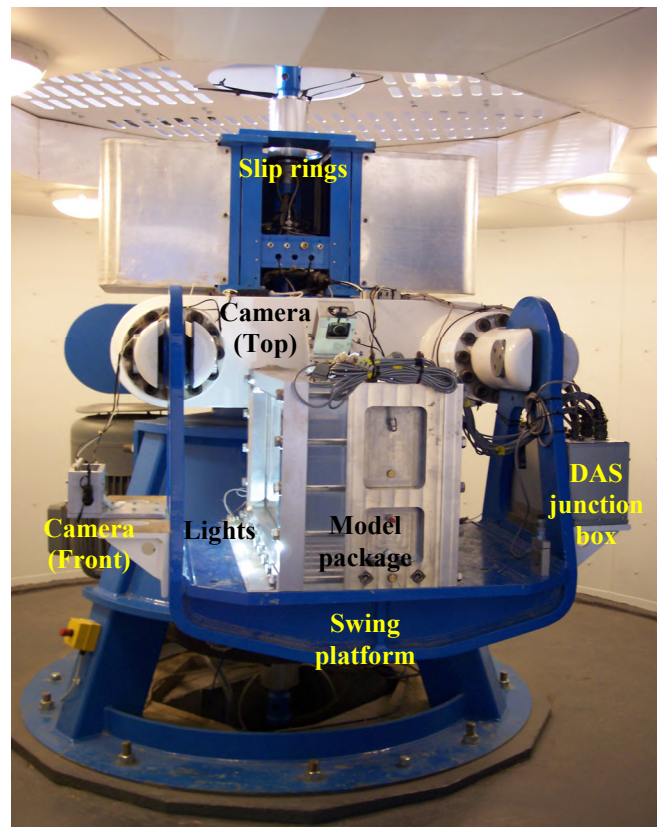


Figure 3.18 - Vertical stress distributions with depth in the centrifuge model at $50g$ and corresponding prototype

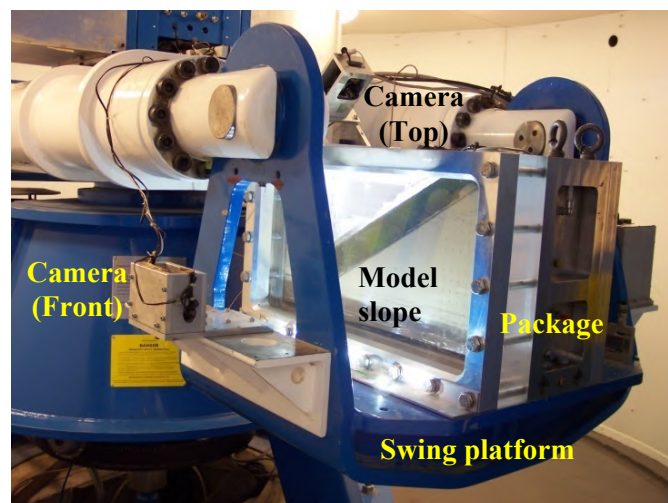
3.7 Test procedure

After completing preparation of a test model (as explained above) the test package was secured to the swinging platform (Figure 3.19), and the instrumentation was connected to the DAS and checked. Two cameras were also mounted on the swinging platform and on the test package.

During the test centrifugal acceleration was increased gradually in 1 g increment from 5 g to 16 g. After that, increments of 2 g from 16 g to 30 g, and then 4 g increments from 30 g to 50 g. A sequence of images was taken using the two digital cameras at every gravity increment.



(a) Arrangement of test



(b) Complete test package on the centrifuge swing

Figure 3.19 - Complete arrangement of a test package in the centrifuge

3.8 Summary

Geotechnical centrifuge modelling is widely recognised to approximately replicate a stress regime corresponding to an equivalent prototype in laboratory simulation. A centrifuge model conventionally considers a specific prototype, and is subjected to the relevant scaling relationship.

The NCG Geotechnical centrifuge is a typical medium-size beam centrifuge with 2.0 m platform radius and a payload capacity of 500 kg at 1.7 m nominal radius up to 100 g. An advanced control and data acquisition system, and in-flight digital photography are available.

The centrifuge model used represents an unstable frictional slope that is inclined at 30° to the horizontal. A prescribed translational slip (with very low resistance) at 70 mm depth (model scale) was used to generate loading on a pile row. The model piles (3/8" 20 SWG aluminium tube) were installed in a row at discrete intervals across the slope, penetrating through the unstable layer into stable underlying material. Plane strain was assumed (except for the pile row). The model soil was Leighton Buzzard Sand (Fraction E), and a silicon-greased aluminium sheet was used for the slip interface. One model pile was instrumented to measure bending moment with 10 BMTs along the pile length.

The modelling focused on pile-soil interaction in the unstable ground rather than the slope stability of a specific prototype. The test programme was therefore established based on factors affecting this mechanism:

- (1) the ratio of the upslope length to the thickness of sliding soil ground (l/h)
- (2) the normalised centre to centre pile spacing along the row (s/d).

The centrifuge test results will be presented in Chapter 4.

CHAPTER 4

CENTRIFUGE MODELLING: TEST DATA

4.1 Introduction

This chapter presents the centrifuge test data, with some analysis and discussion of the results. Further discussion and analysis are given in Chapter 5.

4.1.1 Note on data presentation

General

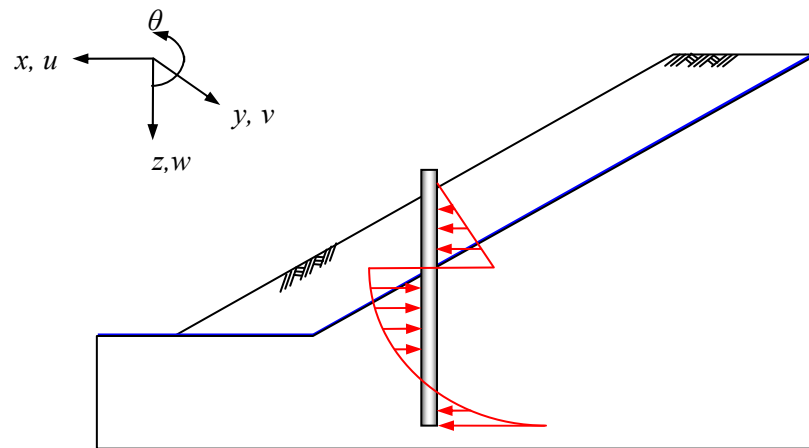
In the present study, the centrifuge test model used focused on investigating the fundamental understanding of passive stabilisation behaviour rather than considering a specific prototype. Thus some of the data are discussed based on the centrifuge model at model scale, or in ‘normalised’ terms in order to eliminate scaling effects.

Some of the data is presented either at a specific point in time for a particular g -level, or as a continuous record of a particular variable with time (and g -level, which varied with time throughout the test).

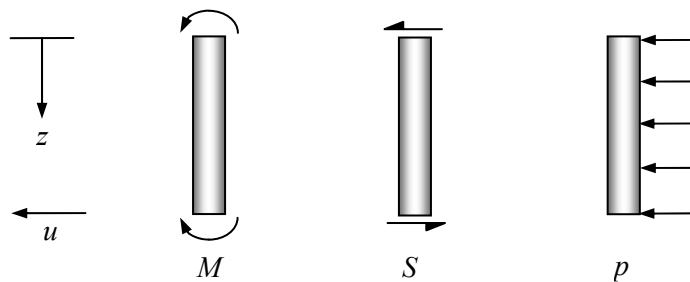
Sign conventions

Figure 4.1 shows general sign conventions and notation for position, displacements and loading in the test. In Figure 4.1(a) positions of test components are denoted using xyz -coordinates (see Chapter 3), and pile and soil displacements use the u -coordinates (v is the zero strain direction). Rotation (θ) is positive in the anticlockwise sense.

The convention for bending moment (M), shear force (S), and pressure (p) acting on the pile are shown in Figure 4.1(b). The sign convention for the bending moment diagram is that compression on the downslope face of the pile is positive. The pressure is positive when the net lateral pressure on the pile acts downslope.



(a) Coordinate system and displacements



(b) Positive sign conventions for bending moment, shear force, and pressure

Figure 4.1 - General notation and conventions for position, displacement and loading

4.1.2 Structure of the chapter

Figure 4.2 illustrates the various geometries used in the tests in terms of the length of the upslope section compared to its thickness (l/h) (Figure 3.2) and centre-to-centre pile spacing compared to the pile diameter (s/d). Table 3.3 also showed this information. Examples having quite different (l/h) and (s/d) (Figure 4.2) have been selected to provide insight into the general behaviour of passive loading in sections 4.2 and 4.3:

- 4.2 Ground and pile movement data (based on PIV analysis)
- 4.3 Pile data (based on analysis of moment data and PIV analysis)
- 4.4 Summary

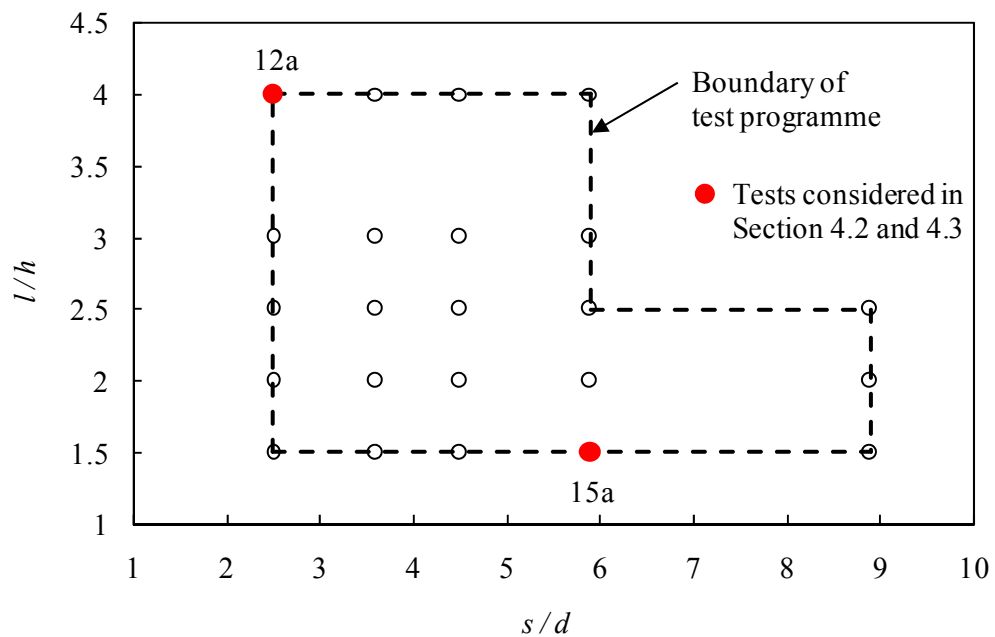


Figure 4.2 - Selection of representative examples (BSY12a and BSY15a)

4.2 Ground and pile movement data

In-flight photography and digital imaging processing (based on PIV analysis) were used to monitor and deduce movements of the unstable soil mass in the cross sectional plane and on the ‘face’ of the slope during a test. Results from two tests (Figure 4.2) will be considered below.

4.2.1 Displacements in the cross sectional plane

Displacement profiles of the unstable soil layer in the ‘exposed’ cross sectional plane were deduced via PIV analysis of latex sprayed with a ‘texture’, as viewed through the transparent front window of the model at elevated g -level during the test. Separate pieces of latex were used upslope and downslope of the pile row to allow discontinuity of displacement here if there was a tendency for this to occur.

A sequence of images for BSY12a ($(s/d) = 2.5$, and $(l/h) = 4.0$) were taken from a digital camera mounted on the swing platform at 1, 10, 20, and 30 g (Figure 4.3). The predefined failure interface is at 70 mm depth below the surface of the slope at model scale. The movement of the slope in the plane strain direction is zero at the window interface, which represents a line of symmetry in terms of pile-soil-pile interaction along the row.

Figure 4.3 shows images taken for processing. The unstable layer is clearly distinguished by the black latex used at the edge of this layer adjacent to the window (a similar arrangement was used at the interface with the inside back face of the box). The position of the pile row is shown by a dotted yellow line.

Without PIV analysis it was hard to identify typical deformation characteristics. Nevertheless two features can be observed (referring to Figure 4.3(e)): (1) separation of the upslope and downslope latex panels at the pile row location, and (2) bulging of the toe of the slope downslope of the pile row. At the end of the test, a ‘passive wedge’ mechanism can be seen immediately upslope of the pile row as indicated in red – further discussion of this will be given later.

Figure 4.4 shows a series of contour plots of soil displacement in the downslope direction derived after PIV analysis, corresponding to the images in Figure 4.3. As anticipated the unstable soil layer tends to slide downwards along the predefined interface, and significant soil movements (up to 40 mm) are observed downslope of the piles. Movement upslope of the piles is considerably restrained by the pile row.

A ‘passive wedge’ developed above the pile row can be identified in the PIV analysis (Figure 4.4(c)). Displacement of the soil immediately behind the pile row is relatively small, but it is higher at the crest. This implies two aspects of behaviour:

1. Restraint of soil immediately behind the pile row. Since the soil is loading the pile row there is analogy with a ‘passive wedge’
2. Increasing possibility of a potential slip upslope of the passive wedge which does not interact with the pile row

The upward bulge immediately behind the pile row in Figure 4.3(e) supports both these hypotheses, and the mechanisms potentially ‘interact’ since the bulge could either be attributed to the passive wedge, or a ‘toe bulge’ for the upslope mechanism.

This kind of failure mechanism tended to develop with an increase of (l/h) for a given (s/d) and decrease of (s/d) for a given (l/h) . The former increases the probability of a mechanism

upslope of the piles, whilst the latter implies greater resistance from the pile row corresponding to the passive wedge loading the row.

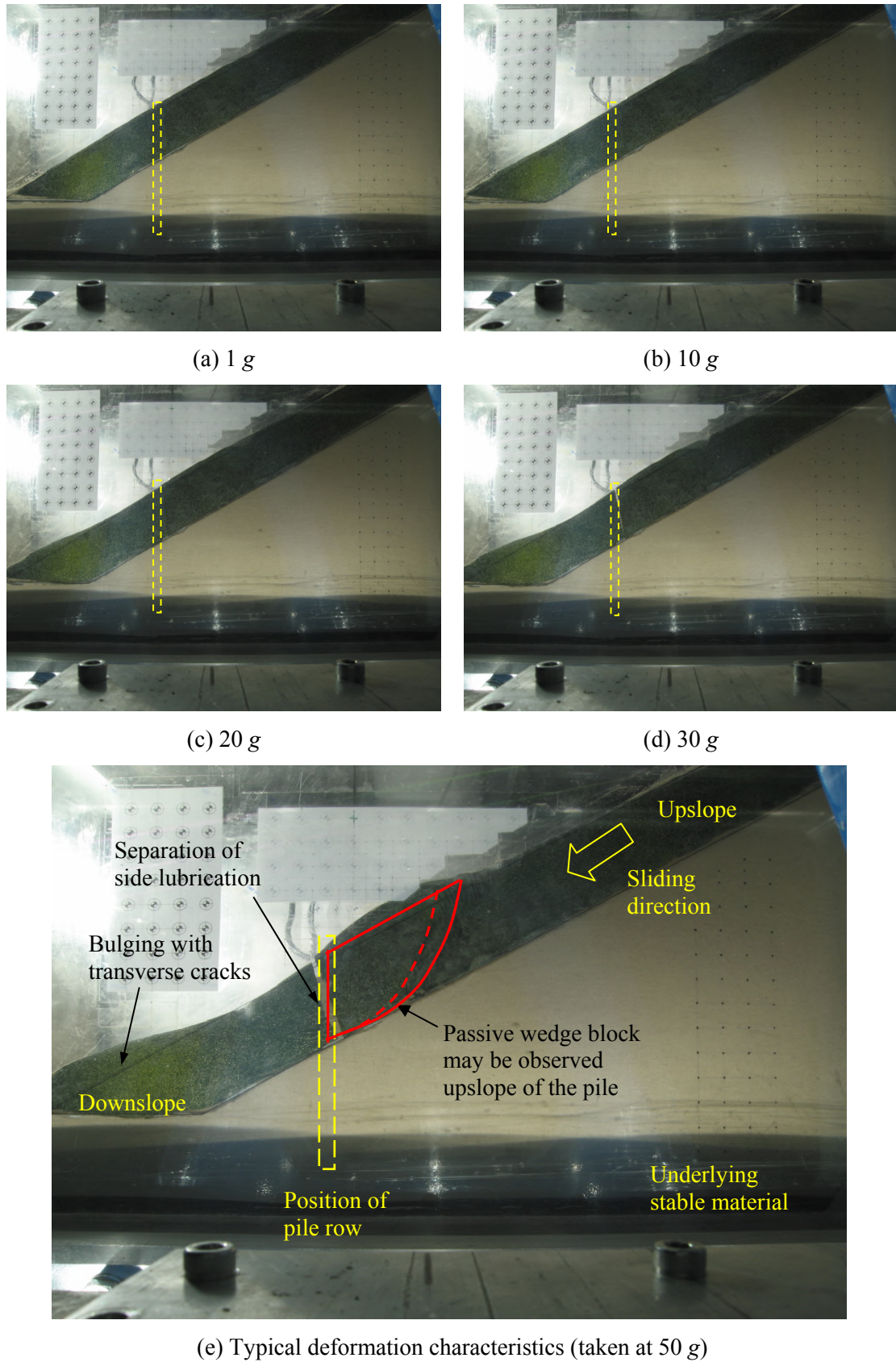
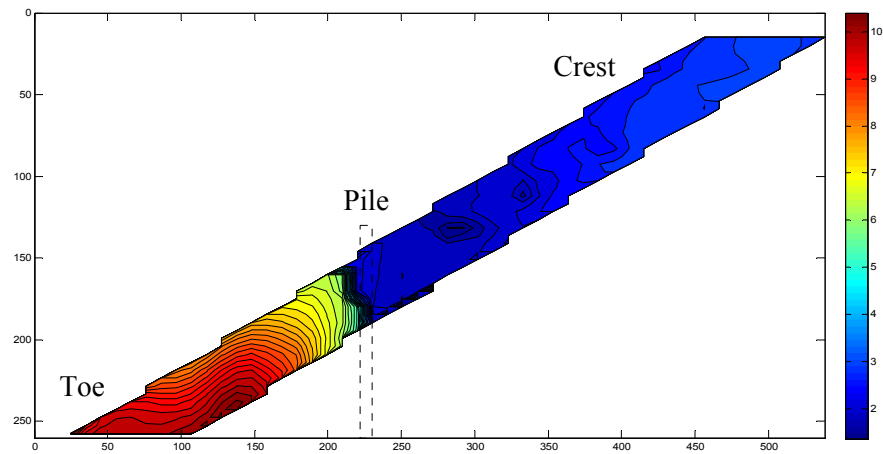
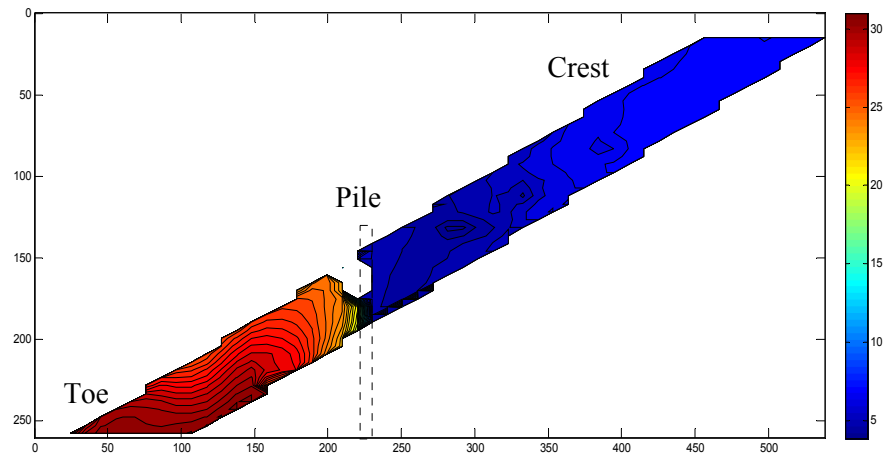


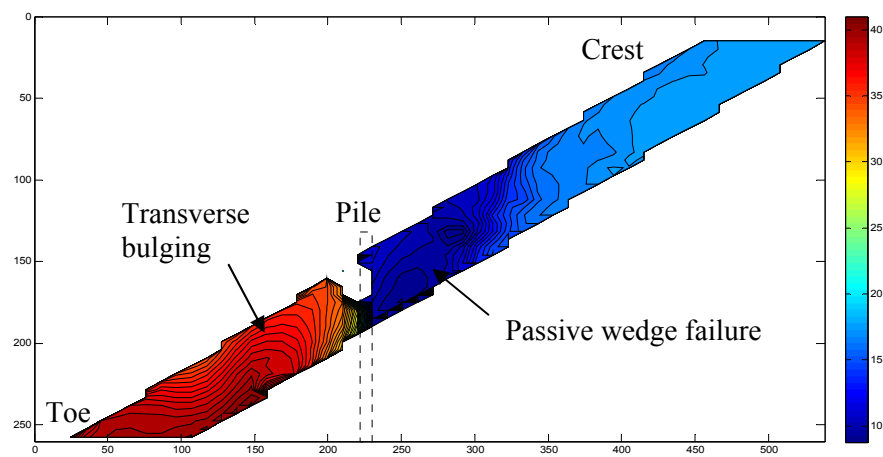
Figure 4.3 - Example of the cross sectional plane view for BSY12a ($(s/d) = 2.5$, $(l/h) = 4.0$)



(a) 1 to 10 g



(b) 1 to 20 g



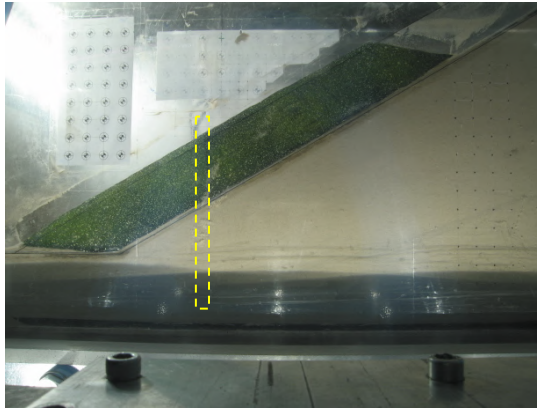
(c) 1 to 30 g

Figure 4.4 - Contours of downslope movement (mm at model scale) for BSY12a ($(s/d) = 2.5$, $(l/h) = 4.0$)

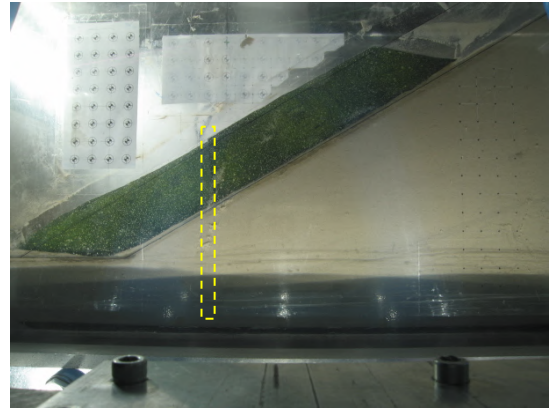
Figure 4.5 and Figure 4.6 show equivalent images and contours for BSY15a ($(s/d) = 5.9$, $(l/h) = 1.5$). Note that the unstable layer does not extend to the top of the interface since $(l/h) = 1.5 < 4$. In fact the latex panel extends beyond the top of the unstable sand layer, and thus it misleadingly appears that (l/h) is somewhat greater than 1.5. The results are generally similar to BSY12a, except that there is no significant evidence of a ‘passive wedge’ upslope of the pile row at 30g.

Figure 4.6 illustrates the upslope movement derived from images taken in the cross sectional plane with increase of g -level. Generally speaking the upslope displacement tends to increase with (s/d) for a given (l/h) , and for a given (s/d) displacement tends to increase with (l/h) . This is a reasonable trend of behaviour, as would be anticipated.

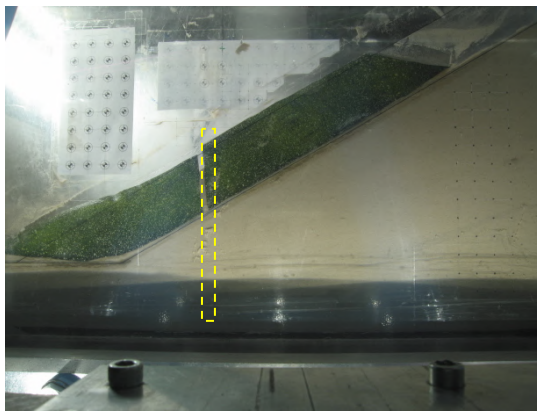
In summary, the ground movements in the cross sectional plane are satisfactorily deduced using digital image processing (PIV analysis) on a series of images taken during a test, including some important features of ground deformation.



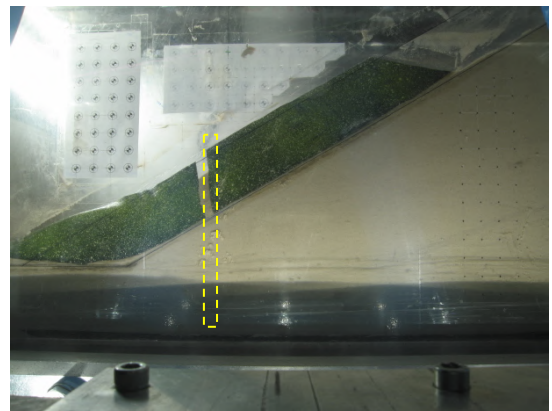
(a) 1 *g*



(b) 10 *g*

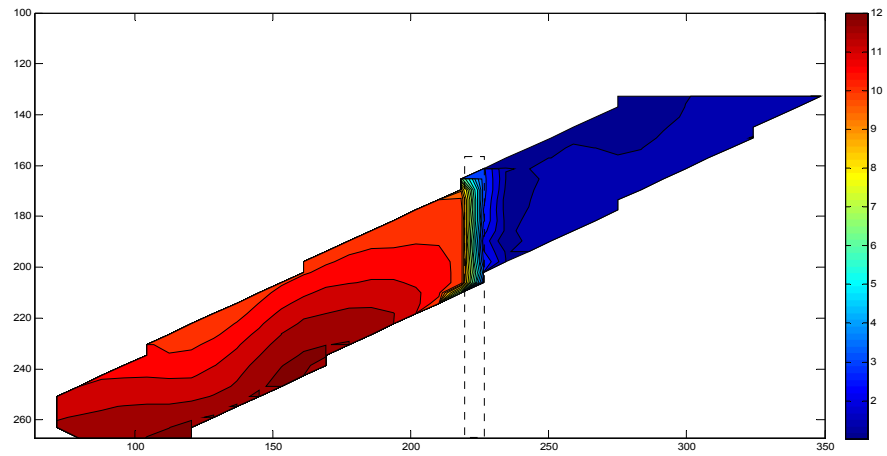


(c) 20 *g*

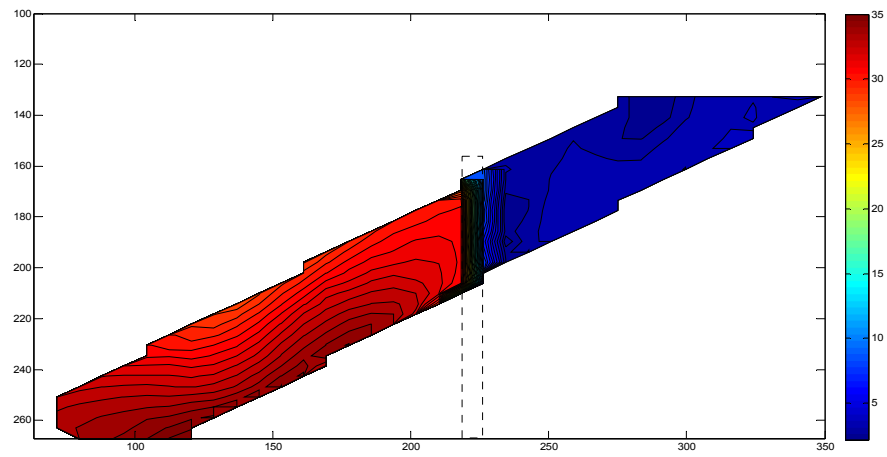


(d) 30 *g*

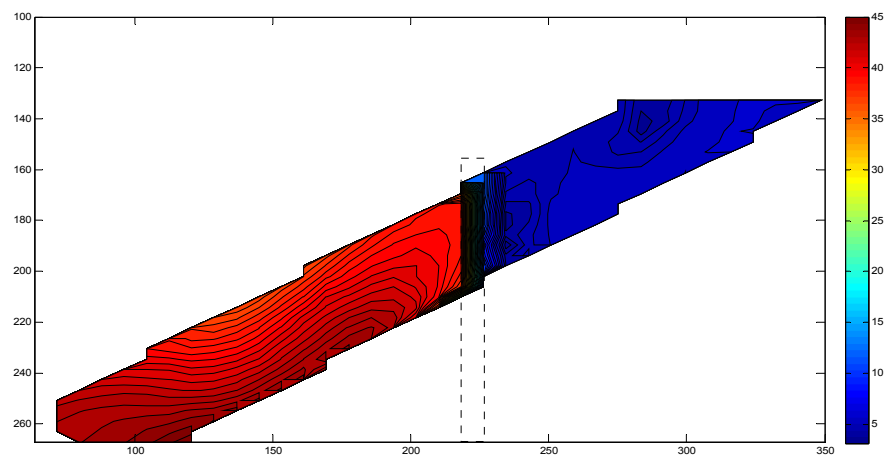
Figure 4.5 - Examples of the cross sectional plane view for BSY15a ($(s/d) = 5.9$, $(l/h) = 1.5$)



(a) 1 to 10 g



(b) 1 to 20 g



(c) 1 to 30 g

Figure 4.6 - Contours of downslope movement (mm at model scale) for BSY15a ($(s/d) = 5.9$, $(l/h) = 1.5$)

4.2.2 Movement of the slope face

Displacements of the slope surface (mainly ‘upslope’ of the pile row) were obtained by image analysis of the dyed sand texture in a view of the model approximately perpendicular to the face. Figure 4.7 shows visual observations of the unstable soil layer in BSY12a at 1, 10, 20, and 30 g. Seven piles were installed at spacing of $2.5d$, and the ratio of upslope length and sliding mass thickness was 4.0.

The bulge at the toe of the slope and passive wedge upslope of the pile row (already described in Section 4.2.1) are indicated on the figure. In Figure 4.7(d), the back of the passive wedge is clearly visible as a black line – the orientation of the lighting in the test causes a shadow along this feature.

A series of contour plots of downslope movement above the pile row at 10, 20, and 30 g (Figure 4.8) indicate some tendency for increase in movement nearer the crest (further from the piles), but deformation is fairly uniform. It was impossible to obtain reliable soil displacement data in the zone of local shallow surface failure due to significant loss of texture on the slope surface. Therefore the mean values (averaging the available displacement vectors) are used to estimate the nominal upslope displacement.



(a) 1 g



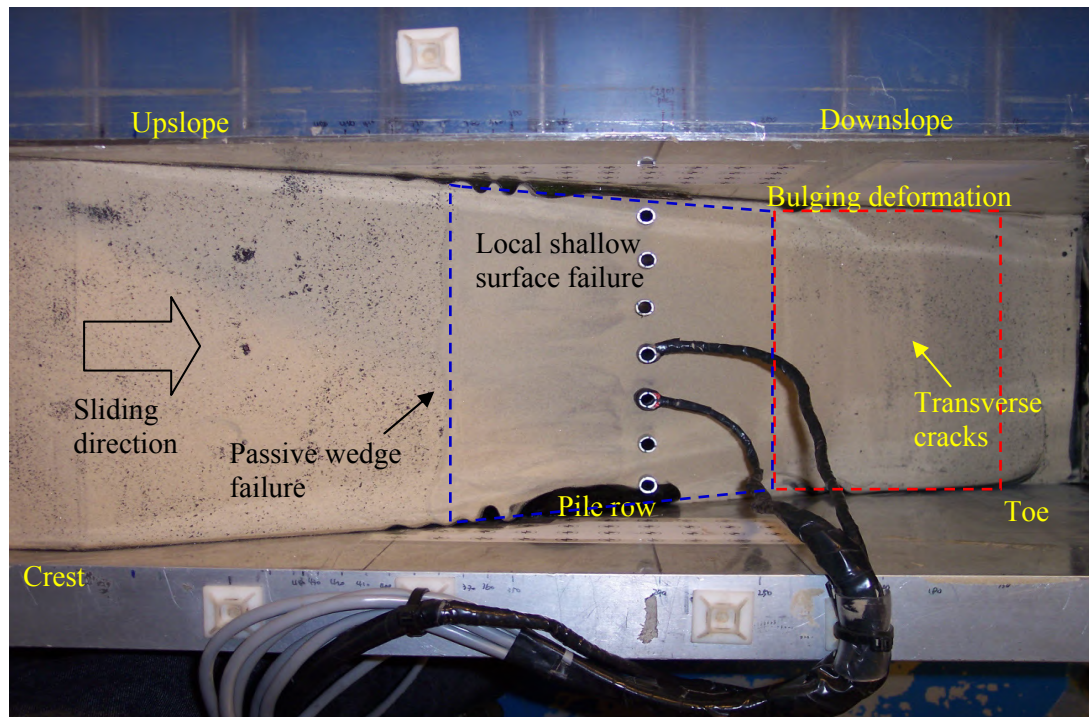
(b) 10 g



(c) 20 g

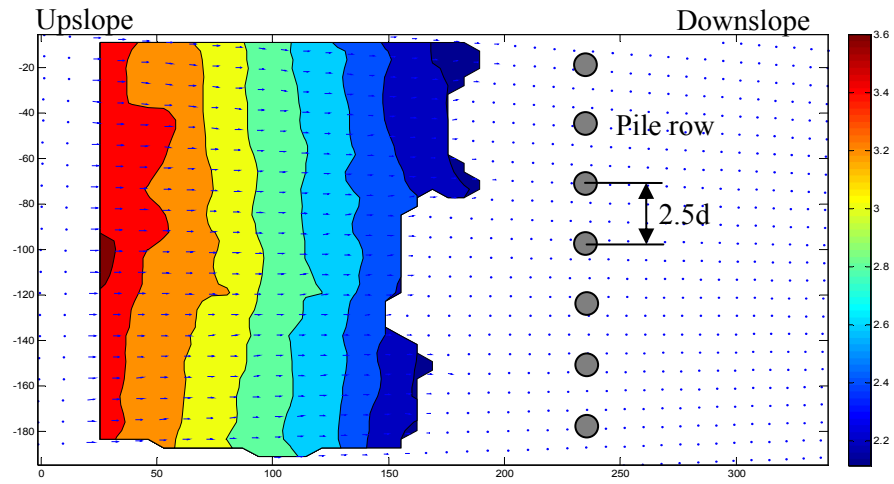


(d) 30 g

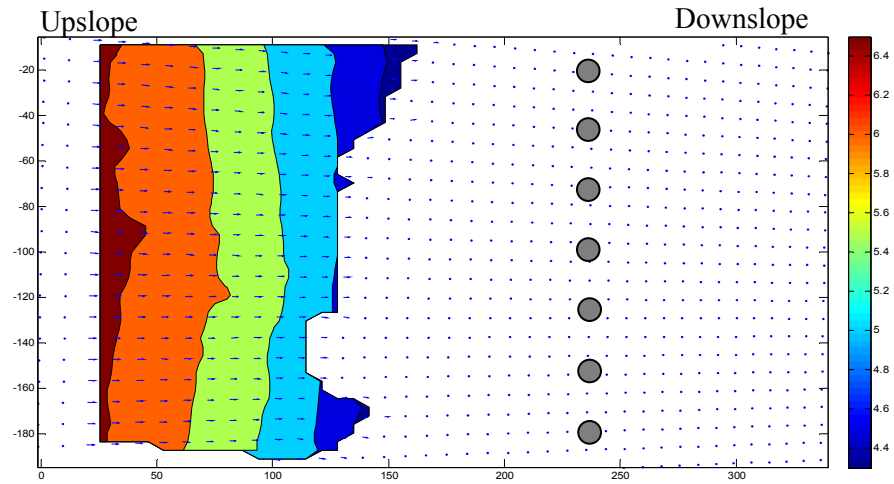


(e) post-test

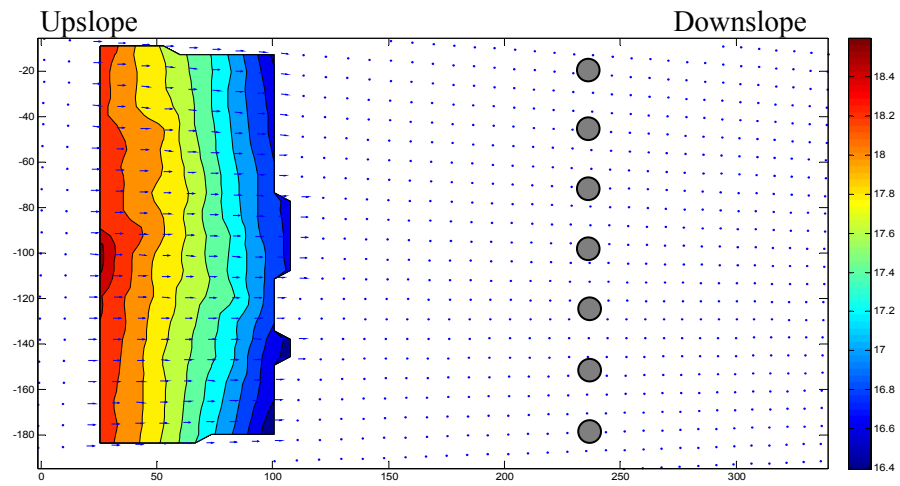
Figure 4.7 - View of the slope face for BSY12a ($(s/d) = 2.5$, $(l/h) = 4.0$)



(a) 1 to 10 g



(b) 1 to 20 g



(c) 1 to 30 g

Figure 4.8 - Contour plots of downslope movement (mm, model scale) on the slope face for

BSY12a ($(s/d) = 2.5$, $(l/h) = 4.0$)

Variation of the average upslope and downslope movement (normalised by the pile diameter) for BSY12a are compared in Figure 4.9, showing increase with g -level. As expected, it appears that there is significant differential displacement between the upslope and downslope. Up to 22 g the stabilising effect of the pile row on the upslope compared to the downslope is clearly evident. The events resulting in significant upslope movement at 22 and 38 g are likely to be associated with failure of a passive wedge above the pile row.

At low g -levels (8 and 14 g) significant downslope movement events are observed in the absence of corresponding upslope movement. This seems to indicate failure events downslope of the piles (but not upslope). At higher g -levels (22 and particularly 38 g) significant upslope and downslope events occur simultaneously. This indicates a failure mechanism upslope of the piles (Section 4.2.1), but also more general widespread movement of the slope probably including ‘flow’ through the piles which causes downslope movement in response to the upslope movement.

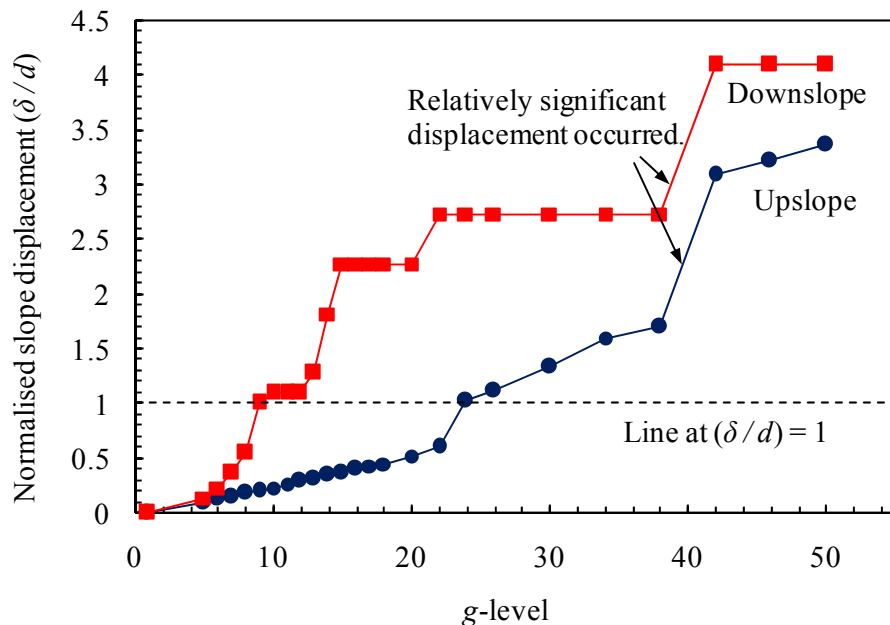
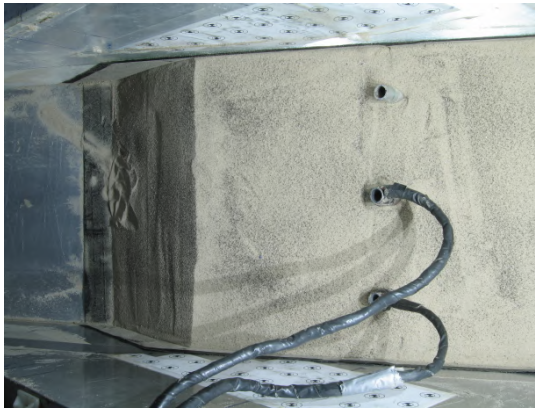


Figure 4.9 - Upslope and downslope displacement (δ) normalised by pile diameter (d) showing variation with g -level for BSY12a ($(s/d) = 2.5$, $(l/h) = 4.0$)

Figure 4.10 and Figure 4.11 illustrate the case for which three piles were spaced at 5.9 pile diameters and $(l/h) = 1.5$ (BSY15a). There is no evidence of passive wedge failure above the pile row. In contrast to BSY12a, there is a smaller zone of uniform upslope displacement (Figure 4.11), reflecting the smaller (l/h) . Again ‘shallow surface failure’ is indicated by loss of the surface texture applied by sprinkling dyed sand on the slope. This kind of failure is broadly observed in the whole area upslope of the pile row, especially when (l/h) is small. This is likely to be caused by the deformed slope angle being oversteepened at the end of the test (exceeding the critical state friction angle of the sand – Figure 4.12). This shallow sliding material is also probably responsible for the loss of texture below the pile row.



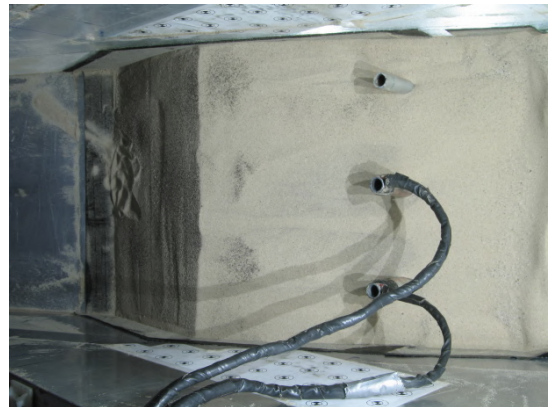
(a) 1 g



(b) 10 g

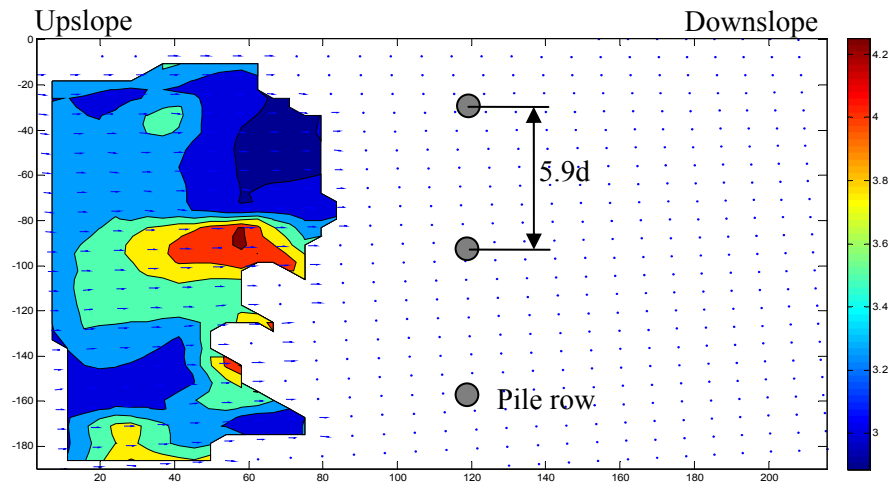


(c) 20 g

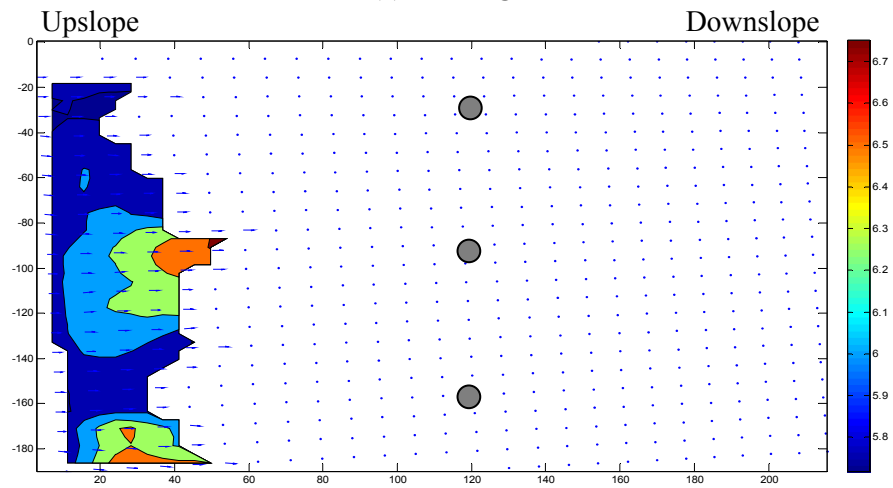


(d) 30 g

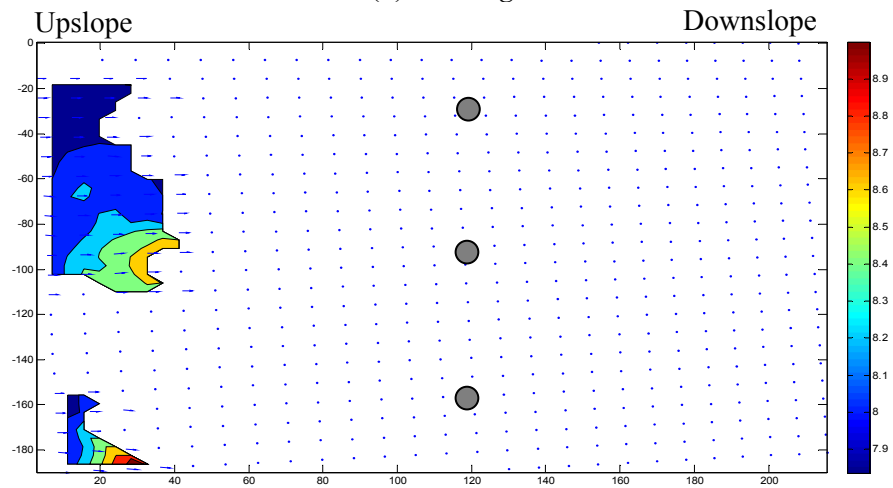
Figure 4.10 - View of the slope face for BSY15a ($(s/d) = 5.9$, $(l/h) = 1.5$)



(a) 1 to 10 g



(b) 1 to 20 g



(c) 1 to 30 g

Figure 4.11 - Contours of upslope movement (mm, model scale) on the slope face for BSY15a ($(s/d) = 5.9$, $(l/h) = 1.5$)

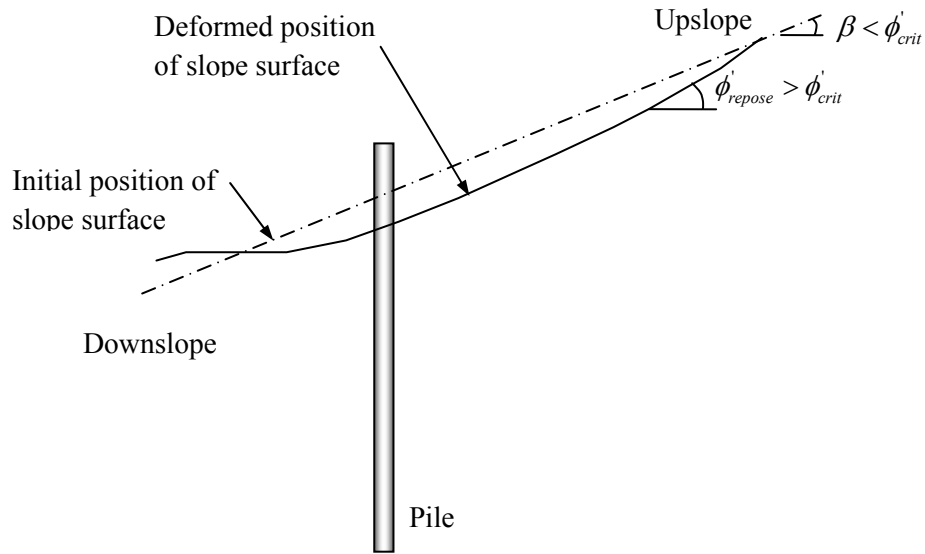


Figure 4.12 - Shallow surface failure

Figure 4.13 shows comparison of the upslope movement with g -level for the two examples discussed previously. The upslope displacement for BSY12a increases gradually up to 22 g but there are dramatic rises between 22 and 24 g and between 38 and 42 g where a passive failure is believed to occur immediately upslope of the pile row. A more steady increase of displacement is shown for BSY15a, without significant events causing sudden increase in movement. Nevertheless there has been quite significant normalised displacement at the end of the test.

From the above results, it can be seen that the ratio of the upslope length to the failure slip thickness is also an important factor in stabilising a slope with the piles, as well as the pile spacing. For a slope with a higher (l/h) ratio, there is a greater mass of upslope material loading the pile row. Thus piles at a wider spacing initially gave similar upslope deformation with smaller (l/h). As the test proceeds upslope failures actually mean that the closer spacing (and greater upslope length) gives larger deformation. The relationship between (l/h) and (s/d) is considered further in Chapter 5.

Figure 4.14 shows the upslope movement as it increases with g -level for all tests. Generally speaking the upslope displacement tends to increase with (s/d) for a given (l/h) , and for a given (s/d) displacement tends to increase with (l/h) . This is a reasonable trend that would be anticipated.

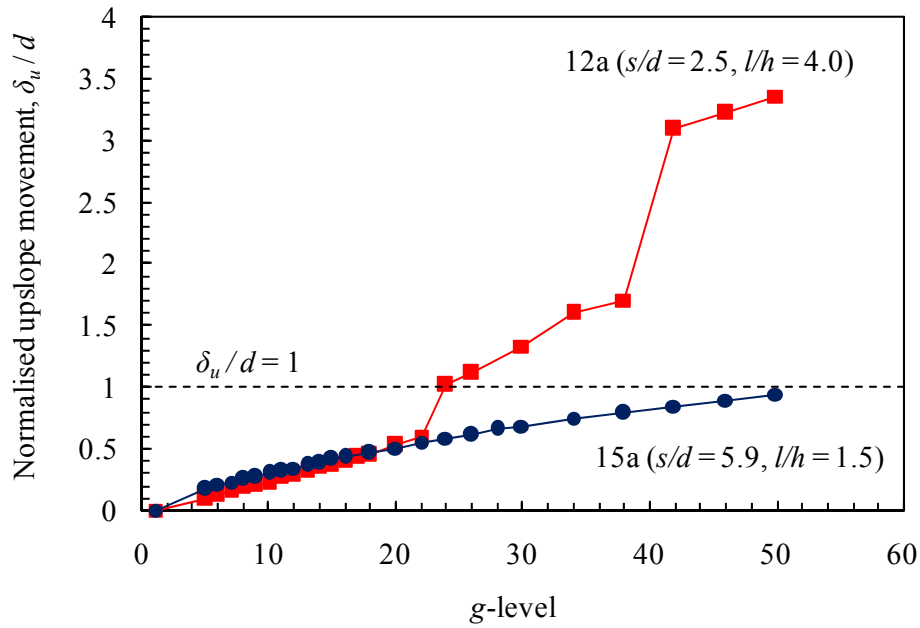


Figure 4.13 - Upslope displacement (δ_u) normalised by pile diameter (d) showing variation with g -level for BSY12a and 15a

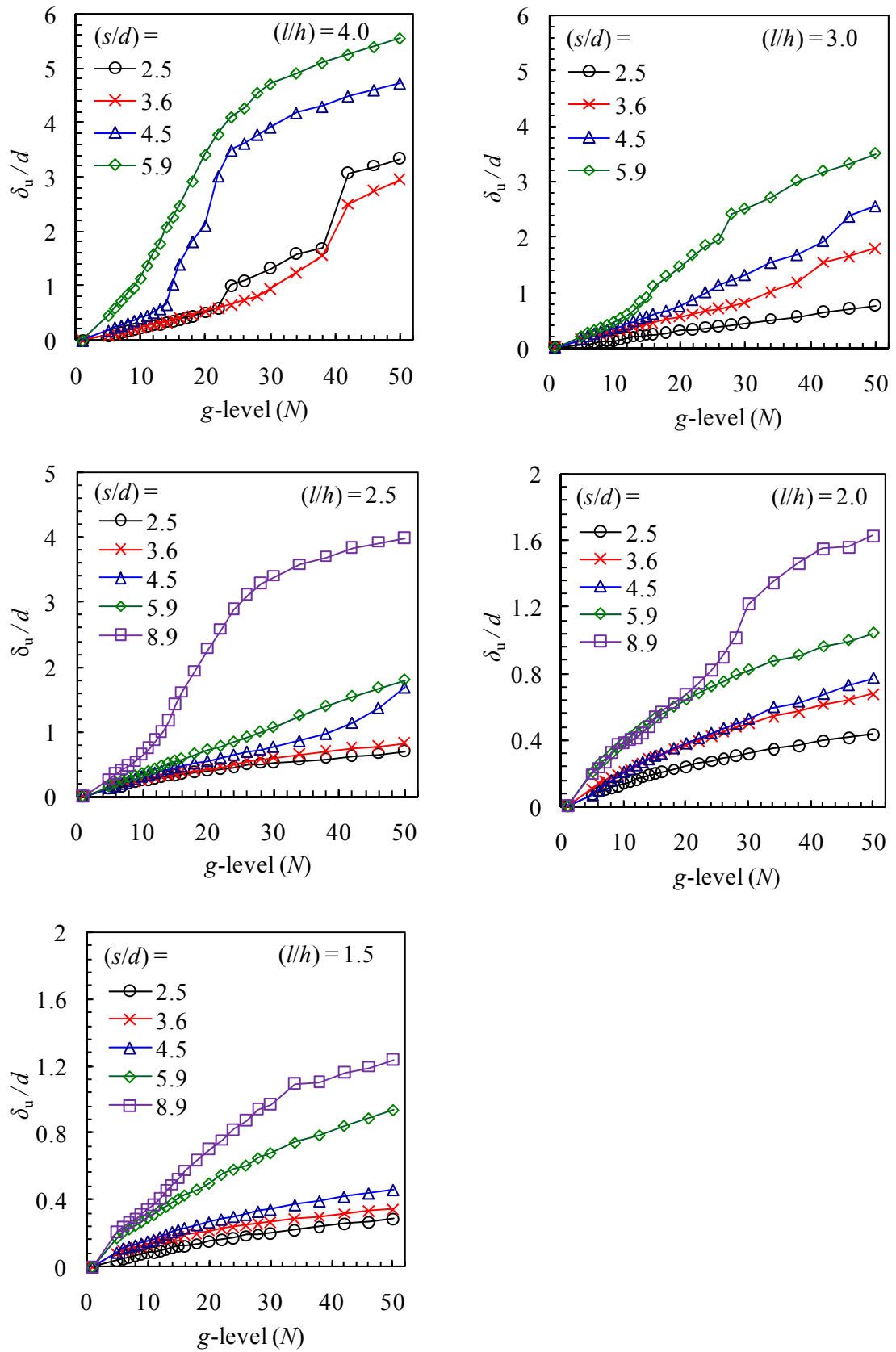


Figure 4.14 - Upslope displacement (δ_u) normalised by pile diameter (d) showing variation with g-level for all tests

4.2.3 Ground deformation characteristics

Characteristics of behaviour

Figure 4.15 illustrates typical types of behaviour, depending on the combination of (l/h) and (s/d):

1. 'Upslope failure' with passive wedge and probably potential upslope slip above the wedge at high (l/h) and small (s/d). The displacement is also prone to show discontinuous 'jumps' (Figure 4.4) seemingly corresponding to specific upslope failure events.
2. 'Flow' through the piles with large deformation at high (l/h) and (s/d)
3. 'Stable' condition (with small deformation) at small (l/h) and (s/d)
4. 'Potentially shallow surface failure' passing through the piles or 'ravelling' between the piles at small (l/h) and high (s/d)

For many cases behaviour was a combination of two types of behaviour described above. However, the specific mechanisms referred to above become dominant at each 'corner' of the test boundary (see Figure 4.15).

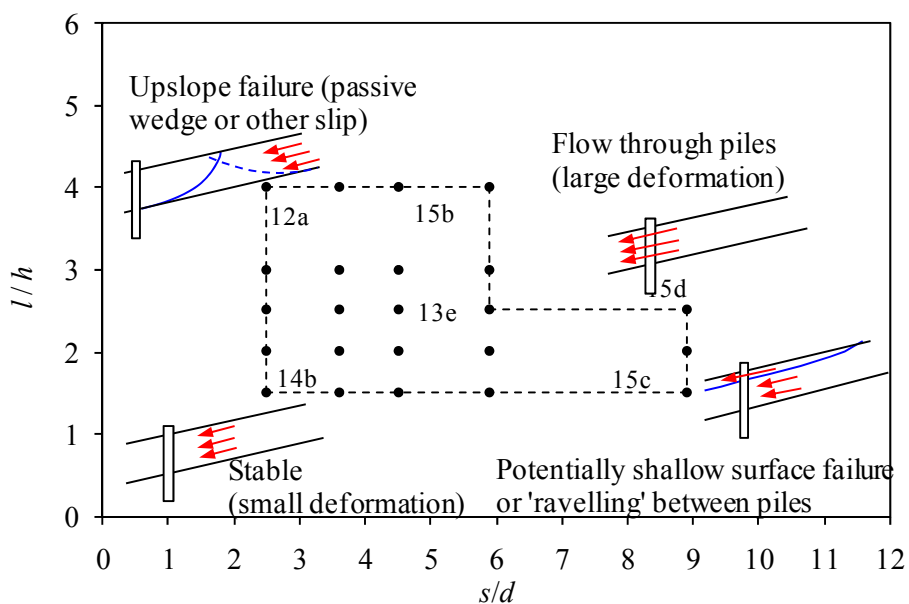
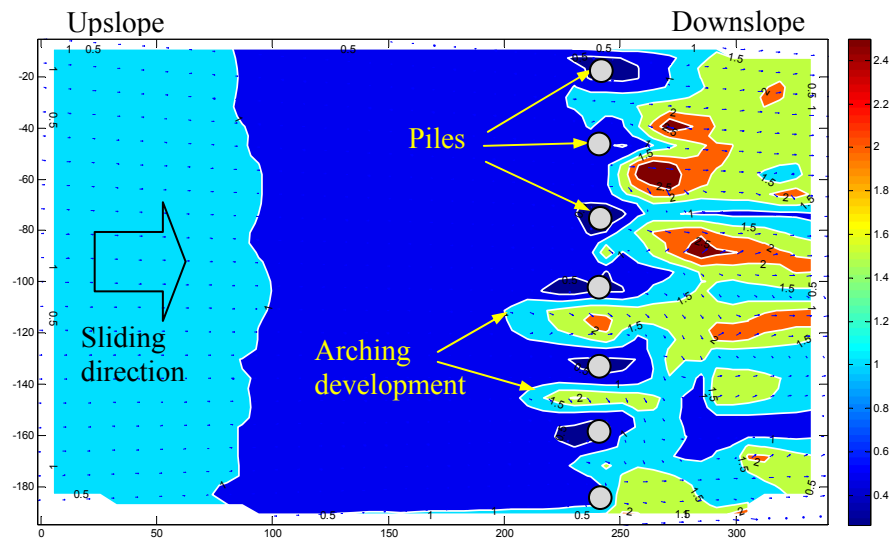


Figure 4.15 - Typical characteristics of passive yielding behaviours

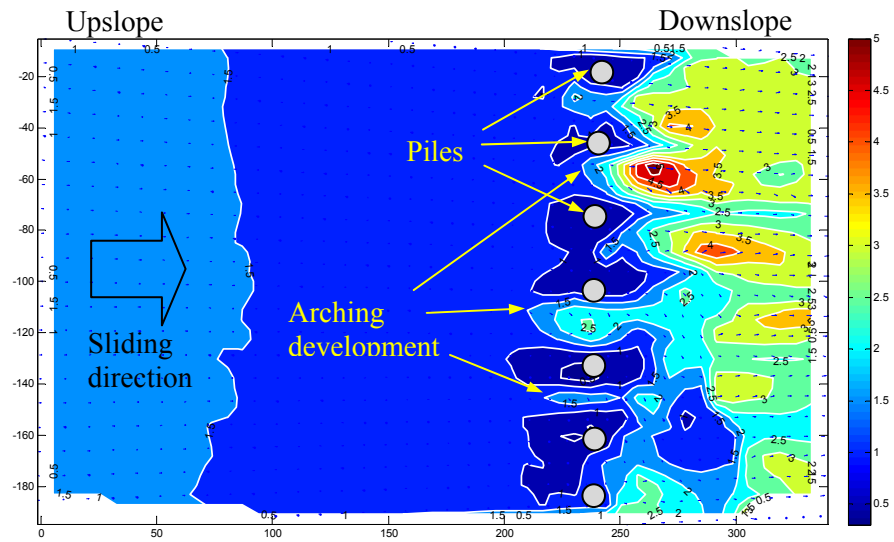
Arching and/or flow between piles

As described in Chapter 2 the efficiency of discrete pile ‘walls’ relies primarily on passive interaction between adjacent piles – maximising arching whilst simultaneously minimising flow between the piles. Direct evidence of arching/flow between adjacent piles was limited due to loss of surface texture in the zone immediately above and below the piles. Nevertheless, contour plots at low gravity levels (e.g. 5 and 6 g) did give some indication of this behaviour. BSY12a ($(l/h) = 4.0$, $(s/d) = 2.5$) is used to illustrate arching action whereas BSY15d ($(l/h) = 2.5$, $(s/d) = 8.9$) illustrates flow.

For closely spaced piles (BSY12a) Figure 4.16 shows an arch-shaped deformation that is progressively developed between the piles. Displacement above the arching zone (referred to Figure 1.1(b) in Chapter 1) was relatively small compared to that below it. The soil shows a tendency to flow between the widely spaced piles (BSY15d) in Figure 4.17. This is in good agreement with general expectation for pile-soil-pile interaction. These deformations are only known at the soil surface, and unfortunately do not give direct evidence of the presence of arching or otherwise at greater depth.

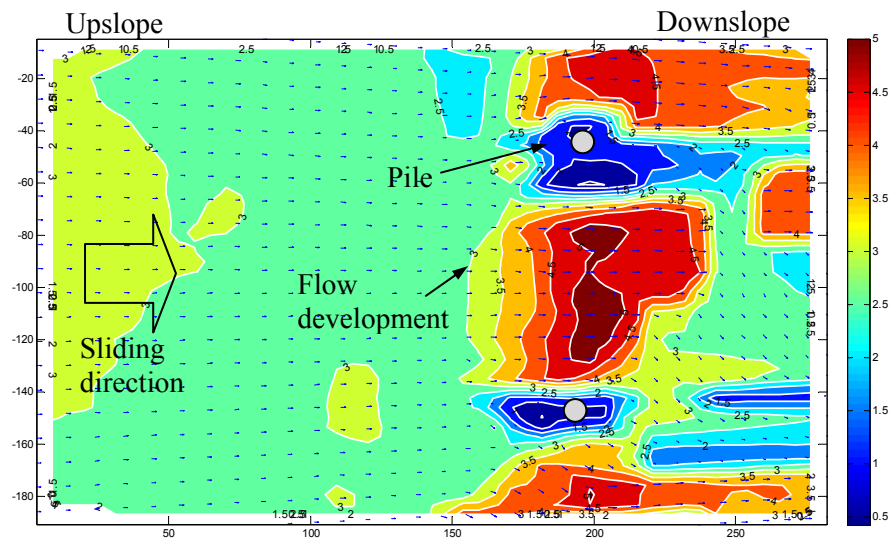


(a) 5 g

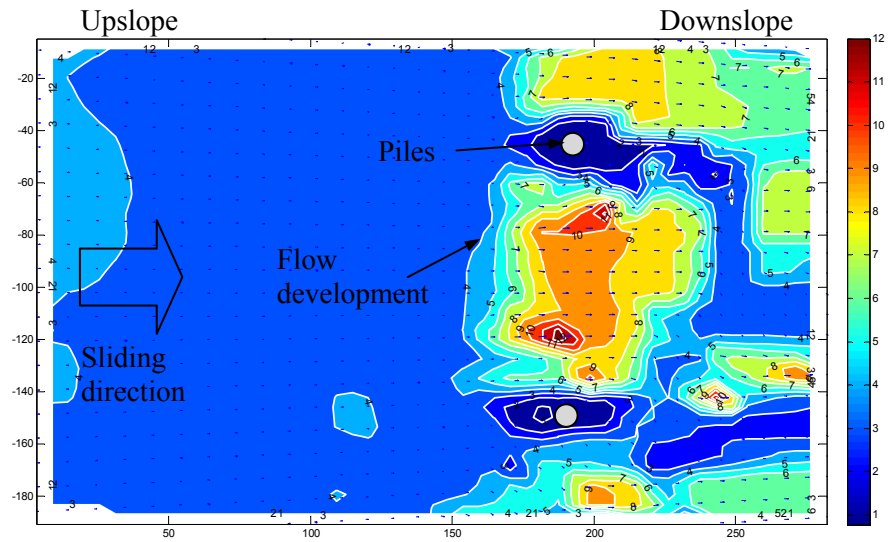


(b) 6 g

Figure 4.16 - Investigation of arching development between the piles for BSY12a



(a) 5 g



(b) 6 g

Figure 4.17 - Flow action between the piles for BSY15d ($(l/h) = 2.5$, $(s/d) = 8.9$)

4.2.4 Pile head displacements

Pile head displacement has been deduced using PIV analysis of a series of images of the slope face. Figure 4.18 shows that the pile head displacement (δ_p , results normalised by pile diameter) increases with an increase of gravity level (N) and (s/d) for a given (l/h), and with (l/h) for a given (s/d). These trends all seem reasonable.

‘Normalisation’ of this data in this respect is considered in Figure 4.19, by dividing by the product of all three variables above. It can be seen that the normalised displacements for all tests generally tend toward consistency regardless of N , (s/d) and (l/h), although the value tends to be slightly higher at low g -level in some tests. At higher g -level the results tend towards an approximately unique value.

In fact the series of ‘normalising’ parameters reflect the total load on a single pile, which tends to increase in proportion to N , (s/d) and (l/h) – this idea is pursued further in the theoretical framework which is developed in Chapter 5. This indicates that the piles show broadly consistent active response to loading throughout the tests, and have sufficient active capacity in the underlying stable soil (significant active failure at any stage would presumably have been indicated by increase of the ‘normalised’ secant displacement).

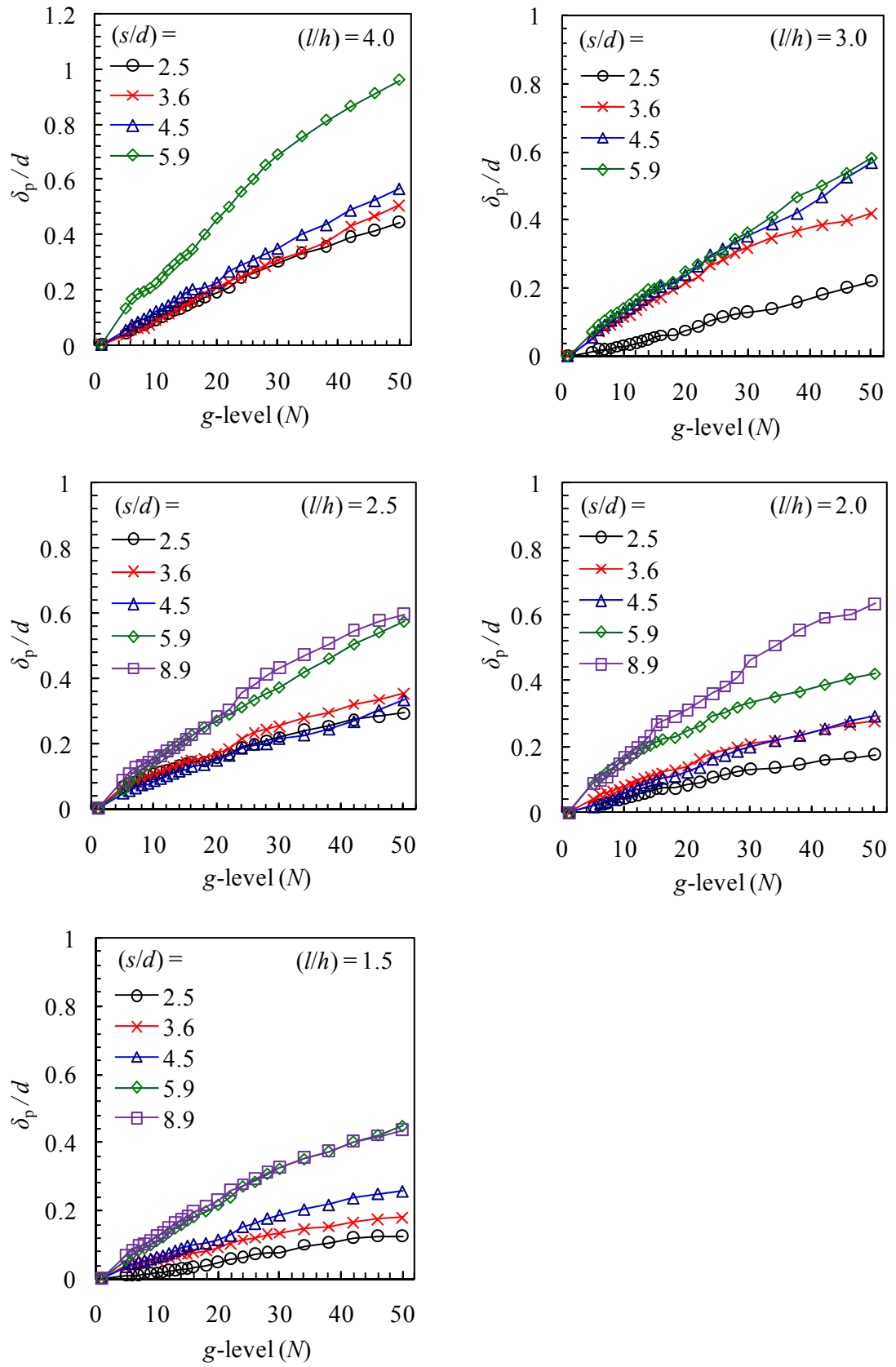


Figure 4.18 - Pile head displacements with g-level for all tests

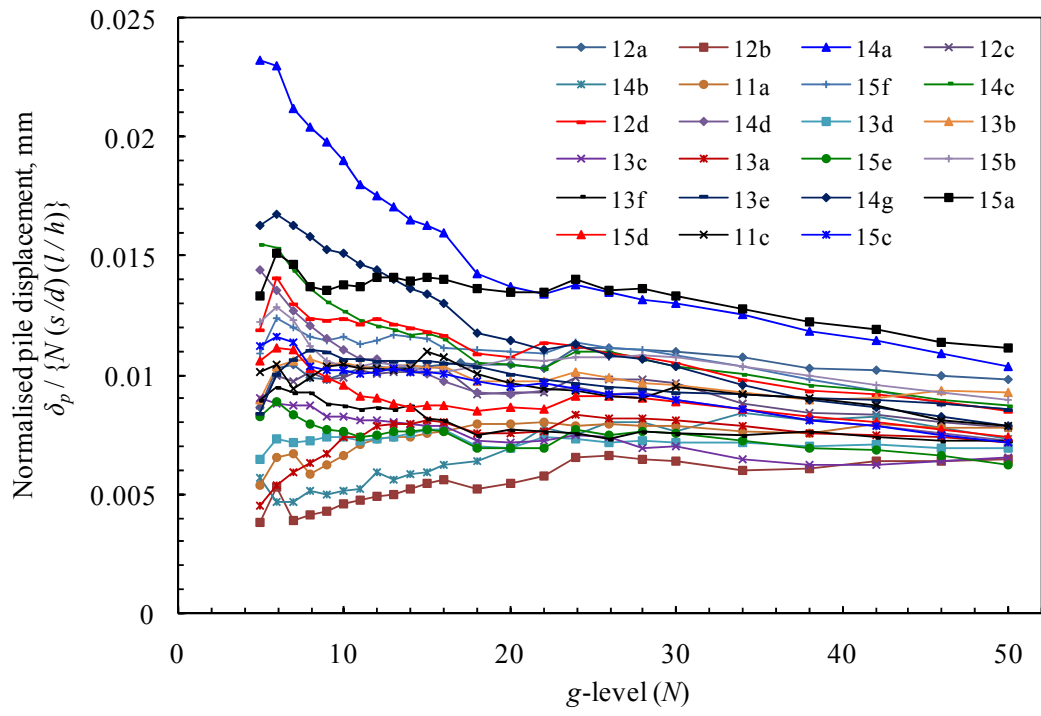


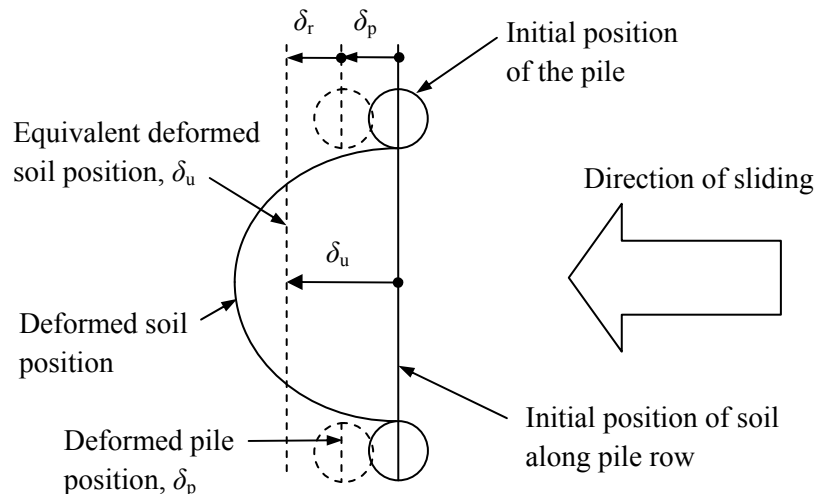
Figure 4.19 - 'Normalisation' of pile displacement with g-level for all tests

4.2.5 Relative pile-soil displacement

‘Relative’ pile-soil displacement (δ_r) is often used in the analysis of passive behaviour. Figure 4.20 shows the general concept of δ_r that is employed frequently in numerical analysis. Here the difference between the upslope soil movement observed at the ground surface (δ_u) and the pile head movement (δ_p) is taken as a broad indicator of relative pile-soil displacement.

Figure 4.21 shows results of relative pile-soil displacement for all tests – δ_r tends to increase as both (s/d) and (l/h) increase. Note that the upslope soil movements were estimated by averaging the available displacement vectors (upslope of the piles) in a test due to significant loss of texture on the slope (also previously stated in Section 4.2.2). This trend seems to logically indicate that:

1. Passive restraint of the stabilising piles to sliding of the slope becomes less effective at wider (s/d) for given (l/h)
2. Large (l/h) generates greater passive loading for a given (s/d) .



where, $\delta_r (= \delta_u - \delta_p) = \text{Relative pile-soil displacement}$

Figure 4.20 - General definition of relative pile-soil displacement in numerical analysis

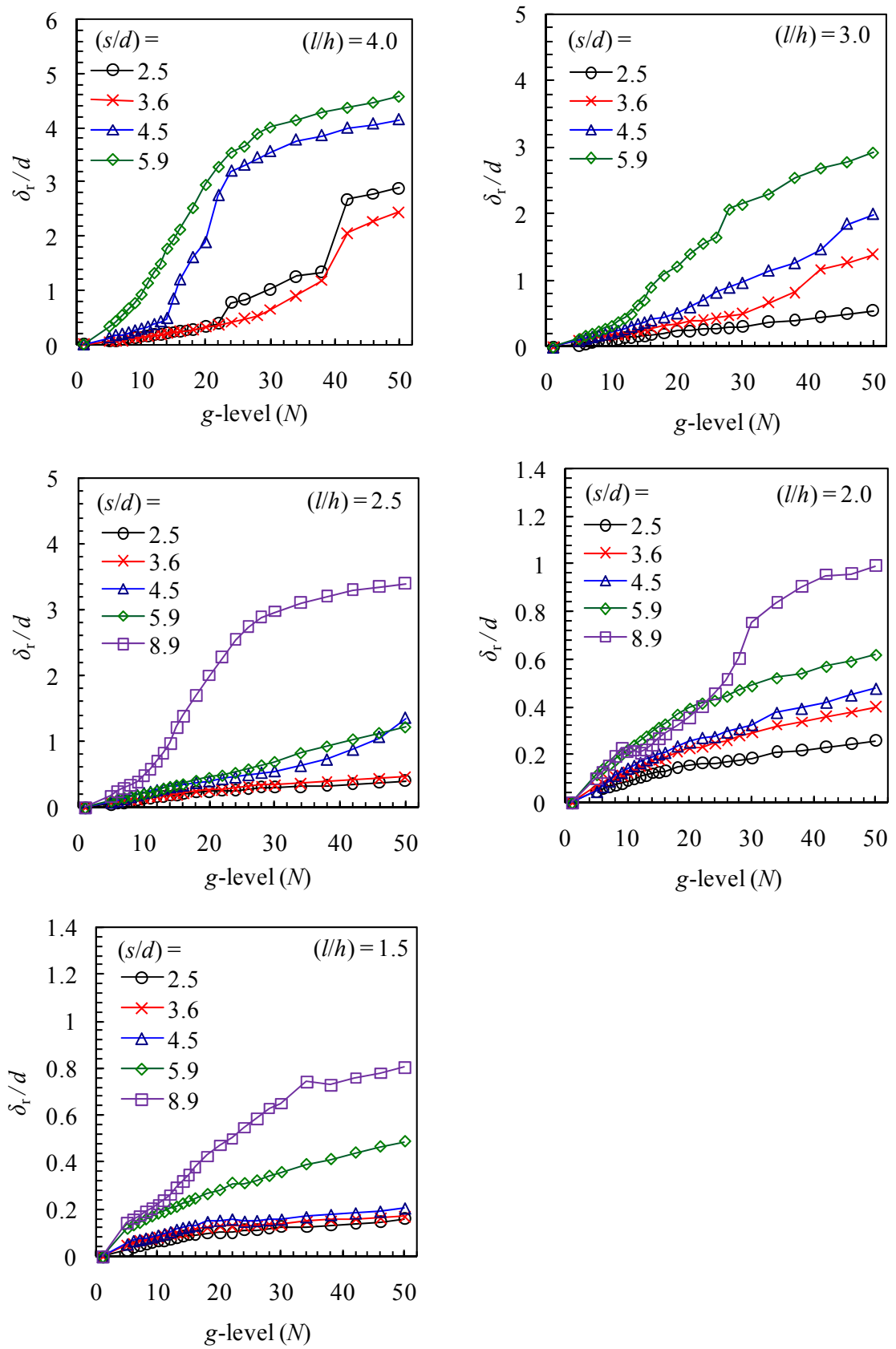


Figure 4.21 - Relative pile-soil displacement with g-level

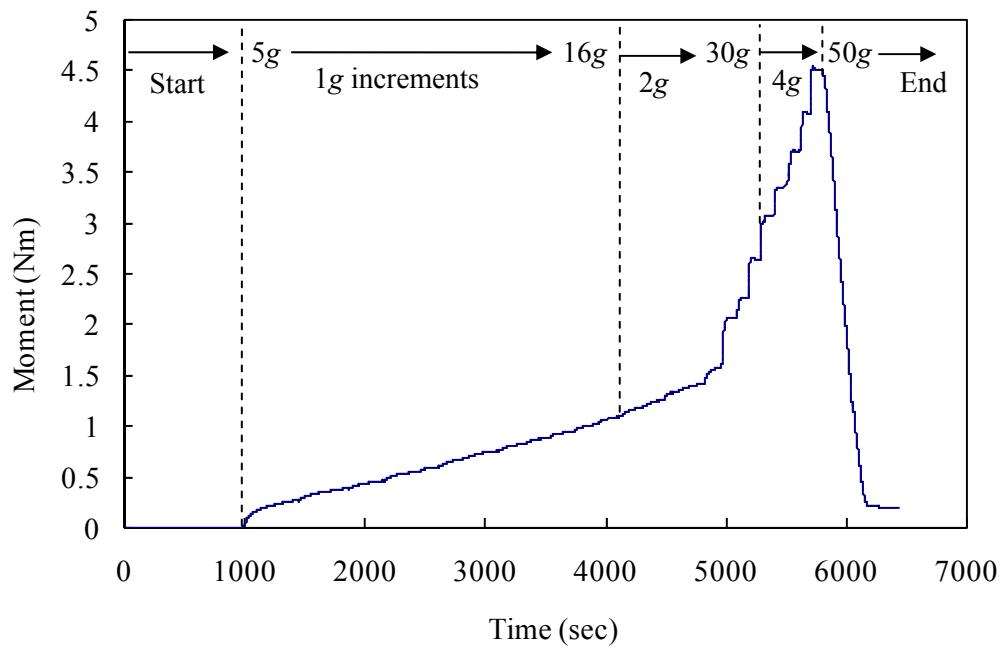
4.3 Pile moment data

Bending moment transducers (BMTs) were used to measure the moment at discrete points along the length of the pile (see Section 3.4.3). A curve-fitting technique was then used to approximate continuous profiles of moment, shear force, and pressure from the measured moment data.

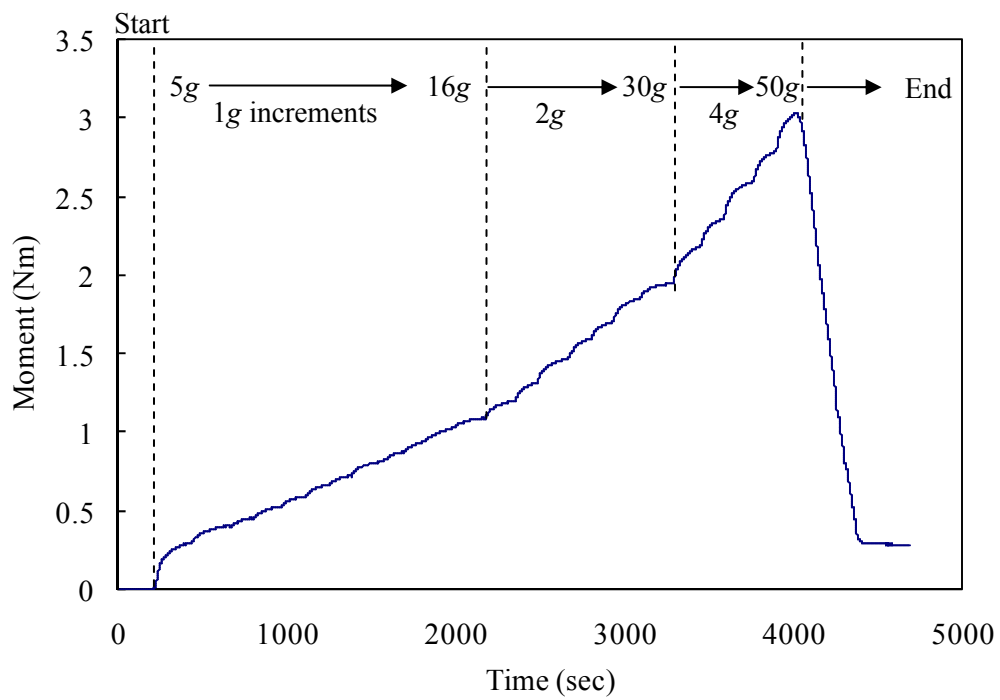
4.3.1 Variation of moment with time

The continuous variations of electrical signals from each strain gauge location were recorded for the pile during a test. Figure 4.22 shows typical variations of moment (differential output voltages multiplied by a calibration factor) with time for BMT 6 (located at the elevation of the interface) slip. Gravity level was increased throughout the test and the increments used are also labelled.

Both results (BSY12a and BSY15a) show similar behaviour – larger increments in gravity level at the end of the test tend to give correspondingly larger increments in moment. Generally, the immediate response to increasing g -level (and hence passive loading) is usually sizable, although there is also generally a surprisingly large time-related response (particularly at low g -levels) given that the soil is dry sand. Each g -level was normally held constant for approximately 5 minutes, so that an asymptotic value was approached. The origins of the time-related behaviour were not established with certainty, but it seems likely that creep in the greased interface caused ongoing downslope movement of the soil with time.



(a) BSY12a



(b) BSY15a

Figure 4.22 - Variation of bending moment for BMT 6 (at the interface elevation) with time

4.3.2 Moment, shear force, and pressure profiles with depth

The pile is embedded through the unstable soil (passive loading) and into the stable material (active loading) beneath. There is continuity of bending moment and shear force in the pile across the predefined failure interface (i.e. silicon-greased latex/aluminium interface). However there is a discontinuity of lateral pressure at the slip, due to the discontinuity of soil displacements (and corresponding change from passive to active loading).

A form of spline curve-fitting technique was therefore employed, with separate polynomials used to fit the measured bending moment data in each layer. The use of this technique is advantageous in reducing the order of polynomials required to achieve satisfactory results, and allowing pressure discontinuity at the slip. The polynomials were constrained to give:

- (1) continuity of moment and shear force in the pile at the slip
- (2) zero moment and shear force at the pile head and tip, and
- (3) zero lateral pressure at the pile head (where the overburden stress is zero and hence the strength of a cohesionless soil tends to zero).

The method of least squares is often used to give a unique ‘best fit’ of a polynomial to data. Partial derivatives are derived to minimise the error between the data and the polynomial fit, and the resulting equations give a unique solution via solution of simultaneous equations (i.e. inversion of a matrix).

A cost function is a popular alternative technique for optimisation of mathematical problems, which generally requires considerably more computational effort, but avoids the necessity of deriving an explicit set of equations by hand to be solved. The additional computational effort for a problem such as this is not that onerous by today’s standards, and the approach offers considerable flexibility and convenience. The resulting solution is not strictly unique,

but provided it has been obtained ‘correctly’ any such analysis would give a similar optimised result.

Here a ‘cost function’ was implemented as follows:

- Derive the value of the polynomial multipliers a_n (passive zone) using one of the methods described below. These values would then remain fixed.
- Make an initial arbitrary assumption regarding the value of the polynomial multipliers b_n (active zone) (see Figure 4.23 below).
- Define the total error in fitting the bending moment data at discrete depths as the sum of the square errors for all data points compared to the polynomial fit.
- Add to this terms for ‘error’ in continuity of moment and shear force at the interface, with an increased ‘weighting’ compared to fitting the data. Conditions at the head and toe of the pile are inherently incorporated as described below, and hence do not need to be considered in the cost function.
- Use optimisation functions in Matlab to minimise the total error from fitting the data and continuity at the interface by adjusting the values b_n . The increased weighting for continuity at the interface means that this is satisfied accurately whilst the data is subject to a ‘least squares’ fit.

The precise result obtained will depend on the technique for optimisation and the number of iterations, as well as the weighting factor given to continuity at the interface. However, provided there is sufficient iteration and the weighting factor is sufficiently large without allowing even very small errors at the interface to have undue influence on the solution, the result should be reasonable. The Matlab code to do this was developed in house (Cox, 2006).

One problem in polynomial curve fitting is the selection of an appropriate order for the polynomial. It can be argued that in principle the use of higher order of polynomials

provides a more detailed profile, allowing greater freedom of curve fitting. However the results are generally unsatisfactory since high order curves tend to ‘oscillate’ between the data points and are highly sensitive to relatively small variations (or errors) in moment. In fact, the lowest order polynomial which gives a reasonable fit to the data is often most suitable.

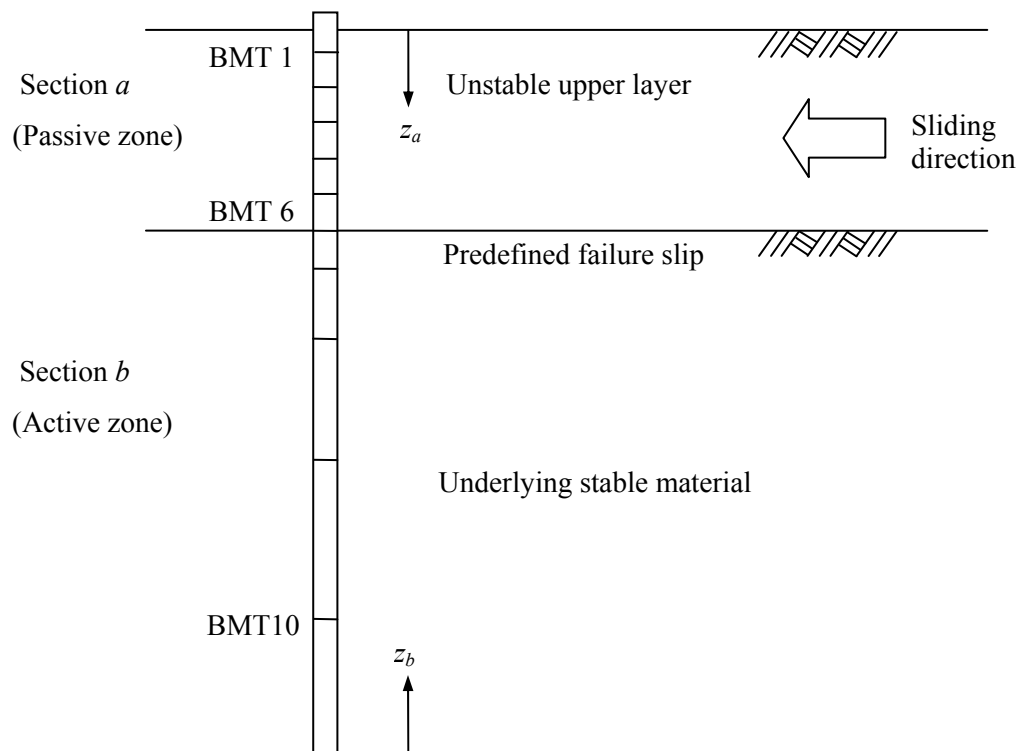


Figure 4.23 - Bending moment, shear force, and lateral pressure acting on the pile

Figure 4.23 shows a schematic diagram for the curve-fitting technique used here. BMT1 to 5 are in the passive zone (section *a*) and BMT 7 to 10 are in the active zone (section *b*). BMT6 is at the interface. Two different vertical co-ordinates systems are used (z_a and z_b), measured from the head and toe of the pile respectively. This offers considerable convenience in inherently satisfying the conditions that moment and shear force should be zero at these points.

Table 4.1 summarises the polynomials P_1 and P_2 used in the passive zone (z_a), and P_3 used in the active zone (z_b). In the passive zone either the P_1 or P_2 approach was used – not both simultaneously. In fact the initial polynomials describe the pressure distribution, and are integrated to give shear force and bending moment. However no constants of integration are introduced since shear force and bending moment are zero for z_a and $z_b = 0$, and these constraints are inherently incorporated. The assumption of zero lateral pressure at the pile head also implies that there is no a_0 term in P_1 and P_2 .

The P_1 approach allows ‘direct derivation’ of the only polynomial multiplier a_1 based only on the value of bending moment at the interface (BMT 6). The P_2 approach used a true ‘least squares’ approach by inversion of a 2×2 matrix to obtain a_1 and a_2 based on all bending moment data above the interface. The values b_n were then optimised using a cost function as described above.

Table 4.1 Curve fitting functions used for deriving moment, shear force, pressure profiles

P_1 approach (direct derivation from BMT 6)	P_2 approach (least squares matrix inversion)
$p(z_a) = a_1 z_a$	$p(z_a) = a_1 z_a + a_2 z_a^2$
$S(z_a) = \int_0^{z_a} p(z_a) dz_a = a_1 \frac{z_a^2}{2}$	$S(z_a) = \int_0^{z_a} p(z_a) dz_a = a_1 \frac{z_a^2}{2} + a_2 \frac{z_a^3}{3}$
$M(z_a) = \int_0^{z_a} S(z_a) dz_a = a_1 \frac{z_a^3}{6}$	$M(z_a) = \int_0^{z_a} S(z_a) dz_a = a_1 \frac{z_a^3}{6} + a_2 \frac{z_a^4}{12}$
P_3 approach (cost function)	
$p(z_b) = b_0 + b_1 z_b + b_2 z_b^2$	
$S(z_b) = \int_0^{z_b} p(z_b) dz_b = b_0 z_b + b_1 \frac{z_b^2}{2} + b_2 \frac{z_b^3}{3}$	
$M(z_b) = \int_0^{z_b} S(z_b) dz_b = b_0 \frac{z_b^2}{2} + b_1 \frac{z_b^3}{6} + b_2 \frac{z_b^4}{12}$	

Derived profiles of moment, shear force, and pressure from the P_1 and P_2 approaches are illustrated in Figure 4.24 and Figure 4.25 for typical data at 10, 20, and 30 g, where the red dashed line shows the P_1 data fit and the blue solid line is the P_2 data fit. Use of the P_1 or P_2 curve in the passive zone also affects the P_3 curve in the active zone due to the condition of continuity of shear force at the interface. The numerical values of the polynomial terms which have been derived for the moment data fit are recorded on the plots. ‘AAE’ is the Average Absolute Error in fitting the data, whilst ‘RMSE’ is the root mean square error. Both are expressed as a percentage of the maximum moment in the pile. The values shown refer to the P_2 (rather than P_1) data fit.

Figure 4.24 shows reasonable consistency between the P_1 and P_2 data fits in all derived profiles for BSY12a. However, in Figure 4.25 the P_1 data fit for BSY15a gives problems in the passive zone when the moment data at mid-depth in the passive zone is low, and the cubic moment curve does not allow sufficient curvature as the moment data increases rapidly towards the bottom of the passive zone.

Problems with the P_1 data fit for BSY15a persist below the interface since the shear force at the interface has potentially been underestimated, and hence the shear force is initially approximately constant immediately below the interface (compared to reduction with depth for the P_2 data fit). This implies approximately zero pressure immediately below the interface for the P_1 data fit, increasing rapidly with depth. This does not seem consistent with the general mode of pile deformation and the assumption that the soil below the interface undergoes little movement. The pressure profile in the active zone given by the P_2 data fit (in the passive zone) seems more reasonable.

In the passive zone a triangular distribution of limiting stress might be anticipated, corresponding to increase of nominal overburden stress with depth. The greater than linear

increase with depth shown for the P_2 data fit in Figure 4.25 seems unlikely - somewhat less than linear increase indicating some reduction in mobilisation compared to the ultimate value with depth would be more plausible.

In general, 11 tests with a large (l/h) and small (s/d) gave similar (satisfactory) curve-fitting to BSY12a, but the others (12 tests) with small (l/h) and large (s/d) tended to give similar problems to BSY15a. This corresponds to the postulated mechanism of ‘shallow failure passing through the piles’ in Figure 4.15. It seems likely that the surface of the slope may actually have become slightly lower at the location of the pile row in these tests. This could explain the difficulty in obtaining a good fit to the bending moment data using the P_1 approach, since the nominal position assumed for the soil surface was no longer completely accurate. With large (l/h) and small (s/d) a ‘bulge’ of soil tended to form behind the row (Figure 4.3(e)), and hence there was less tendency for the level of the soil surface to drop, and the P_1 curve fit gave better results.

In conclusion, the P_1 approach is considered to be more ‘robust’ in the passive loading zone and less sensitive to any error in position of the soil surface, or inaccuracy in small moment measured at mid-depth in passive zone. Hence it will be used in preference to the P_2 approach in the remainder of the thesis when considering passive loading.

From Figure 4.24 and Figure 4.25, it can be seen that the general trends of behaviour do not change with g -level. Passive loading (positive pressure, Figure 4.1) increases with depth and shows a maximum value at the slip – the rather unlikely shape of the P_2 data fit in some cases was discussed above. Below this loading is actively resisted (negative pressure) in the stable ground with a point of pressure reversal near the toe of the pile in the active zone to give moment equilibrium of the pile. The bending moment reaches a maximum in the active zone where the shear force is zero.

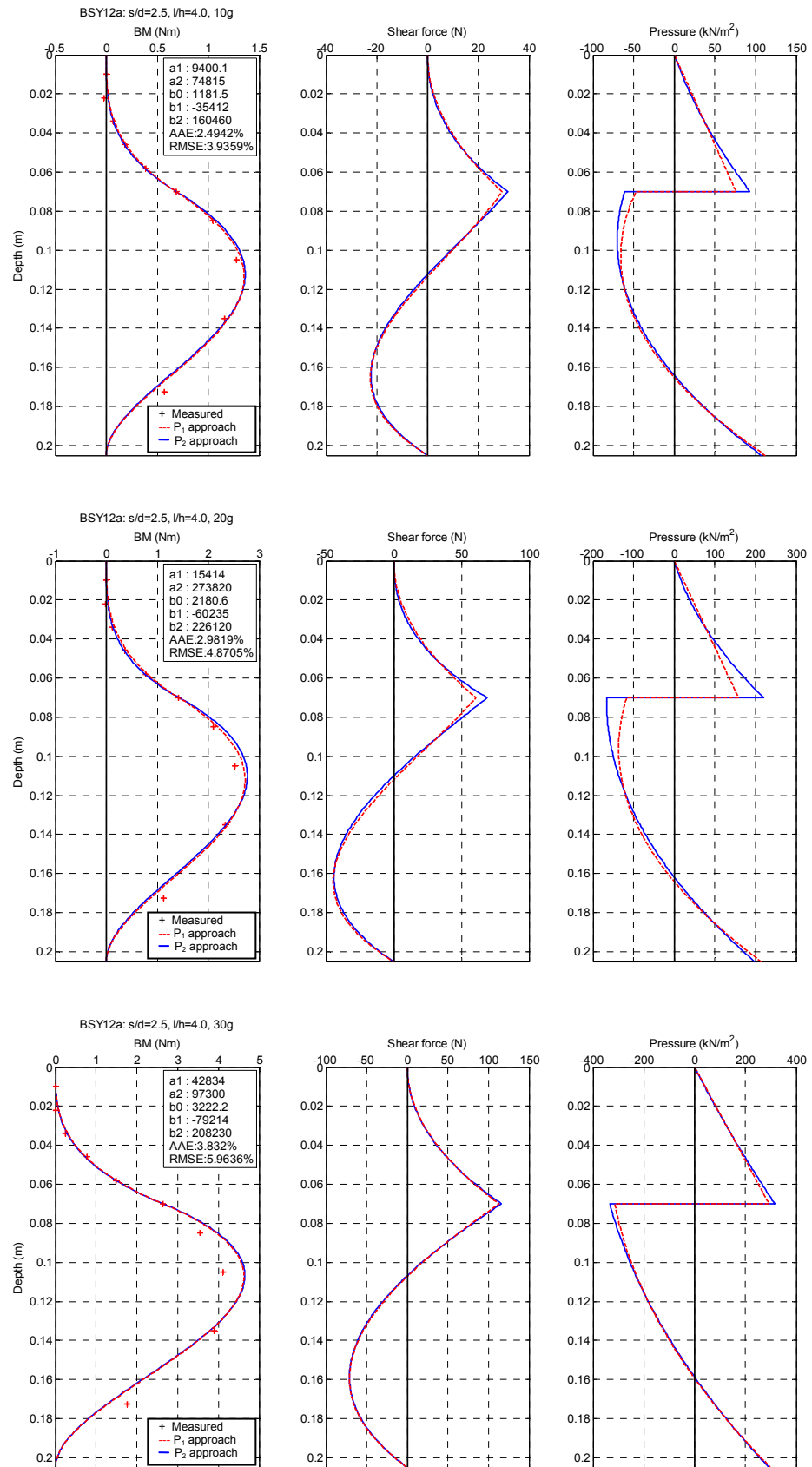


Figure 4.24 - Moment, shear force, and pressure profiles for BSY12a ($s/d = 2.5$, $l/h = 4.0$)

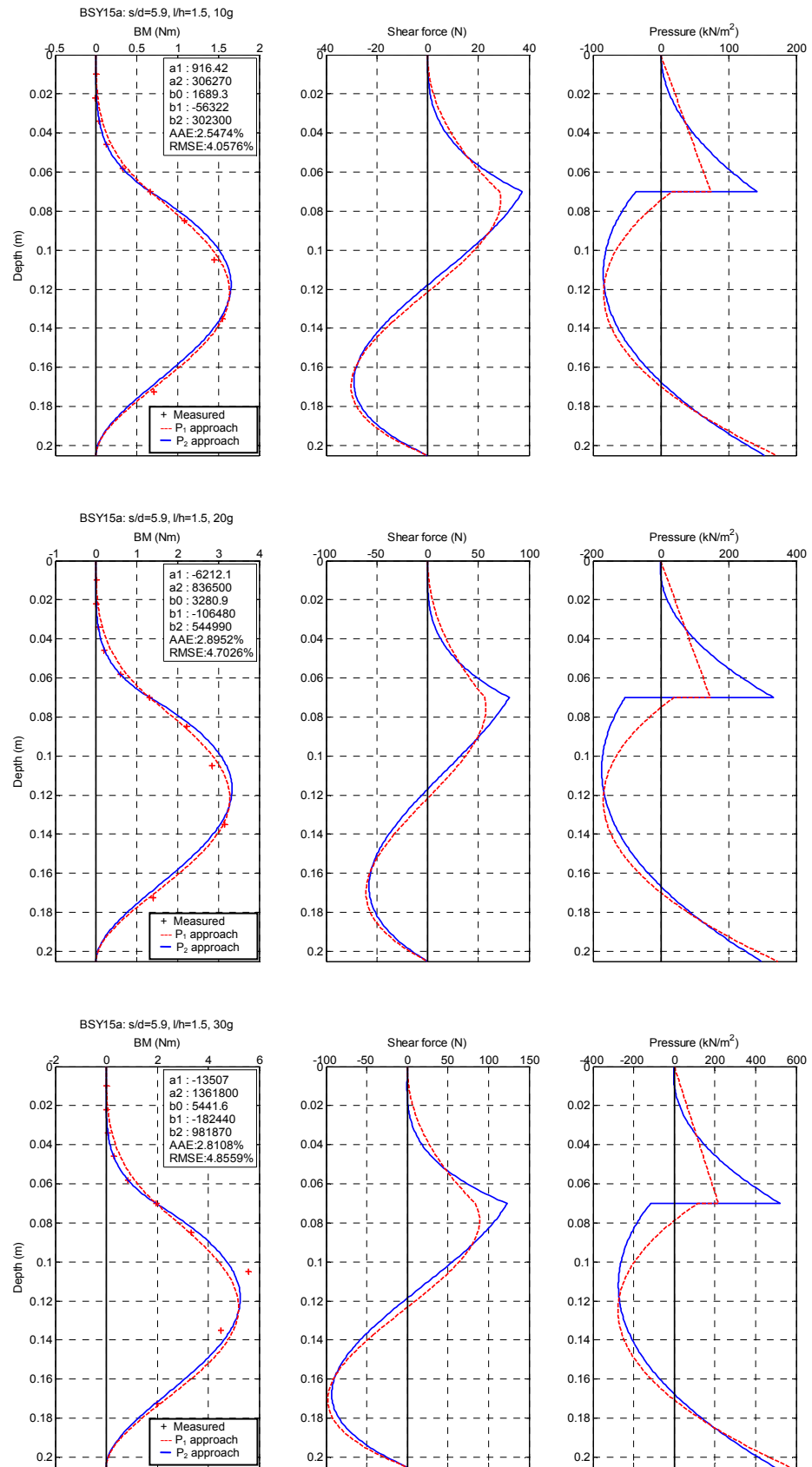


Figure 4.25 - Moment, shear force, and pressure profiles for BSY15a ($s/d = 5.9$, $l/h = 1.5$)

4.3.3 Derived and idealised pile displacements with depth

The pile displacement profile with depth can be derived by integrating the moment polynomials (see Table 4.1) twice, as follows:

Passive zone (based on P_2 approach)

$$\theta(z_a) = \int_0^{z_a} M(z_a) dz_a = \frac{1}{EI} \left(a_1 \frac{z_a^4}{24} + a_2 \frac{z_a^5}{60} \right) + A_1$$

$$u(z_a) = \int_0^{z_a} \theta(z_a) dz_a = \frac{1}{EI} \left(a_1 \frac{z_a^5}{120} + a_2 \frac{z_a^6}{360} \right) + A_1 z_a + A_2$$

Active zone (based on P_3 approach)

$$\theta(z_b) = \int_0^{z_b} M(z_b) dz_b = \frac{1}{EI} \left(b_0 \frac{z_b^3}{6} + b_1 \frac{z_b^4}{24} + b_2 \frac{z_b^5}{60} \right) + B_1$$

$$u(z_b) = \int_0^{z_b} \theta(z_b) dz_b = \frac{1}{EI} \left(b_0 \frac{z_b^4}{24} + b_1 \frac{z_b^5}{120} + b_2 \frac{z_b^6}{360} \right) + B_1 z_b + B_2$$

The total four constants of integration (A_1 , A_2 , B_1 , and B_2) are obtained by assuming:

- (1) the pile deflection at the head is equal to the pile head displacement deduced from image analysis in the test.
- (2) continuity of gradient (rotation, θ) at the interface.
- (3) continuity of pile displacement (u) at the interface.
- (4) the point of pressure reversal in the active zone is assumed to correspond to zero absolute pile deformation. In fact, this point is associated with zero differential displacement between the pile and soil. However, this assumption will be acceptable since lateral soil displacement is likely to be very small at this depth.

This allows four independent equations to be written in terms of the four unknown constants of integration. Hence a unique solution exists and can be derived (see Appendix A).

For convenience the profile of pile displacement with depth could be idealised assuming that the pile is completely rigid. The idealised linear profile is assumed to be defined by the pile displacement at the pile head, and zero absolute pile displacement at the point of pressure reversal near the tip.

The resulting pile displacement (normalised by pile diameter) for BSY12a at 30 g (Figure 4.26) shows a typical results. The pile deflects downslope (the positive direction) – rotation and flexure of the pile both contribute to this movement. The linear profile overestimates the displacement above the point of pile rotation, which is around 40 % higher than the value derived including the effect of flexure at the predefined slip.

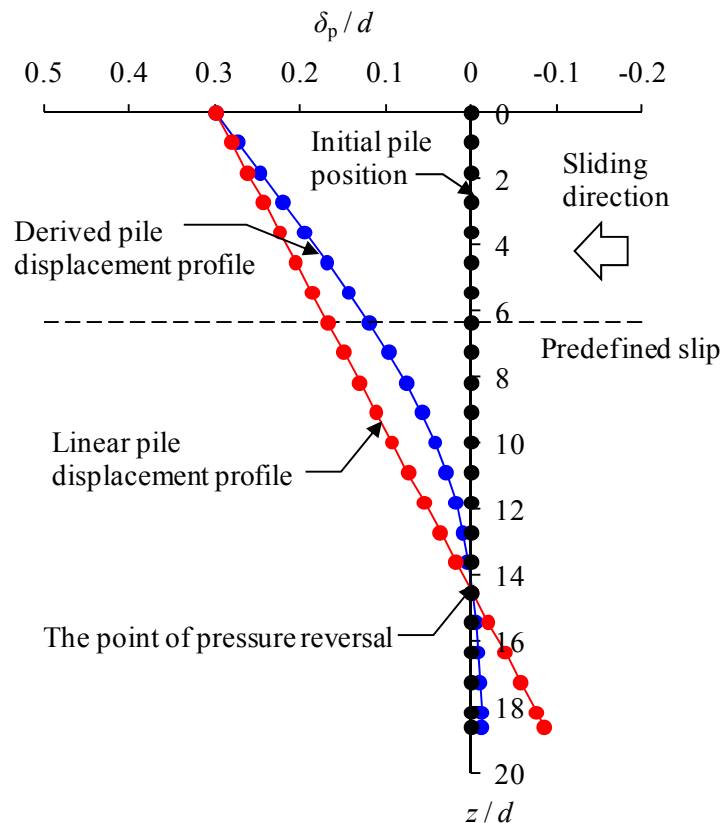


Figure 4.26 Derived and idealised pile displacement profiles with depth (BSY12a at 30g)

4.4 Summary

Movements of the unstable soil mass in the cross sectional plane and on the face of the slope during tests were successfully deduced from In-flight photography and digital image processing (PIV analysis), including some important aspects of ground deformation. General trends of displacement of the slope and the pile head can be described as follows:

- the ground and pile head displacements, and relative pile-soil displacement increase with (s/d) for a given (l/h) and with (l/h) for a given (s/d)
- ‘upslope failure’ with a passive wedge above the pile row occurred for high (l/h) and low (s/d)
- flow through the piles with large displacement occurred for high (l/h) and (s/d)
- shallow surface failure passing through piles occurred for low (l/h) and high (s/d)
- the slope was stable with small displacement at low (l/h) and (s/d)

Continuous distributions of moment, shear force, and pressure were derived from the measured moment data using a curve-fitting technique (combined with the least squares matrix inversion method or direct derivation in the passive zone and cost function in the active zone). General behaviour of the piles can be summarised as follows:

- the bending moment increases with depth and reaches a maximum in the active zone where the shear force is zero
- the pressure in the passive zone increases approximately linearly with depth, showing a maximum at the slip
- below the slip the pressure is actively resisted in the stable material with a point of pressure reversal in the active zone to give moment equilibrium of the pile

Interpretation of the centrifuge test data will be presented in Chapter 5

CHAPTER 5

CENTRIFUGE MODELLING: INTERPRETATION AND COMPARISON

5.1 Introduction

This chapter presents a theoretical framework that is based on analysis of a semi-infinite slope. The centrifuge test data are interpreted by comparison with the proposed framework. Some of the previous work presented in Chapter 2 is then compared with the framework.

5.2 Theoretical framework for a piled slope

A theoretical framework (based on a conventional analysis of a semi-infinite slope under ‘plane strain’ conditions) is proposed to enhance generic understanding of slope stabilisation using a row of piles. The framework primarily considers stabilisation of a potentially unstable layer, focusing on evaluating the force required to stabilise the layer upslope of the piles and the maximum stabilising force available from passive interaction.

5.2.1 Problem definition

A uniform slope inclined at an angle β° to the horizontal is considered. A translational failure slip has developed on a plane parallel to the surface of the slope and at a depth h m below it (Figure 5.1). The l m long failing upslope soil block above the pile row (ABCD) was considered to represent the effect of a failing mass of soil acting on the pile row. The analogy with the centrifuge test approach (described in Chapter 4) is clear.

The end forces P_1 and P_2 due to the earth pressure on the interfaces AD and BC are assumed to be equal and opposite (P_1 does not include the effect of pressure on the piles, which will be considered in due course). It is probable that the earth pressure will be close to active at both these locations. The material downslope of the piles was unstable but active earth pressure represents minimum support to the upslope material from the downslope material.

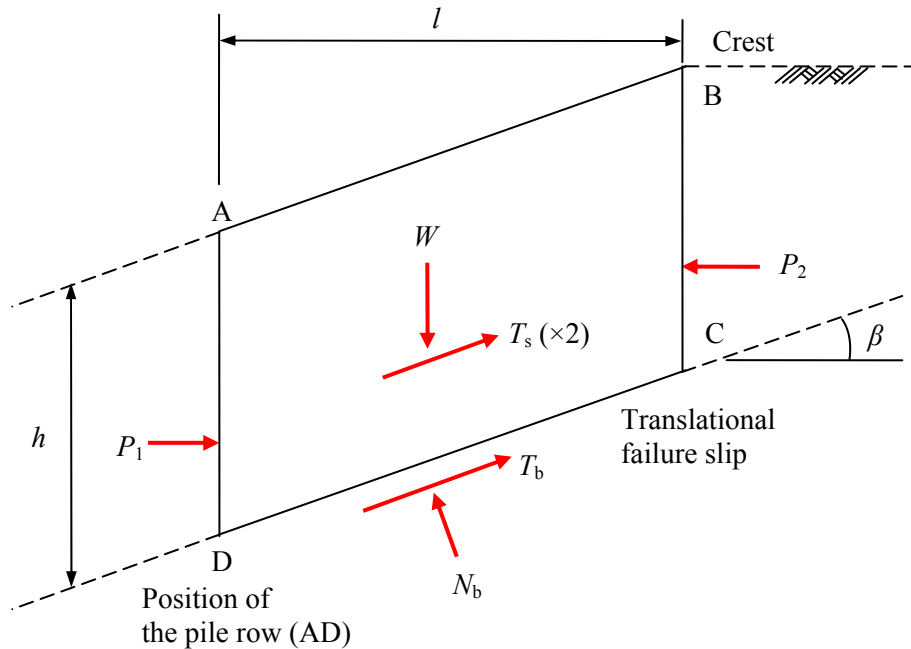


Figure 5.1 - Idealisation of a piled slope problem for semi-infinite slope

The factor of safety (in terms of force equilibrium) is generally calculated by comparing resisting forces with driving forces, and defined as

$$\text{FoS} = \frac{\text{Resisting forces } (F_r)}{\text{Driving forces } (F_d)} \quad (5.1)$$

Here resisting forces are the shear strength of the soil along the failure plane, and resistance induced from any reinforcing members. An additional small component of resistance results from side friction in the centrifuge tests. The driving force is the component of the gravity load of the soil mass acting down the slope.

The weight of the upslope block of the failing soil (for a width b normal to the plane strain section along the pile row) is given by

$$W = lhb\gamma \quad (5.2)$$

where,

$$\begin{aligned} l &= \text{length of upslope 'block'} \\ h &= \text{thickness of slip (from the surface to the slip)} \\ b &= \text{width into page} \end{aligned}$$

The ‘disturbing’ component of this force will be taken as the component acting ‘down’ the slope, giving

$$F_d = W \sin \beta \quad (5.3)$$

Movement of the failing upslope block in the centrifuge model is resisted by friction mobilised on the ‘front’ and ‘back’ sides T_s (assumed to act parallel to base), as well as friction on the base, T_b . The general magnitude of these effects will be considered before proceeding to consider resistance from the pile row.

$$T_s = \mu_s N_s = \frac{1}{2} \mu_s K_s \gamma h^2 l = \frac{1}{2} \mu_s K_s \frac{h}{b} W \quad (5.4)$$

and

$$T_b = \mu_b N_b = \mu_b W \cos \beta \quad (5.5)$$

(assuming $N_b = W \cos \beta$ by resolving perpendicular to the base)

where,

$$\begin{aligned} T_s, N_s &= \text{Shear and Normal forces on each side} \\ T_b, N_b &= \text{Shear and Normal forces on base} \\ \mu_s, \mu_b &= \text{Coefficients of friction on sides and base (= } \tan \delta) \\ K_s &= \text{Coefficient of earth pressure on sides} \end{aligned}$$

The total resistance from friction on the sides and base opposing the driving force F_d is

$F_\mu = (2T_s + T_b)$ (there are 2 sides). Thus expressing this relative to the nominal value of F_d

$$\frac{F_\mu}{F_d} = \frac{2T_s + T_b}{W \sin \beta} = \frac{1}{\sin \beta} \left(\mu_s K_s \frac{h}{b} + \mu_b \cos \beta \right) = \alpha \quad (5.6)$$

where α is the total frictional resistance expressed relative to the driving force.

For a truly plane strain situation μ_s is effectively zero, so that

$$\frac{F_\mu}{F_d} = \frac{\mu_b}{\tan \beta} \quad (5.7)$$

corresponding to the normal equation for an infinite slope in purely frictional soil.

Coefficients of friction on the sides and base, μ_s and μ_b , have been determined by shear box tests in the lab, e.g. $\mu_s = \mu_b \approx 0.03$ (for $\phi'_{\text{int}} \approx 2^\circ$ in Section 3.6.1) but this is likely to vary in the test models to some extent. Since the soil is assumed not to deform in the plane strain direction, K_s may be estimated using the earth pressure coefficient at rest ($K_0 = 1 - \sin \phi'$).

Considering an upper bound on the effect of friction, taking $\mu_s = \mu_b \approx 0.1$ (corresponding to

$\phi'_{\text{int}} \approx 6^\circ$), $K_s = 0.47$ (for $\phi' = 32^\circ$), and $h/b = 0.36$ (for $h = 0.07$ m and $b = 0.196$ m), $\alpha \approx 0.1$, resulting mainly from the friction on the base.

Now consider the effect of a stabilising (shear) force S acting on the unstable soil mass, compared to the disturbing force. The forces are pragmatically assumed to act upward along the slip and hence can be directly compared (assuming that S maintains equilibrium by resisting the driving force after subtracting the effect of friction).

$$S = F_d - F_\mu = F_d(1 - \alpha) = AW \quad (5.8)$$

where

$$A = (1 - \alpha)\sin\beta \quad (5.9)$$

Note that the total horizontal stabilising force required for equilibrium is sometimes considered (e.g. two part wedge method in HA68/94; Department of Transport, 1994) so that $\tan\beta$ replaces $\sin\beta$. However, for typical values of β for soil slopes there is little practical difference between these results.

5.2.2 Stabilising (shear) force

A stabilising (shear) force that each pile can provide to resist sliding of the slip is now taken into account. A triangular passive load distribution is assumed and hence the stabilising interaction force on a pile is given by

$$S_p = \frac{1}{2} B_{\text{mob}} \gamma h^2 d \quad (5.10)$$

where,

S_p = total stabilising interaction force on a pile (normal to the pile),
equivalent to the shear force at the sliding interface

$$B_{\text{mob}} = \text{lateral interaction stress on pile / nominal vertical stress, assumed constant with depth}$$

This normalised lateral interaction stress (B_{mob}) may be proposed to tend to a value such as K_p^2 (as proposed in Equation (2.3)) as the interaction reaches its ultimate state.

For stability of the slope the required stabilising force (Equation 5.8) and the interaction forces for n piles across the width b can be equated:

$$S = nS_p = \frac{1}{2}B_{\text{mob}}\gamma h^2 nd = AW = Albh\gamma \quad (5.11)$$

Rearranging the above equation gives

$$B_{\text{mob}} = 2A\left(\frac{l}{h}\right)\left(\frac{b}{nd}\right)$$

Substituting for pile spacing $s = (b/n)$:

$$B_{\text{mob}} = 2A\left(\frac{l}{h}\right)\left(\frac{s}{d}\right) \quad (5.12)$$

This relationship shows how the lateral interaction stress on the piles (expressed as B_{mob}) required for stabilising the slope increases in proportion to:

1. A which incorporates the slope angle (β) and any reduction in ‘driving’ force due to friction in the model
2. the length of the upslope soil block above the pile row relative to the thickness of the sliding block (l/h)
3. the centre-to-centre spacing relative to the pile diameter (s/d)

5.2.3 Pile row interaction

The general behaviour of a pile row due to passive interaction can potentially be specified by considering the following concepts of limiting interaction capacity for a pile in a row (Durrani, 2006):

- The pile behaves as an ‘isolated pile’, with the ultimate lateral resistance predicted by (Fleming et al., 1994, Figure 5.2(a))

$$p_{p,ult} = K_p^2 \sigma'_{v0} \quad (5.13a)$$

- The pile behaves as if it is part of a ‘continuous wall’ (i.e. arching is effective, Figure 5.2(b)), with passive and active earth pressure in front of and behind it respectively. In some cases there may be complete loss of support rather than active earth pressure. However numerically $(K_p - K_a)$ and $(K_p - 0)$ are quite similar. If the piles are not required for stability the upslope and downslope earth pressures may be equal. Hence the equivalent pressure on the pile itself is given by

$$p_{p,ult} = (K_p - K_a) \sigma'_{v0} \left(\frac{s}{d} \right) \quad (5.13b)$$

where,

$p_{p,ult}$ = ultimate equivalent pressure on the pile (defined as the load per unit length along the pile divided by the diameter)

K_p, K_a = the passive and active earth pressure coefficients respectively

$$K_a = \frac{1 - \sin \phi'}{1 + \sin \phi'}$$

$$K_p = \frac{1}{K_a} = \frac{1 + \sin \phi'}{1 - \sin \phi'}$$

σ'_{v0} = the nominal vertical effective stress in the soil for a given depth

s = centre-to-centre pile spacing
 d = pile diameter

The ultimate equivalent pressure on the pile can be normalised by the initial vertical stress in the soil since this term appears in both equations.

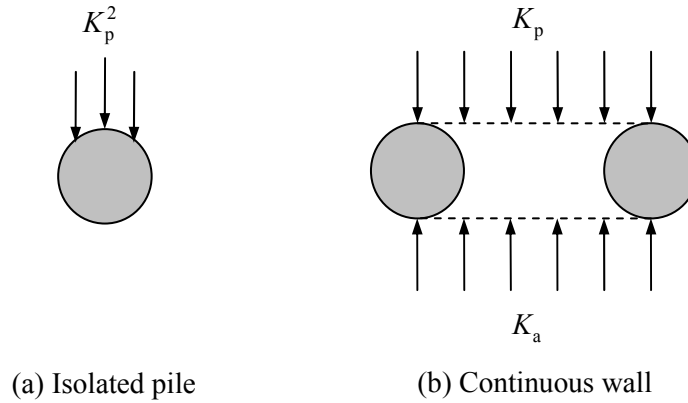


Figure 5.2 - Concepts of limiting interaction capacity for a pile in a row

For sloping ground K_p and K_a can be sometimes expressed as a function of slope angle (β°) and internal friction angle of soil (ϕ'). In Equation (5.13a) the term K_p is associated with inherent limiting strength for a Mohr circle of stress, and modification of the value due sloping ground would not be consistent with the basis of the formula. In Equation (5.13b) the value of $p_{p,ult}$ derived using unmodified earth pressure coefficients is ‘conservative’, whereas using values modified for a slope could potentially be ‘non-conservative’ (giving a higher value of ultimate interaction). It is therefore considered pragmatic to use the ‘standard’ (unmodified) values of K_p and K_a .

The relationship between two equations (Equations (5.13a) and (5.13b)) proposes a rational approach for predicting a critical spacing, $(s/d)_{crit}$ where the two equations intersect, and is given by (Durrani, 2006)

$$\left(\frac{s}{d}\right)_{\text{crit}} = \frac{K_p^2}{K_p - K_a} \quad (5.14)$$

This expression represents a ‘general’ limit of the spacing ratio (s/d) at which arching is effective. At wider spacings the piles are supposed to behave approximately as an isolated pile (at least in terms of ultimate capacity). For instance for $\phi' = 32^\circ$, $(s/d) = 3.6$ - this value shows good general correspondence with generally accepted limits on the critical spacing for arching to occur when using discrete pile rows for slope stabilisation.

5.3 Interpretation and comparison

Throughout this section, the centrifuge test results will be interpreted and compared with the theoretical framework proposed in Section 5.2.

5.3.1 Interpretation of test data

Interpretation of the centrifuge test data will focus on the effect of the stabilising force at the pre-defined slip interface (see Section 4.3.2), in order to determine the two variables A and B_{mob} :

1. The total stabilising interaction force on an instrumented pile is derived from the bending moment measured at the pre-defined slip interface (M_{int}), assuming that the lateral force acts at a distance of $(h/3)$ above the interface (corresponding to a triangular distribution of load on the pile over the height h of unstable material, Figure 5.1). Thus

$$S_{\text{p, int}} = \frac{M_{\text{int}}}{(h/3)} \quad (\text{N}) \quad (5.15)$$

2. The weight of the upslope unstable soil block above the pile row (W) is calculated by considering the volume, density, and centrifugal acceleration (Ng),

$$W = lbh\gamma = lbh\rho gN \quad (\text{N}) \quad (5.16)$$

For the purposes of this calculation any small change (reduction) in l due to movement of the upslope block is neglected.

3. The value A is calculated using the following relationship where n is the number of the piles in the test,

$$A = \frac{S}{W} = \frac{nS_{p,int}}{W} \quad (5.17)$$

According to the model of behaviour proposed this value is theoretically given by Equation (5.9) as $(1 - \alpha) \sin\beta$ and thus correspondence with the model can be tested.

4. The value of B_{mob} is determined directly by substituting the derived stabilising force into Equation (5.10)

$$B_{mob} = \frac{2S_{p,int}}{\gamma h^2 d} = \frac{2S_{p,int}}{\rho g N h^2 d} \quad (5.18)$$

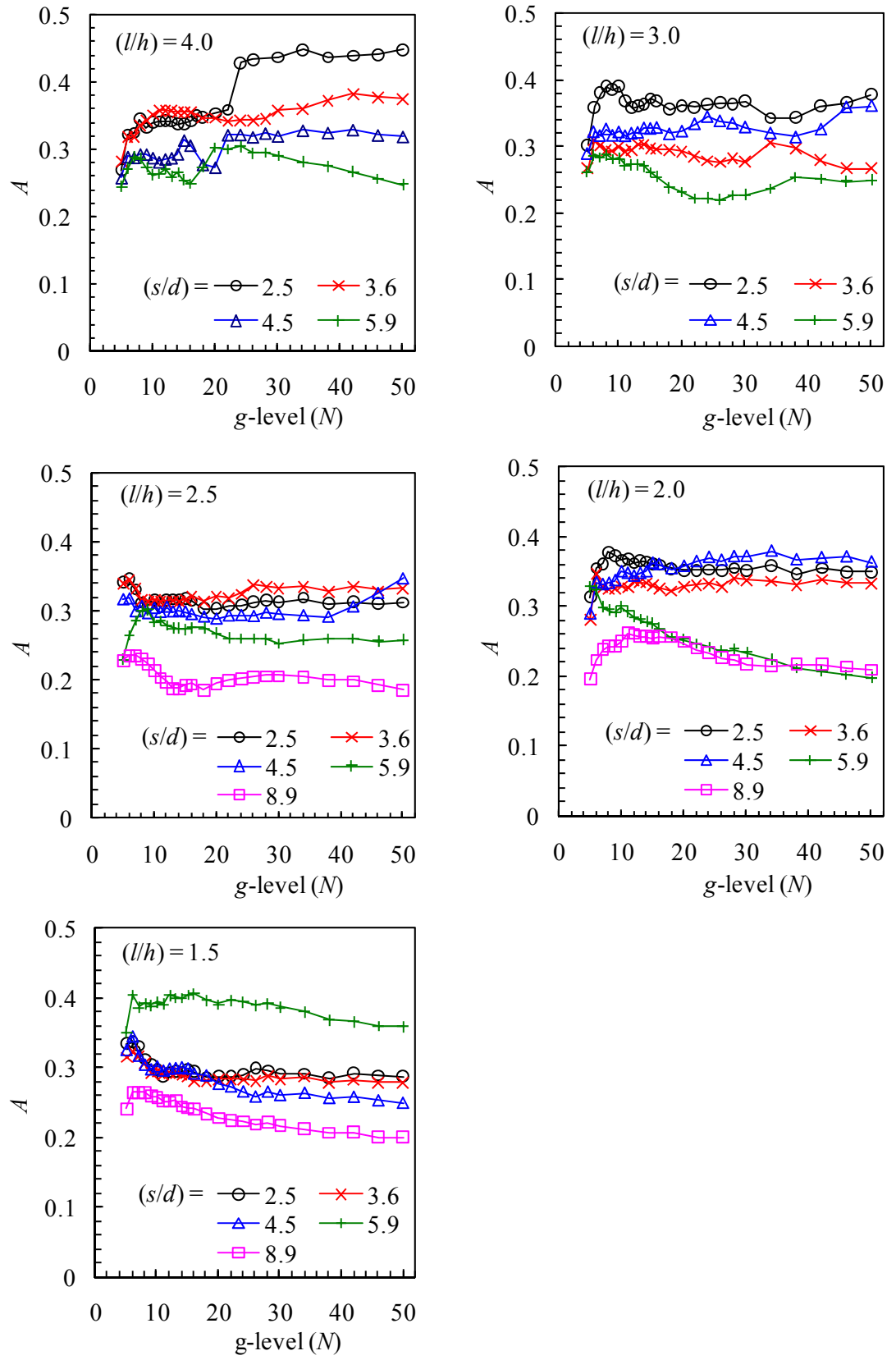
Again this theoretical value is given by Equation (5.11) as $2A(l/h)(s/d)$ and thus correspondence with the model can be examined.

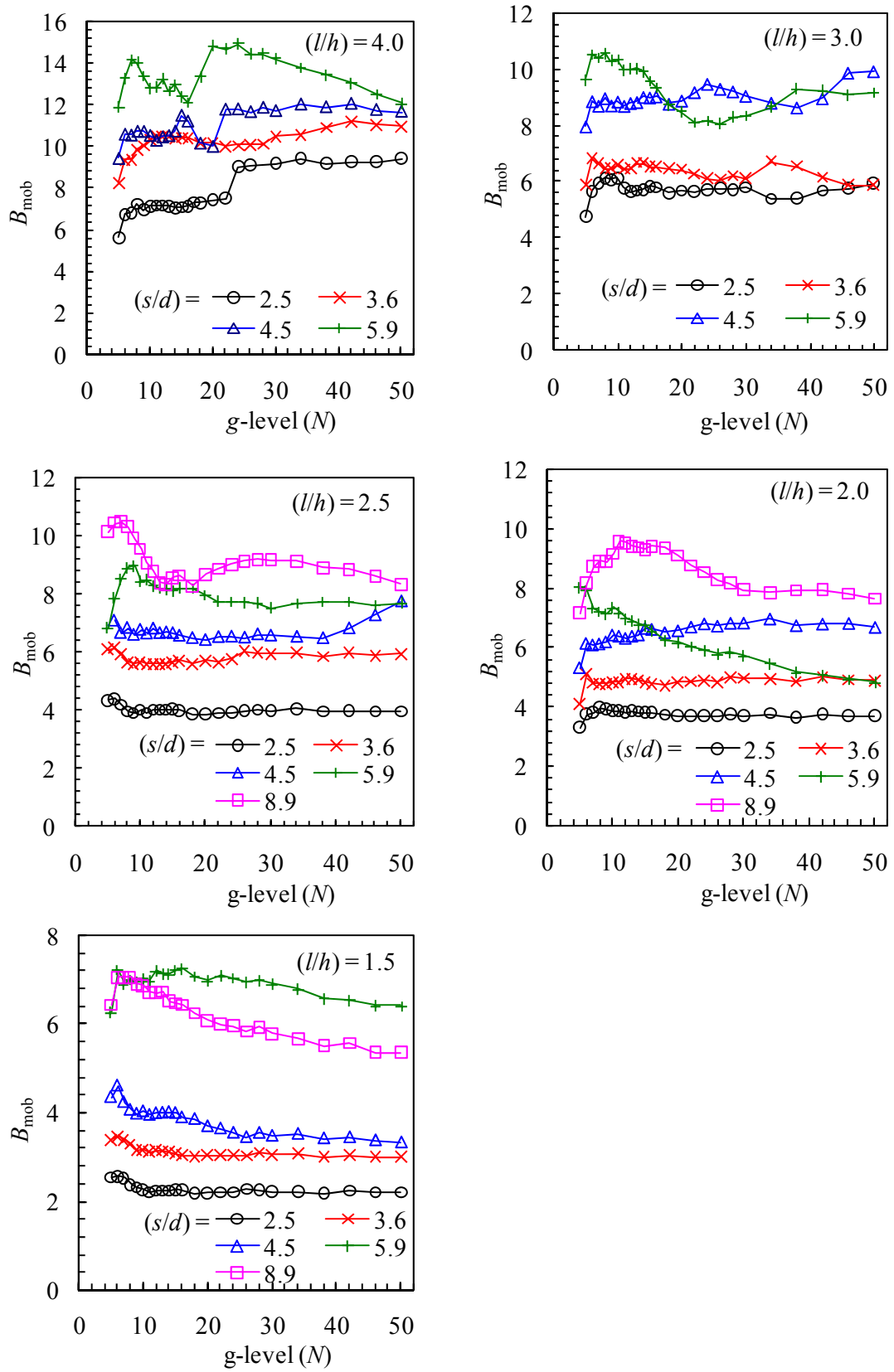
5.3.2 Variation of A and B with g -level in each test

Figure 5.3 and Figure 5.4 show variation of the values of A and B_{mob} derived from the test data (M_{int} and hence $S_{\text{p,int}}$) as described above, and plotted against increasing g -level in all the tests. Each subplot shows a particular value of (l/h) , whilst the various lines show various (s/d) .

Generally speaking, A is approximately constant with g -level for each test (Figure 5.3). This is reasonable since the effect of g -level is accounted for by the γ term in Equation (5.16). The maximum value is approximately 0.3 to 0.4, which is broadly consistent with the theoretical value (according to Equation (5.9) $A_{\text{max}} \approx 0.45$ for $\mu_b = \mu_s \approx 0.1$ used in Section 5.2). Tests with high (s/d) can show lower values due to the effect of B_{max} – further discussion will be given in Section 5.3.4.

Again, it can be seen that B_{mob} is approximately constant with g -level for each test (Figure 5.4) since this effect is again accounted for by the γ term in Equation (5.18). The maximum value observed in any of the tests is $B_{\text{max}} \approx K_p^2$. This normalised value is constant with depth for the approximately triangular distribution of stress over the depth of passive loading (Section 4.3.2), but this observation is probably associated with the use of a pre-defined low friction failure interface. In a more general situation the passive pressure is likely to reduce more gradually to zero at some depth. Generally speaking for a given value of (l/h) B_{mob} tends to increase with (s/d) , and for a given value of (s/d) B_{mob} tends to increase with (l/h) – this is consistent with Equation (5.12).


 Figure 5.3 - Variation of A with g -level for all tests


 Figure 5.4 - Variation of B_{mob} with g -level for all tests

5.3.3 Variation of A and B_{mob} with (s/d)

The values of A and B_{mob} deduced from all the tests are compared with the proposed theoretical model in Figure 5.5 and Figure 5.6 respectively. The plots show variation with (s/d) for a given (l/h) .

As previously noted the value of A throughout a test showed relatively little variation (Figure 5.3). The ‘representative’ value of A shown in Figure 5.5 as a data point was taken over the range from 6 g to 10 g where the values were less affected by upslope displacement and passive failure – this was also often the maximum value observed in the test. The approximate upper limit (AUL) and lower limit (ALL) of A_{max} for the data are taken as 0.4 and 0.3 respectively, with the mean value of A_{max} also plotted at 0.35. As noted previously this value shows reasonable correspondence with the theoretical estimate (Equation (5.9)).

In fact, the model of behaviour developed earlier in this Chapter indicates that the ‘true’ theoretical maximum value of A may not be observed in the pile loading. Re-arranging Equation (5.12) in terms of B_{mob} (although it is more fundamentally related to $S_{\text{p,int}}$ in terms of it’s derivation from the data):

$$A = \frac{B_{\text{mob}}}{2(s/d)(l/h)} \leq A_{\text{max}} \quad (5.19a)$$

For low (s/d) or (l/h) A_{max} will be observed, with a corresponding value of B_{mob} loading the piles. In other words the action of the unstable soil mass dictates the load on the piles.

However, if the limiting interaction pressure (B_{max}) is mobilised this limits the value of A which is ‘observed’ in the test

$$A = \frac{B_{\text{max}}}{2(s/d)(l/h)} < A_{\text{max}} \quad (5.19b)$$

This also implies that the interaction has reached its ultimate ‘failure’ state. Taking B_{\max} as $K_p^2 = 10.6$ this curve is plotted at high (s/d) in Figure 5.5. The interaction of this line with A_{\max} is given by

$$\left(\frac{s}{d}\right)_{\text{int}} = \frac{1}{2} \frac{B_{\max}}{A_{\max}} \frac{1}{(l/h)} \quad (5.20)$$

and hence tends to increase as (l/h) reduces. Based on the model, for a given (l/h) , as (s/d) increases initially B_{mob} increases (see Equation 5.21 below), since there are less piles to carry the same load. Eventually B_{\max} is reached, with subsequent increase in (s/d) leading to reduction in A as deduced from the limiting interaction.

The data points representing the tests in Figure 5.5 generally represent (s/d) less than the intersection value (particularly for low (l/h)), and hence A_{\max} is observed in the test. However, there is some evidence of tendency for A to reduce as the intersection point is approached and exceeded.

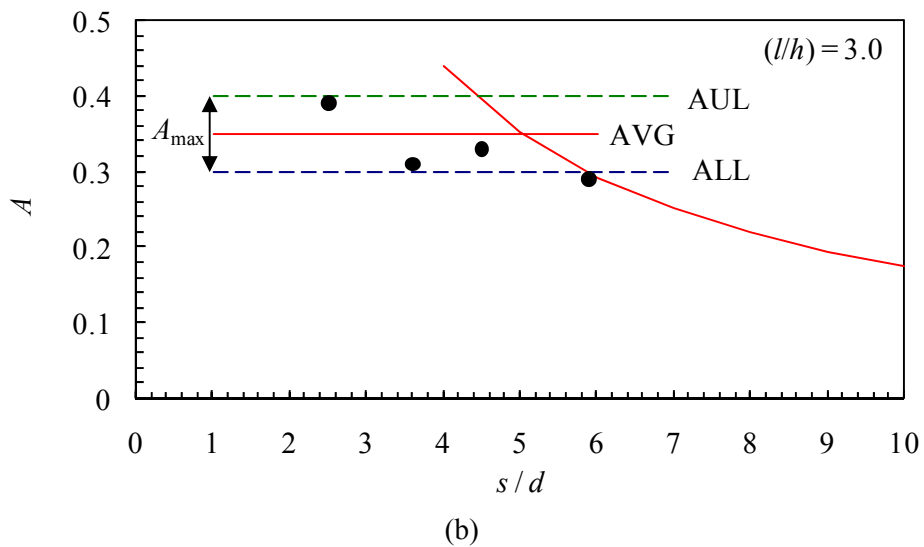
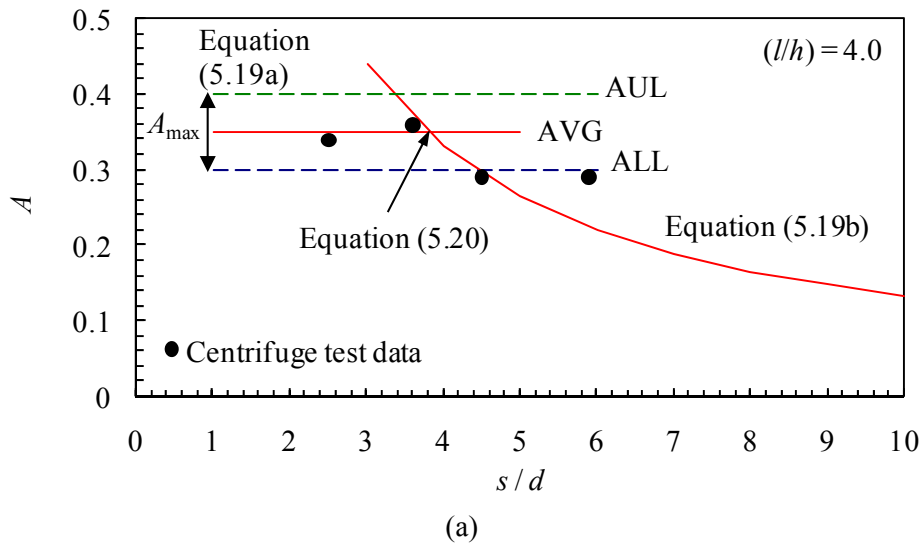
The ‘representative’ value of B_{mob} was obtained from Figure 5.4 in the same way as described above for A . The results are plotted as data points in Figure 5.6. The corresponding form of the equation for the model of behaviour is:

$$B_{\text{mob}} = 2A_{\max} \left(\frac{s}{d}\right) \left(\frac{l}{h}\right) \leq B_{\max} \quad (5.21)$$

As (s/d) or (l/h) increase B_{mob} tends to increase until the limiting value of interaction is reached. The value of (s/d) where the limit B_{\max} is reached is the same as above.

Again the data generally represent (s/d) less than the intersection value (particularly for low (l/h)). In fact the data have been derived from the same value of $S_{p,int}$ and thus show the same relationship with the proposed model of behaviour as in Figure 5.5.

Plotting the data in this way it is evident that for BSY15b ($(s/d) = 5.9$ and $(l/h) = 4.0$) B_{mob} somewhat exceeds the proposed value of B_{max} , whilst for BSY15c ($(s/d) = 8.9$ and $(l/h) = 1.5$) it is somewhat less. Nonetheless the centrifuge test data derived generally shows good agreement with the theoretical lines.



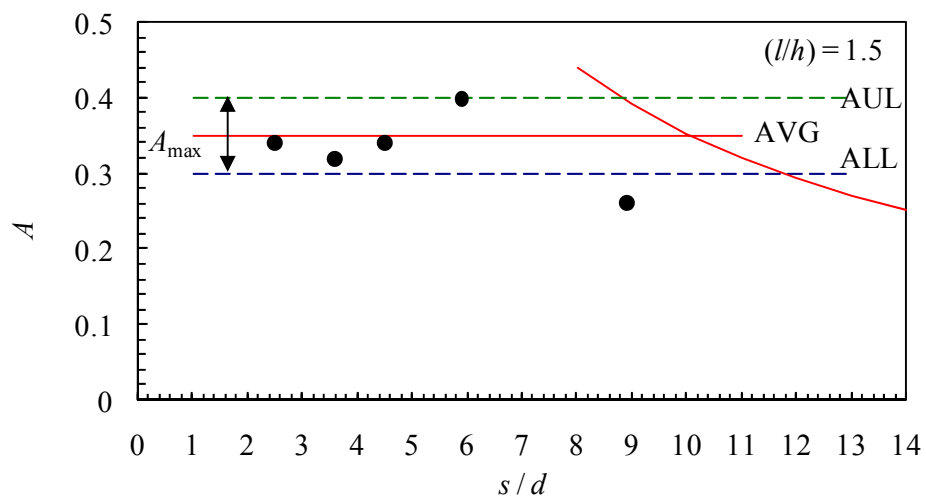
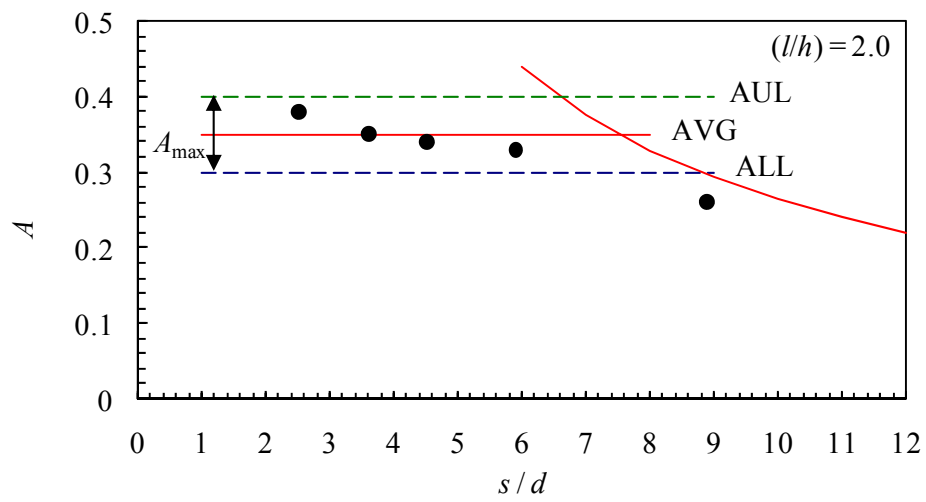
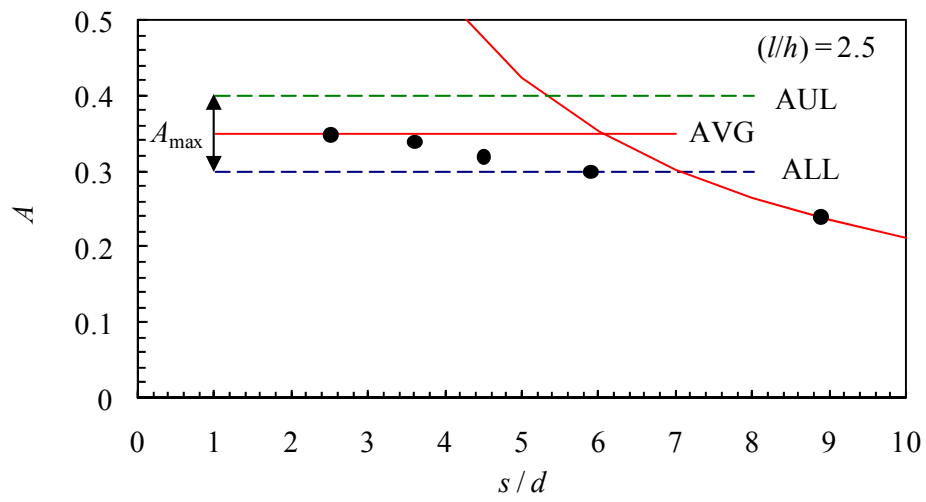
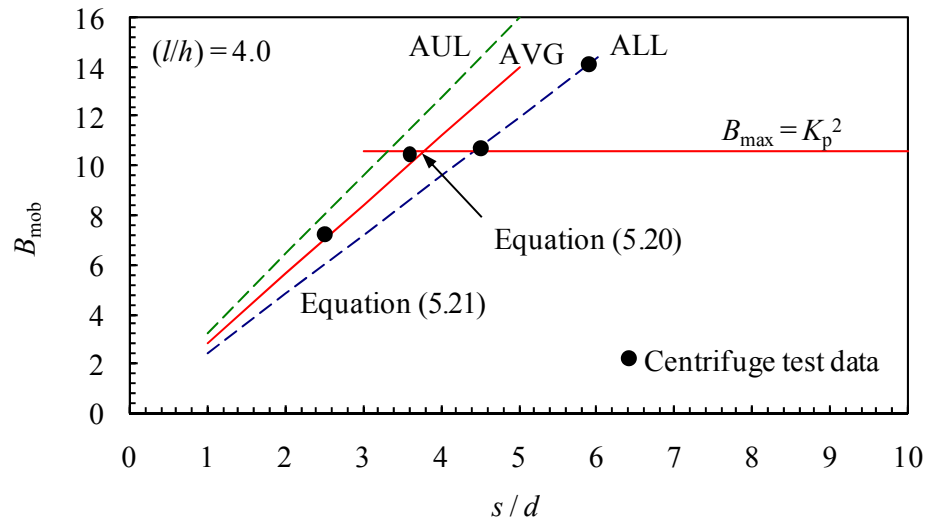
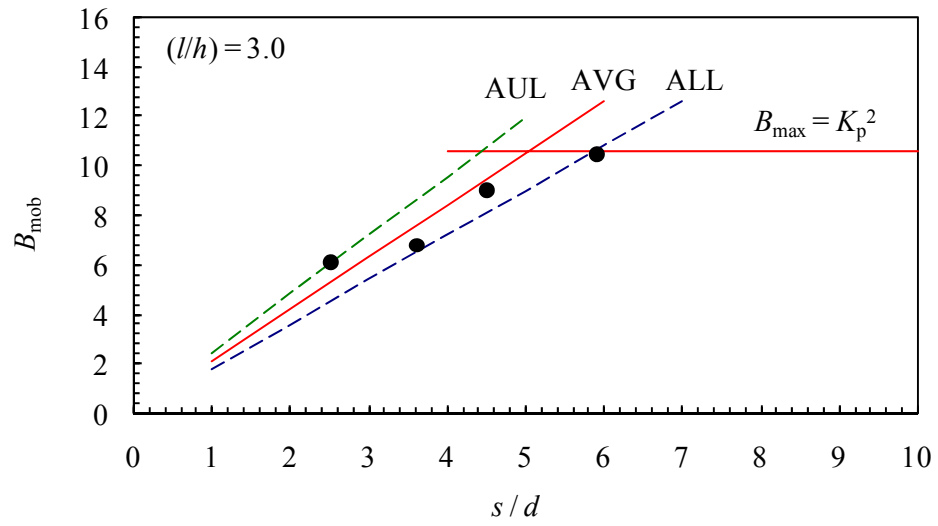


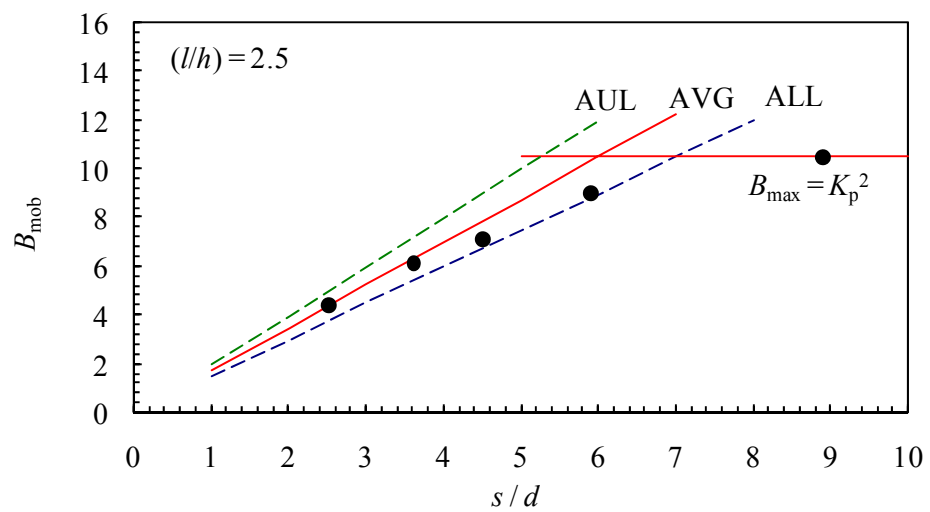
Figure 5.5 - Variation of A with various (s/d) for a given (l/h)



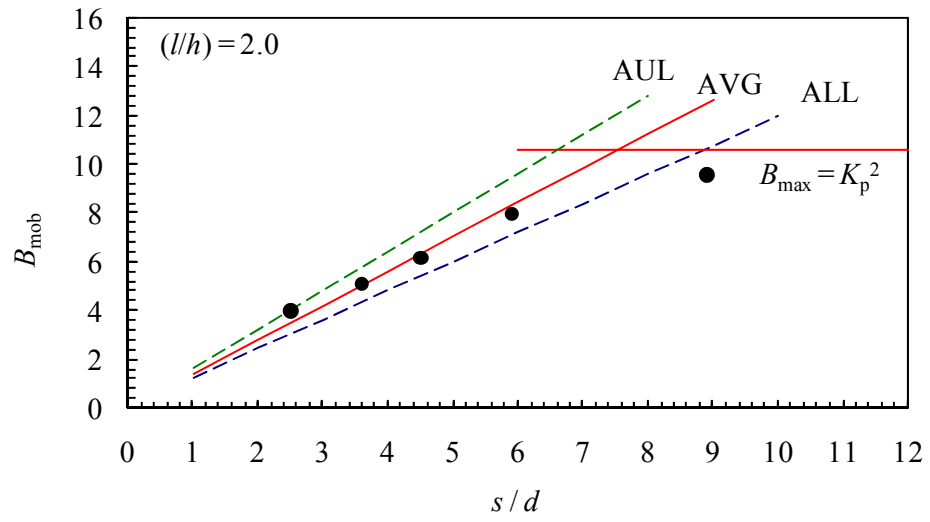
(a)



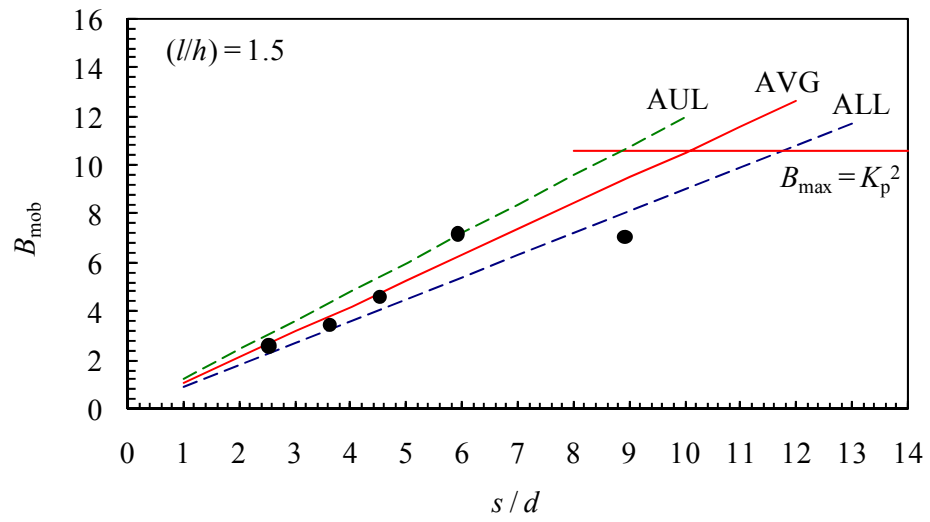
(b)



(c)



(d)



(e)

 Figure 5.6 - Variation of B_{mob} with (s/d) for a given (l/h)

5.3.4 Relationship between pile row interaction, (s/d) and (l/h)

Figure 5.7 summarises the previous observations regarding variation of A and B_{mob} as (s/d) changes for given (l/h) .

Re-arranging Equation (5.21) above:

$$\left(\frac{l}{h}\right) = \frac{1}{2} \frac{B_{\text{mob}}}{A_{\text{max}}} \frac{1}{(s/d)} \quad (5.22)$$

Thus expressing the value of (l/h) theoretically required to mobilise a given value of B in terms of pile-soil interaction for a given value of (s/d) . It is assumed that $B_{\text{mob}} \leq B_{\text{max}}$, and thus $A = A_{\text{max}} = 0.35$.

Figure 5.8 shows this relationship for $B_{\text{mob}} = K_p^2$ and $B_{\text{mob}} = K_p$. As above, the former value is proposed as the limiting interaction stress (for an ‘isolated’ pile). The latter value is a ‘factored’ value of interaction which represents reduced mobilisation of interaction (Durrani, 2006). In fact the model of behaviour proposed by Durrani incorporates a minimum value of (s/d) below which ‘isolated’ behaviour is no longer applicable, and the limiting resistance offered by the pile row shows no further increase (the pile row acts as a ‘continuous wall’). This limit is given by Equation (5.14), and is shown on Figure 5.8. The value of (l/h) for each value of B_{mob} shows no further increase as (s/d) reduces beyond this point.

For the purpose of simplification three labels are defined on the plot (Figure 5.8):

- A. small interaction pressure required for stability
- B. increasing interaction pressure required for stability
- C. proposed ultimate interaction pressure exceeded

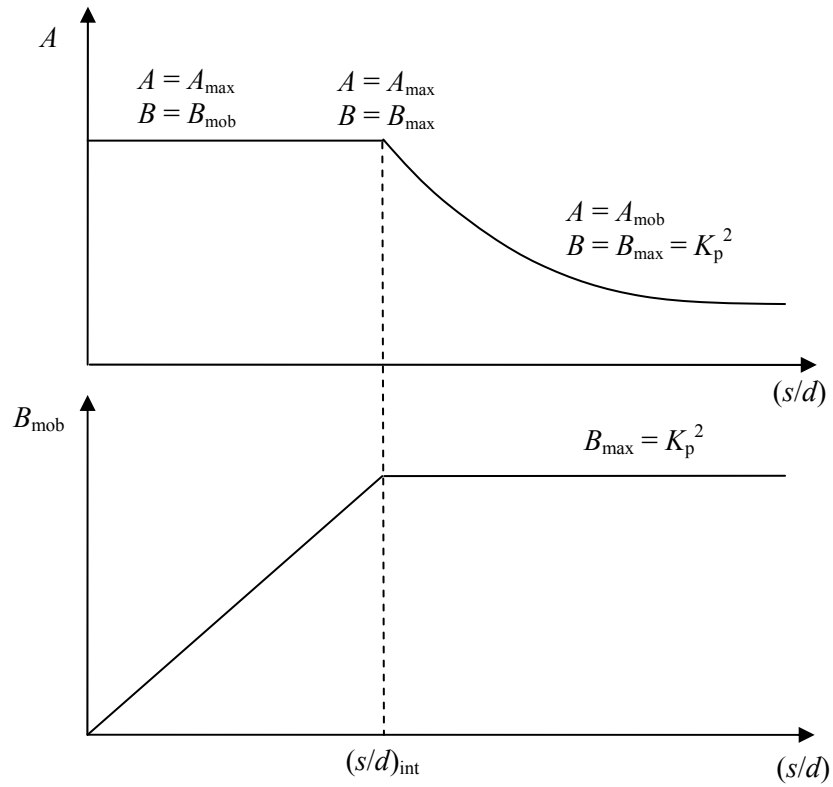
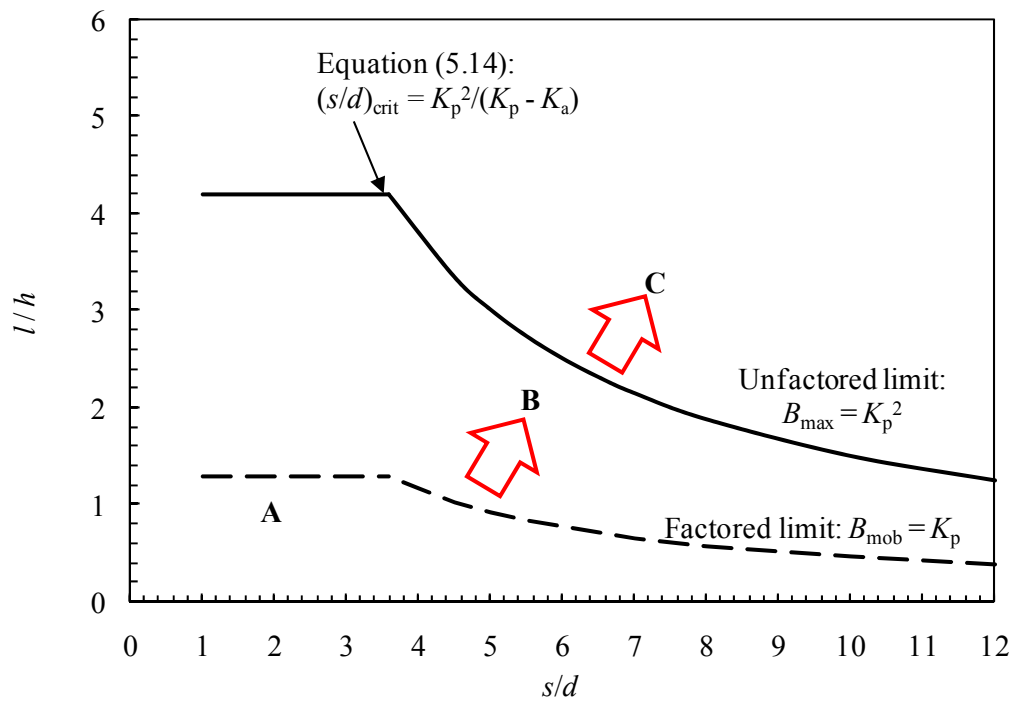

 Figure 5.7 - Concept of the pile row interaction in terms of A and B_{mob}

 Figure 5.8 - Concept of the pile row interaction in terms of (l/h) and (s/d)

Figure 5.9 attempts to correlate the amount of interaction which is ‘mobilised’ in a test (based on the proposed model of behaviour) with the normalised relative displacement measured at 50 g on the plot of (l/h) and (s/d) . Different data symbols have been used to show different amounts of displacement, with corresponding line colours showing lines of approximately equal displacement. Generally speaking deformation tends to increase with mobilisation as expected. This shows good agreement with the deformation characteristics presented in Section 4.2.3 (see Chapter 4).

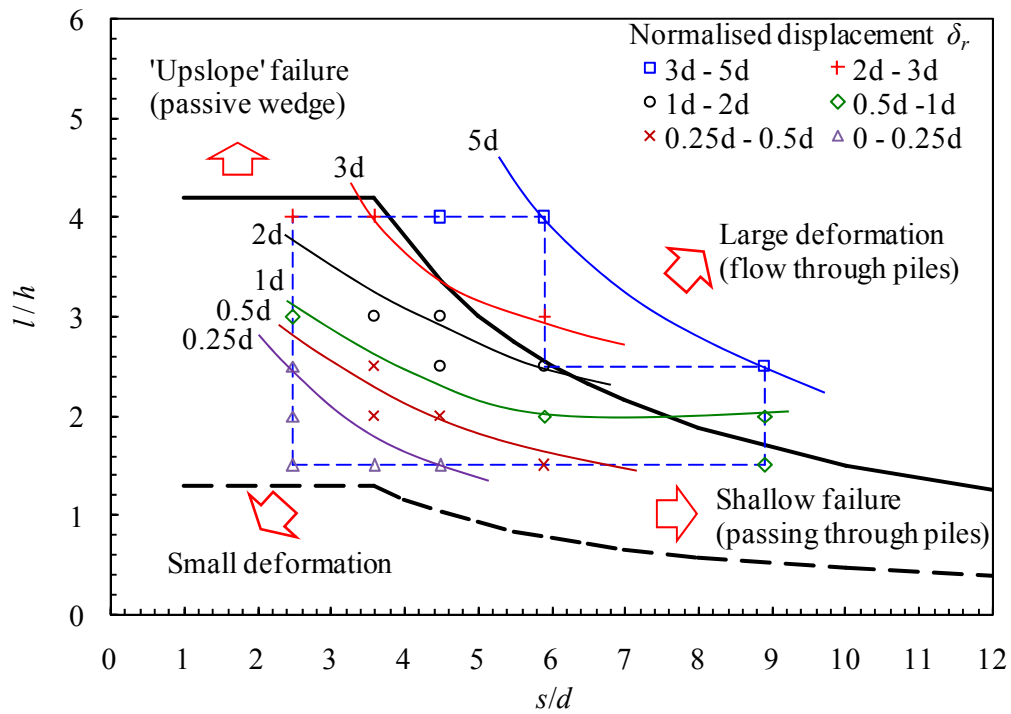


Figure 5.9 - Comparison of test results with the theoretical lines for relative displacement

Figure 5.10 plots the normalised relative displacement at 50 g in all tests against the (approximately constant) value of B_{mob} in the test. Separate data series show each value of (s/d) used in the tests. Moving along a data series from left to right shows increase of (l/h) in various tests, and hence increasing load on the pile row. The movement cannot be interpreted directly as equivalent prototype values since it accumulated at a variety of g -levels. However, the results from the various tests can be compared.

With the exception of one value at very large relative displacement as noted above B_{mob} tends to a maximum value of approximately 10, approximately equal to K_p^2 . It could be argued that a larger value would have been observed at higher δ_r . This would have required a test with $(l/h) > 4$. However, the test package would not allow this, and in any case there would have been very significant tendency for failure upslope of the piles, thus limiting interaction with the piles.

For a given magnitude of B_{mob} less than the limiting value it can be seen that the value of (s/d) does not have significant impact on the corresponding magnitude of δ_r . This supports another observation by Durrani (2006) that piles spaced wider than the critical value still offer support to the upslope material – it is just that the equivalent value per metre along the slope drops in proportion to $(1/s)$ for a given value of B_{mob} .

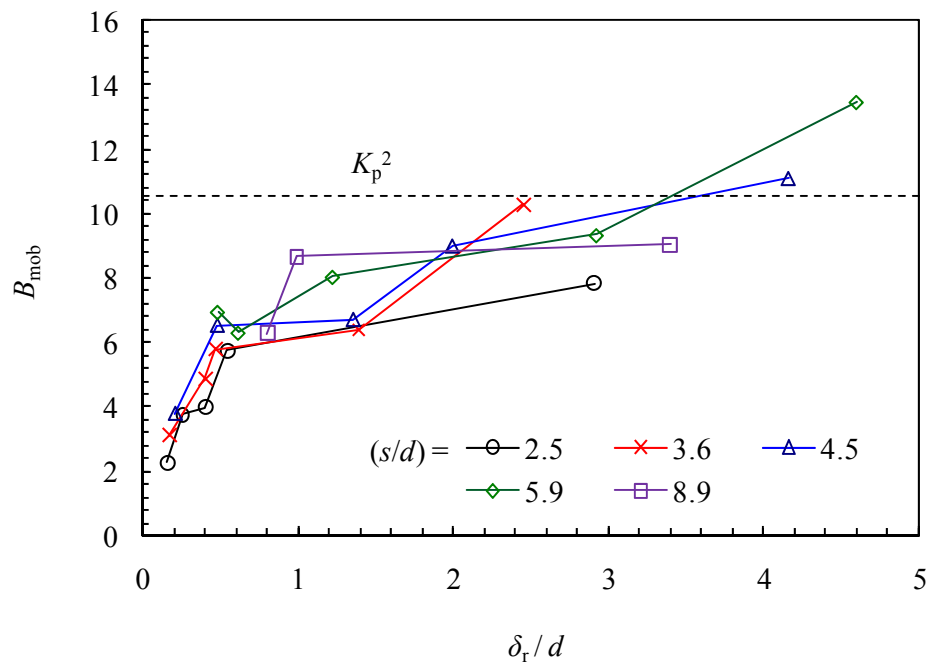


Figure 5.10 - Variation of B_{mob} with relative soil-pile displacement at 50 g showing results from all tests

5.4 Comparison with previous works

It is not possible to give direct comparison of the current work with all the references in Chapter 2. However, it is possible to consider the interaction pressure on piles as it varies with (s/d) , and the design for a case study.

5.4.1 Ito and Matsui (1975)

Ito and Matsui's theory has been specifically discussed in the literature review (Section 2.2.2). The theory considered the following relationship to determine the equivalent lateral pressure acting on a pile ($p = P / d$) for granular soils:

$$p = \frac{\gamma z}{N_\phi d} \left\{ A \exp \left[\frac{D_1 - D_2}{D_2} N_\phi \tan \phi \tan \left(\frac{\pi}{8} + \frac{\phi}{4} \right) \right] - D_2 \right\} \quad (5.23)$$

where

$$A = D_1 \left(\frac{D_1}{D_2} \right)^b$$

D_1 = centre-to-centre spacing between piles

D_2 = $D_1 - d$

d = pile diameter

$b = N_\phi^{1/2} \tan \phi + N_\phi - 1$

$$N_\phi = K_p = \tan^2 \left(\frac{\pi}{4} + \frac{\phi}{2} \right)$$

γ = the unit weight of the soil

ϕ = the friction angle of the soil

z = depth within the moving layer of soil

Here the soil is assumed to be purely frictional and rigid piles spaced at various intervals were considered. The following values are used for the purpose of comparison:

- Friction angle of the soil $\phi' = 32^\circ$
- Unit weight of the soil $\gamma = 16 \text{ kN/m}^3$
- Pile diameter $d = 0.011 \text{ m}$
- Thickness of the slip $z = 0.07 \text{ m}$

Figure 5.11 plots the ultimate pressure ($p_{p,ult}$) on the pile normalised by the nominal overburden stress ($\sigma'_{v0} = \gamma z$) at any depth, which can be derived directly from Equation (5.23). Expressing Equation (5.23) in this way all terms are non-dimensional (D_1 and D_2 are normalised by d). Hence model-scale values can be used and are applicable to any g -level in the centrifuge tests.

Normalising $p_{p,ult}$ in this way is equivalent to B_{mob} in the centrifuge tests (Equation (5.18)), which was indeed found to be approximately constant in each test (Section 5.3.2). Hence data corresponding to Figure 5.6 is plotted in Figure 5.11 for comparison. Equivalent limits proposed by Durrani (2006) (Figure 2.5: ‘continuous wall’ and ‘isolated pile’) are also shown.

Referring to Figure 5.11 some consistency between the centrifuge test data and Durrani’s limits is evident. The ‘isolated pile’ limit is reached at wide spacing except when $(l/h) = 1.5$, where presumably the upslope material was insufficient to generate full passive resistance even at wide pile spacing. The widest spacing for $(l/h) = 4$ somewhat exceeds the isolated pile limit. However, at lower spacing this data supports the ‘continuous wall’ limit proposed by Durrani. For smaller (l/h) it would appear that the upslope material is again insufficient to generate the full ‘continuous wall’ load.

However, from Figure 5.11 it can be seen that the Ito & Matsui method predicts the opposite of the general trend observed from the centrifuge tests and Durrani’s method. The result was found to tend toward the lower ‘factored limit’ proposed by Durrani as spacings get wider. This is because the solution includes $N_\phi = K_p$ (the same as the factored limit for an isolated pile proposed by Durrani). In conclusion, as noted by previous authors and confirmed here, this method does not appear to give reasonable predictions of ultimate resistance at small pile spacings (where the lateral force on the piles tends to infinity) and at

wide spacings (where it tends to zero). At intermediate spacings (3 to $5d$) the general trend of behaviour with pile spacing is questionable, but the general magnitude of results from the method are comparable with the centrifuge tests, particularly for low (l/h) (which has inherently limited the value of B_{mob} as described in Section 5.2.3).

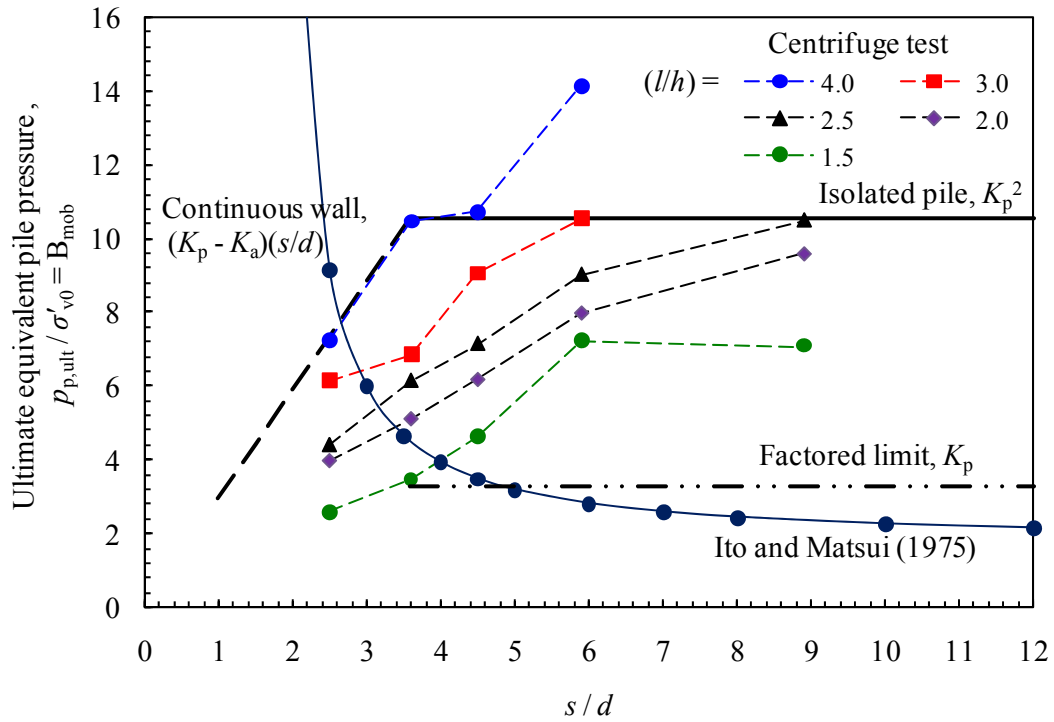


Figure 5.11 - Comparison of ultimate equivalent pressure on pile (B_{mob}) with (s/d) for purely frictional soil ($\phi' = 32^\circ$)

5.4.2 Chen and Martin (2002); Ang (2005); Durrani et al (2006)

Three references based on numerical analysis are selected for comparison with the proposed theoretical limits. Figure 5.12 shows schematic boundary conditions adopted in the 2d and 3d numerical models used. The plane strain model (Chen and Martin, 2002) was used to examine a particular aspect of arching between two piles (principal stress rotation), by applying a constant small velocity to both end boundaries. The horizontal slice model (Ang, 2005) was similar to the constant overburden approach used by Durrani et al. (2006) (see Section 2.2.3), except that pile-soil displacement was generated by moving the end boundaries relative to a static pile rather than moving the pile relative to static boundaries. Note that Chen and Martin have not exploited the line of symmetry at the mid-point between piles - the reasons for this are not clear, and although it has doubled the computation required in their analyses it does not effect the validity of the results.

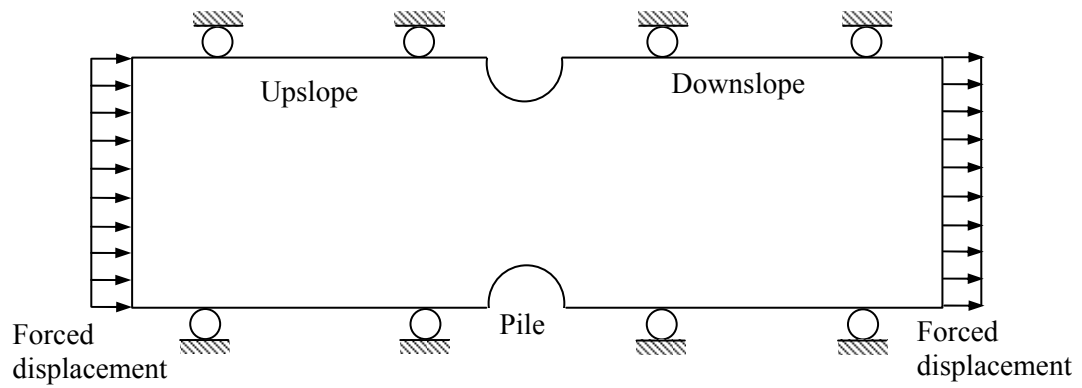
Comparison of the numerical models is summarised in Table 5.1.

Table 5.1 - Analysis specification for comparison

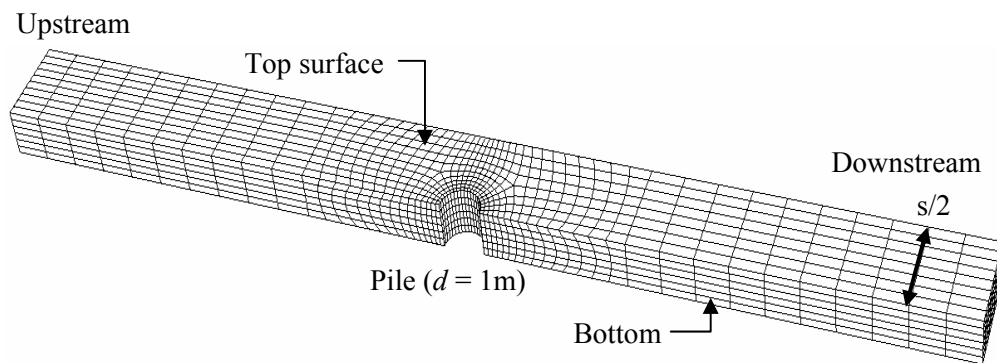
		Chen and Martin (2002)	Ang (2005)	Durrani (2006)
Method		FLAC using 2d plane strain	3d FEM using a horizontal slice	FLAC using 3d constant overburden
Soil properties	Cohesion, c (kN/m ²)	0	0.1	0
	Friction angle, ϕ'	30	30	30
	Unit weight, γ (kN/m ³)	21	21	18
	Dilation, ψ	0	0	0
Pile diameter (m)		1	1	1
Corresponding depth (m)		3	3	1.5

Figure 5.13(a) and (b) show the ultimate equivalent pressure on a pile ($p_{p,ult}$) and on the pile row (p_r) respectively, normalised by σ'_{v0} showing variation with the spacing ratio (s/d). The two results are simply related by $p_r = p_{p,ult}(d/s)$. The limits initially proposed by Durrani (2006) – see Section 2.4, are also shown. It is not surprising that Ang's results are very similar to Durrani's since both use an analogous conceptual modelling approach (although the former uses a finite element technique, whilst the latter uses FLAC – which is a finite difference solution technique). The result of a plane strain model underestimates the ultimate resistance (Durrani, 2006), and this is seen to be the case here.

Nevertheless, all the results indicate that the equivalent pressure on a pile generally increases with pile spacing up to a certain spacing where behaviour of an isolated pile becomes dominant. This pattern is consistent with that observed in the centrifuge tests.

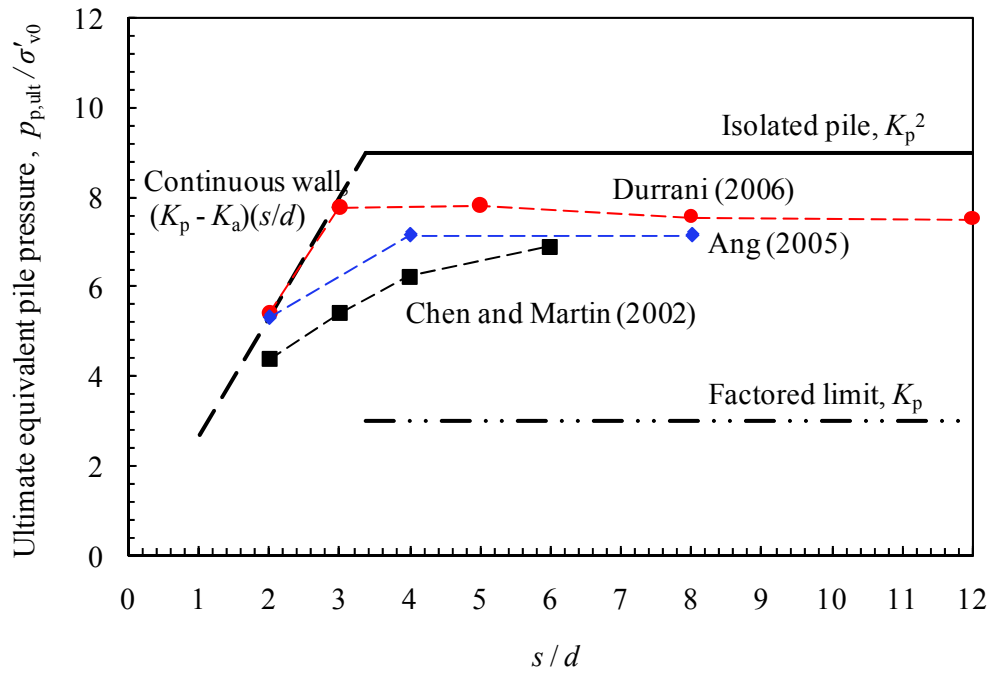


(a) Plane strain model (after Chen and Martin, 2002)

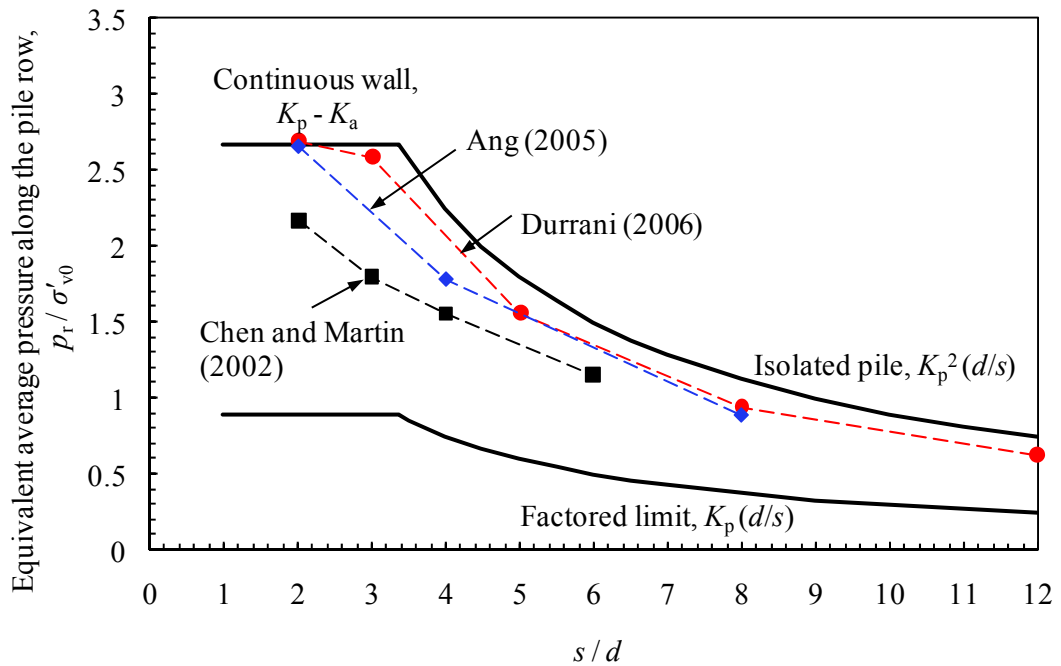


(b) Three-dimensional horizontal slice model (after Ang, 2005)

Figure 5.12 - Boundary conditions of 2d and 3d numerical models used



(a) Ultimate equivalent pile pressure (equivalent to B_{mob})



(b) Equivalent average pressure along the pile row

Figure 5.13 - Ultimate equivalent pressures on a pile and on a pile row with theoretical limits

5.4.3 Davies et al. (2003)

The reference is based on stabilisation works for a large slip on a Southerly section of the M25, Surrey. ‘Section C’ which is the area of the greatest apparent movement will be considered (Figure 5.14(a)).

A translational failure slip (approximately parallel to a slope surface, inclined at 11° to 15° to the horizontal) was developed between 8 – 10 m depth below ground level, extending from a steep backscarp about 80 m up the slope, down to the motorway hard shoulder. The slip was within weathered or unweathered Gault clay, with overlying head deposits covering the upper portion of the slope (Figure 5.14(b)). Properties of soils comprising of the slope are given in Table 5.2.

Table 5.2 - Geotechnical material properties

Material	Design parameters		Other properties		
	c' kPa	ϕ'	c_u kPa	PI	W/C
Head	0	14	50		40
Gault clay	1	24	100	45	35
Residual Gault clay	0	14	50		

The lowest FoS for Section C obtained using a slip circle method (Slope/W software) was 0.93. The pile row was designed to provide an additional stabilising force required for 20% increase in the FoS, based in part on Viggiani’s method (see Chapter 2).

The total weight of the unstable material upslope of the pile row can be estimated as about $\gamma lh = 20 \times 50 \times 8 = 8,000$ kN/m (see Figure 5.14(b)), with a ‘driving’ component acting down the failure surface of about $8,000 \times \sin 11^\circ = 1,500$ kN/m. The stabilising force used

(Figure 5.14(c)) was 250 kN/m, which corresponds to about $250 / 1500 \times 100 \% = 17 \%$ of the driving force, and is thus broadly consistent with a 20 % increase in FoS.

A row of discrete bored piles (1.05 m diameter and 16 m long) was installed at $(s/d) = 2.5$, and positioned at approximately one third of the way up the failure (25m from the back of the motorway kerb). In order to give an additional enhancement of stability, a drainage system was designed to reduce the groundwater level.

The following properties were used for comparison:

- passive earth pressure $K_p = (1 + \sin \phi') / (1 - \sin \phi') = 2.37$ for $\phi' = 24^\circ$ (taking standard soil strength for the soil above the residual shear surface)
- active earth pressure $K_a = (1 - \sin \phi') / (1 + \sin \phi') = 0.42$
- groundwater level after drainage installation $h_w = 3$ m above the slip

For stability of the slope the total stabilising force for n piles across the width b (Equation (5.11) is slightly modified to include the effect of the pore water pressure u due to the groundwater above a slip):

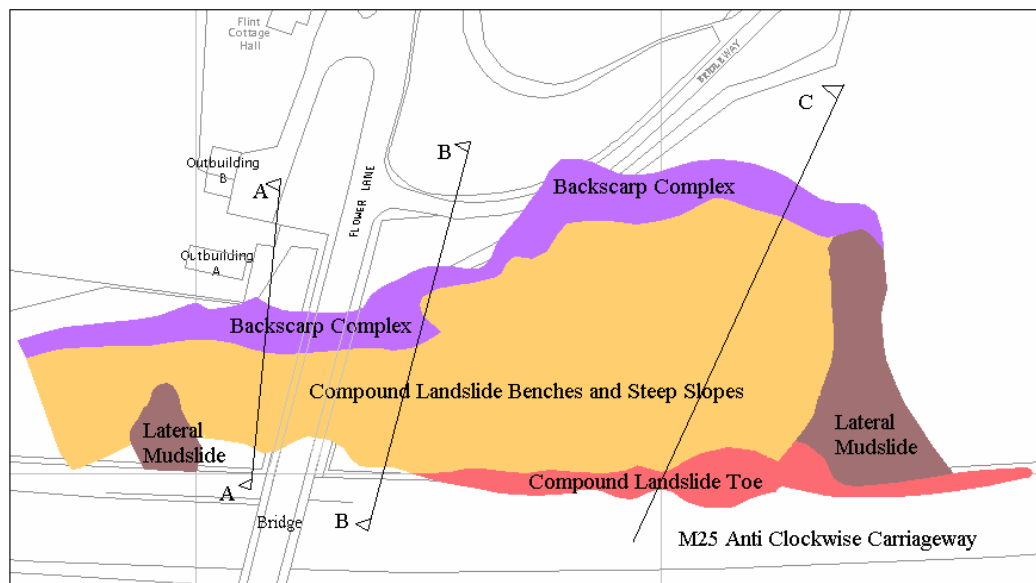
$$S = nS_p = \frac{1}{2} B_{\text{mob}} (1 - r_u) \gamma h^2 n d \quad (5.24)$$

where r_u is the pore pressure ratio that (the ratio of the pore water pressure to the total vertical stress). At the slip surface $r_u = u/(\gamma h) = (\gamma_w h_w)/(\gamma h) = (10 \times 3)/(20 \times 8) = 0.2$. In fact r_u varies with depth, but this value will be considered representative for the entire depth, and is slightly conservative since it is actually the maximum value over this depth provided the drainage remains effective.

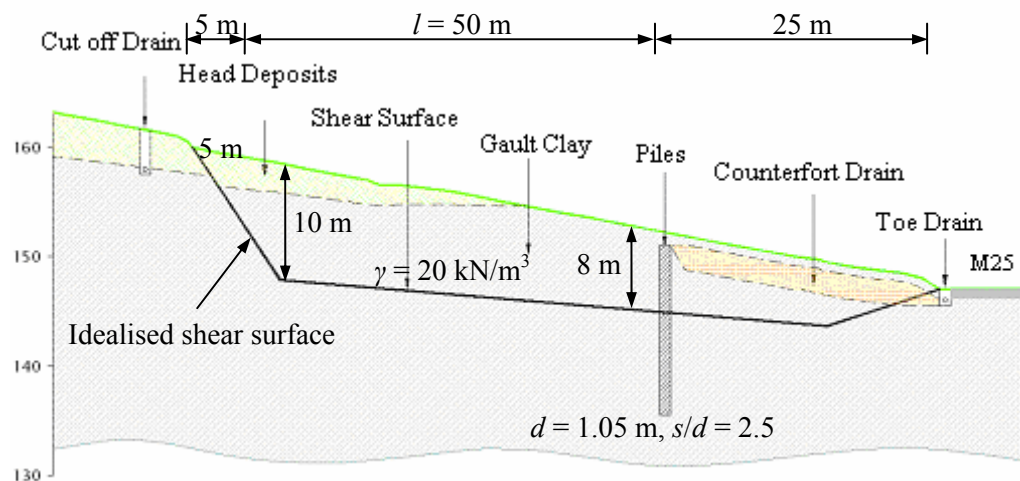
The equivalent stabilising force per unit width along the pile row due to passive interaction is derived by dividing by $b = ns$, and is required to be 250 kN/m (as above):

$$\hat{S} = \frac{S}{b} = \frac{S}{ns} = \frac{1}{2} B_{\text{mob}} (1 - r_u) \gamma h^2 \frac{d}{s} = 250 \text{ kN/m} \quad (5.25)$$

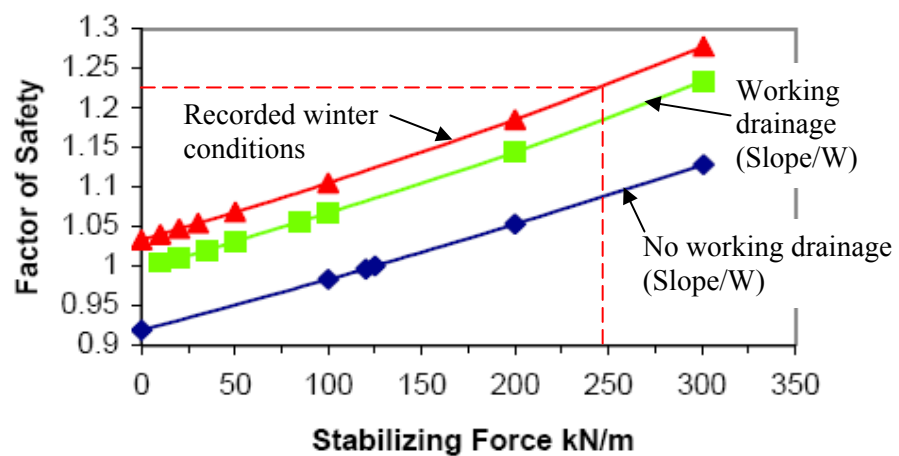
Hence $B_{\text{mob}} = 250 \times 2 / \{(1 - 0.2) \times 20 \times 8^2 \times (1/2.5)\} = 1.2$. This value is plotted in Figure 5.15, which also shows the critical pile spacing, and the ‘unfactored’ (K_p^2) and ‘factored’ (K_p) limits on interaction pressure for individual piles. The spacing is slightly less than the critical value, and quite significantly less than the factored limit on interaction pressure. The impact of passive limiting drained interaction on the stability was not considered in the design (since this effect was not reflected in Viggiani’s method which was used), and thus this results in excessively over-conservative design from the perspective of pile soil interaction (but not necessarily structural capacity etc). Thus it appears that the proposed design is much more robust in this respect so that it can potentially be used to assess the effect of pile spacing for a given load in practice.



(a) Geomorphological map



(b) Schematic layout of cross-sectional plane section



(c) Stabilising force versus improved factor of safety

Figure 5.14 - Geomorphological mapping and schematic layout (after Davies et al., 2003)

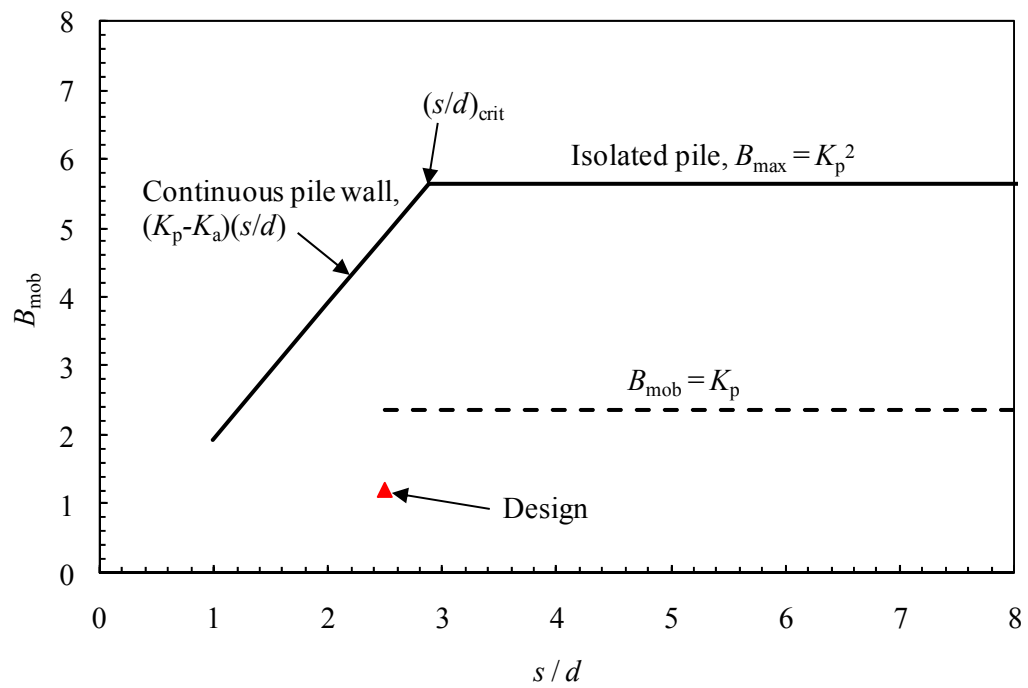


Figure 5.15 Comparison of B_{mob} with the 'factored' and 'unfactored' theoretical limits

5.5 Summary

Based on analysis of a semi-infinite slope under conditions of plane strain, a theoretical method has been established for interpreting the centrifuge test data. The proposed method embodied two important variables A and B_{mob} as follows:

- *loading on the pile row*

A is the proportion of the weight of the upslope material loading the pile row (Equation 5.8). It is related mainly to the inclination of the pre-defined failure interface, with some reduction due to friction on this interface and the sides of the plane strain section.

- *the corresponding interaction pressure on a pile in the row*

B_{mob} is the corresponding interaction pressure mobilised on a pile, expressed as a dimensionless factor normalised by the nominal vertical effective stress in the soil at a given depth (Equation 5.12). This value tends to increase with the weight of the upslope material, and pile spacing.

The above relationships were compared with the centrifuge test data, and showed very good correspondence in general:

- The maximum value of A was observed for low (s/d) or (l/h) , and corresponded quite well with the theoretical prediction. The corresponding B_{mob} was less than the ultimate interaction pressure. However, A tended to reduce relative to its maximum value as the limiting interaction pressure was mobilised (i.e. $B_{\text{mob}} = B_{\text{max}}$), for higher (s/d) or (l/h) , generally indicating inability of the pile row to maintain stability of the upslope material, with corresponding significant displacement.

- The ultimate value of interaction was found to be $B_{\text{mob}} = K_p^2$ as proposed by Fleming et al. (1982). It could be argued that the limiting interaction pressure would be increased due to the inclination of the upslope soil loading the piles. However the limiting value does not appear to be significantly increased, and it is in any case conservative to ignore this potential effect in design. In the centrifuge tests the presence of a pre-defined low friction interface meant that this pressure was observed through the full depth of unstable material as an approximately triangular distribution. However, in a more general situation the passive pressure is likely to reduce more gradually to zero at some depth.
- According to numerical analyses conducted by Durrani et al (2006) the K_p^2 limit on interaction (for an isolated pile) could be used to propose a limit on centre-to-centre spacing (s) where behaviour of the pile row ceases to be a ‘wall’ and becomes more like individual piles at larger spacing. This limiting interaction pressure was verified in the tests.
- For a given magnitude of B_{mob} less than the limiting value the value of (s/d) does not have significant impact on the corresponding magnitude of relative pile-soil displacement. This supports another observation by Durrani (2007) that piles spaced wider than the critical value still offer support to the upslope material – it is just that the equivalent value per metre along the slope drops in proportion to ($1/s$) for a given value of B_{mob} .
- There was some evidence that for closely spaced piles the reduction in limiting pressure predicted by Durrani et al (2006) for the ‘wall’ (as opposed to isolated piles) was observed. It could be argued that greater loading on the pile row would have been required to prove this conclusively, but the test package would not allow

this, and in any case there would have been very significant tendency for failure upslope of the piles, thus limiting interaction with the piles.

Comparison of the centrifuge test results with some of the references reviewed in Chapters 2 was made, focusing on the effect of pile row interaction. Ito and Matsui's approach did not give accurate predictions of the 'full' ultimate resistance – especially at low (s/d), where the trend of behaviour is incorrect. However, as above, the references based on numerical approaches (particularly the 'constant overburden approach', Durrani et al, 2006) showed consistency with the centrifuge test results.

Comparison with a field study indicated that the scheme (which has performed satisfactorily to date) was designed with an appropriate pile interaction pressure for the desired improvement in factor of safety.

CHAPTER 6

CONCLUSIONS

6.1 Work reported in the thesis

6.1.1 Centrifuge model tests

A total of 23 centrifuge model tests (based on plane strain except the pile row) were undertaken, modelling a purely frictional slope comprising sliding (unstable) ground and stable underlying material, separated by the presence of a predefined failure surface. The predefined surface was a translational slip parallel to the slope surface at 0.07m depth at model scale, having a very low shear resistance to increase the tendency for the upper portion of the slope to cause passive loading on the piles over a known depth.

The model piles were installed in a row at discrete intervals across the slope, with the total embedded length 205 mm (at model scale) to give sufficient active pile resistance against lateral passive loading. The pile was instrumented to measure bending moment at ten locations through its depth. The ground displacements (in the cross sectional plane and of the slope face), and the pile head displacement, were measured using in-flight photography and digital image processing (based on GeoPIV). The maximum acceleration used in the centrifuge tests was 50 g, at which point the thickness of sliding material corresponded to 3.5 m at 'prototype' scale, and the pile length was 10.3 m.

The idealised model is intended to investigate the underlying principles controlling passive stabilisation behaviour at a realistic prototype scale rather than to consider a specific

prototype. The ratio of the upslope length to the thickness of unstable soil (l/h) and the normalised pile spacing (s/d) were used for this purpose.

Ground and pile head movements during a test were satisfactorily measured via geoPIV analysis, and ground deformation features were characterised by combination of the ratios (l/h) and (s/d):

- the ground and pile head displacements, and relative pile-soil displacement, tend to increase with (s/d) for a given (l/h), and for a given (s/d) displacements also tend to increase with (l/h)
- upslope failure with a ‘passive wedge’ at large (l/h) and small (s/d)
- flow through the piles with significant deformation at large (l/h) and (s/d)
- a stable condition with small deformation at small (l/h) and (s/d)
- shallow surface failure passing through the piles at small (l/h) and large (s/d)

Back analysis of bending moment data was largely successful in deriving distributions of shear force and lateral pressure, using a number of curve-fitting techniques:

- the bending moment increases with depth until a maximum in the active zone is reached where shear force is zero
- the pressure in the passive zone increases approximately linearly with depth and shows a maximum value at the predefined slip depth. This observation is related to the imposition of the low friction pre-defined slip. In a more general situation the passive pressure would probably reduce more gradually to zero at some depth.
- the passive pressure is actively resisted in the stable ground, with a point of pressure reversal in the active zone to give moment equilibrium of the pile

6.1.2 Analytical model

An approximate analytical model (based on a limit equilibrium method) was developed to enhance generic understanding of slope stabilisation using a row of piles, and particularly to allow interpretation of the centrifuge test results, based on:

- The stabilising force required for the unstable material depending on (1) the mass of the soil upslope of the pile row, (2) the inclination of the predefined failure surface, and some adjustment for friction on the failure surface and sides of the model.
- The amount of passive interaction for the pile row corresponding to the above loading.

The proposed method gave a logical framework for interpretation of the data, and showed good correspondence with the centrifuge test results.

6.2 Implications for design

- The ultimate value of interaction was found to be $B_{\text{mob}} = K_p^2$ as proposed by Fleming et al. (1982). It could be argued that the limiting interaction pressure would be increased due to the inclination of the upslope soil loading the piles. However the limiting value does not appear to be significantly increased, and it is in any case conservative to ignore this potential effect in design. In the centrifuge tests the presence of a pre-defined low friction interface meant that this pressure was observed through the full depth of unstable material as an approximately triangular distribution. However, in a more general situation the passive pressure is likely to reduce more gradually to zero at some depth.

- According to numerical analyses conducted by Durrani et al (2006) the K_p^2 limit on interaction (for an isolated pile) could be used to propose a limit on centre-to-centre spacing (s) where behaviour of the pile row ceases to be a ‘wall’ and becomes more like individual piles at larger spacing. This limiting interaction pressure was verified in the tests, and hence the following relationship;

$$\left(\frac{s}{d}\right)_{crit} = \frac{K_p^2}{K_p - K_a} \quad (5.14)$$

- For a given magnitude of B_{mob} less than the limiting value the value of (s/d) does not have significant impact on the corresponding magnitude of relative pile soil displacement. This supports another observation by Durrani (2006) that piles spaced wider than the critical value still offer support to the upslope material – it is just that the equivalent value per metre along the slope drops in proportion to $(1/s)$ for a given value of B_{mob} .
- There was some evidence that for closely spaced piles the reduction in limiting pressure predicted by Durrani et al (2006) for the ‘wall’ (as opposed to isolated piles) was observed. It could be argued that greater loading on the pile row would have been required to prove this conclusively, but the test package would not allow this, and in any case there would have been very significant tendency for failure upslope of the piles, thus limiting interaction with the piles.

Comparison of the centrifuge test results with some of the references reviewed in Chapter 2 was made, focusing on the effect of pile row interaction. Ito and Matsui’s approach did not give accurate predictions of the ‘full’ ultimate resistance – especially at low (s/d) , where the trend of behaviour is incorrect, which does not give confidence in the use of this approach. Wang and Yen’s approach relies on specifying uncertain geometrical parameters, and there

is no dependency on pile diameter, so the use of this approach is not recommended in practical design. However, as above, the references based on numerical approaches (particularly the ‘constant overburden approach’, Durrani et al, 2006) showed consistency with the centrifuge test results.

6.3 Recommendations for future work

Recent numerical modelling (Durrani 2006) improved generic understanding of interaction for a passively loaded pile row, and this work has now been supplemented and confirmed by physical modelling in a geotechnical centrifuge. Areas for further work mainly consider more detailed aspects of behaviour associated with design in specific circumstances; for instance movement of soil and piles. These areas are generally complicated by the inherent assumptions made in design, such as calculating displacements which are associated with a factor of safety for the slope which is in excess of 1.0, and therefore arguably not relevant to a serviceability calculation. Nevertheless some areas where further work could be undertaken are listed below:

- Horizontal restraint at the pile head can have significant benefit in reducing bending moments in the pile and corresponding displacement. However, there is not likely to be significant effect on the limiting interaction pressure derived from this work.
- The effect of orientation or multiple rows of piles (e.g. miniplies) in a slope could be investigated – particularly with regard to the limiting interaction pressure.
- Use of a lower slope angle compared to the soil friction angle would reduce potential issues with shallow surface failures, also improving PIV on the face of the slope.
- The impact of flexibility of the piles or active behaviour depending on the embedded depth below a slip could be examined. However, such aspects of behaviour are closely related to the wider study of laterally loaded piles.

- Relative pile-soil displacement in relation to B_{mob} was considered in Chapter 5, but the movement cannot be interpreted directly as equivalent prototype values since it accumulated at a variety of g -levels. This aspect of behaviour could be studied in more detail.

APPENDIX

A. Derivation of pile displacement profile with depth

Figure A.1 shows general sign conventions and notation for displacement and rotation of a pile, where subscript ' i ' denotes the position of an interface and ' l_1 ' is the distance from a pile tip to a point of pressure reversal. Rotation (θ) is positive in the anticlockwise and downslope displacement (u) of a pile is positive (see Figure 4.1)

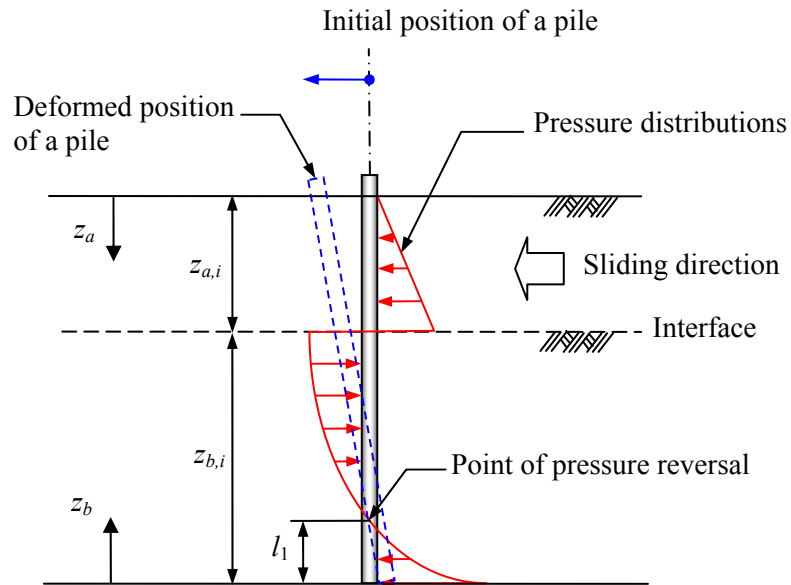


Figure A.1 General definitions and conventions for pile rotation and displacement

The pile displacement profile with depth can be derived by integrating the moment polynomials twice, as follows:

1. Passive zone (based on P_2 approach)

$$M(z_a) = a_1 \frac{z_a^3}{6} + a_2 \frac{z_a^4}{12} \quad (\text{A1a})$$

$$\begin{aligned} \theta(z_a) &= \int_0^{z_a} M(z_a) dz_a = \frac{1}{EI} \left(a_1 \frac{z_a^4}{24} + a_2 \frac{z_a^5}{60} \right) + A_1 \\ &= \theta_a + A_1 \end{aligned} \quad (\text{A1b})$$

$$\begin{aligned} u(z_a) &= \int_0^{z_a} \theta(z_a) dz_a = \frac{1}{EI} \left(a_1 \frac{z_a^5}{120} + a_2 \frac{z_a^6}{360} \right) + A_1 z_a + A_2 \\ &= u_a + A_1 z_a + A_2 \end{aligned} \quad (\text{A1c})$$

2. Active zone (based on P_3 approach)

$$M(z_b) = b_0 \frac{z_b^2}{2} + b_1 \frac{z_b^3}{6} + b_2 \frac{z_b^4}{12} \quad (\text{A2a})$$

$$\begin{aligned} \theta(z_b) &= \int_0^{z_b} M(z_b) dz_b = \frac{1}{EI} \left(b_0 \frac{z_b^3}{6} + b_1 \frac{z_b^4}{24} + b_2 \frac{z_b^5}{60} \right) + B_1 \\ &= \theta_b + B_1 \end{aligned} \quad (\text{A2b})$$

$$\begin{aligned} u(z_b) &= \int_0^{z_b} \theta(z_b) dz_b = \frac{1}{EI} \left(b_0 \frac{z_b^4}{24} + b_1 \frac{z_b^5}{120} + b_2 \frac{z_b^6}{360} \right) + B_1 z_b + B_2 \\ &= u_b + B_1 z_b + B_2 \end{aligned} \quad (\text{A2c})$$

Assuming the following conditions the total four constants of integration (A_1 , A_2 , B_1 , and B_2) are derived by:

- the pile deflection at the head, $u(z_{a,head})$, is equal to the pile head displacement

$$\text{measured from image analysis in the test } (\delta_p), \quad u(z_{a,head}) = \delta_p$$

$$A_2 = u(z_{a,head}) = \delta_p$$

- continuity of gradient (rotation) at the interface, $\theta(z_{a,i}) = \theta(z_{b,i})$

$$\theta_{a,i} + A_1 + \theta_{b,i} + B_1 = 0$$

$$A_1 = -(\theta_{a,i} + \theta_{b,i} + B_1)$$

- the point of pressure reversal in the active zone ($z_b = l_1$) corresponds to zero absolute pile deformation, $u(z_{b,l_1}) = 0$

$$u(z_{b,l_1}) = u_{b,l_1} + B_1 l_1 + B_2 = 0$$

$$B_2 = -(u_{b,l_1} + B_1 l_1)$$

- continuity of pile displacement at the interface, $u(z_{a,i}) = u(z_{b,i})$

$$u_{a,i} + A_1 z_{a,i} + A_2 = u_{b,i} + B_1 z_{b,i} + B_2$$

$$B_1 z_{b,i} = u_{b,i} + B_2 - u_{a,i} - A_1 z_{a,i} - A_2$$

$$B_1 z_{b,i} = u_{b,i} - (u_{b,l_1} + B_1 l_1) - u_{a,i} + (\theta_{a,i} + \theta_{b,i} + B_1) z_{a,i} - \delta_p$$

$$B_1 (z_{b,i} + l_1 - z_{a,i}) = u_{b,i} - u_{b,l_1} - u_{a,i} + (\theta_{a,i} + \theta_{b,i}) z_{a,i} - \delta_p$$

$$B_1 = \frac{u_{b,i} - u_{b,l_1} - u_{a,i} + (\theta_{a,i} + \theta_{b,i}) z_{a,i} - \delta_p}{z_{b,i} + l_1 - z_{a,i}}$$

This allows four independent equations to be written in terms of the four unknown constants of integration. Hence a unique solution exists and can be derived.

REFERENCES

Adachi, T., Kimura, M. and Tada, S. (1989). Analysis on the preventive mechanism of landslide stabilizing piles. *3rd International Symposium on Numerical Models in Geomechanics* , pp. 691-698.

Ang, E. (2005). Numerical investigation of load transfer mechanism in slopes reinforced with piles. *PhD thesis*, University of Missouri-Columbia.

Ausilio, E., Conte, E. and Dente, G. (2001). Stability analysis of slopes reinforced with piles. *Computers and Geotechnics* , 28, pp. 591-611.

Baguelin, R., Frank, R. and Said, Y.H. (1977). Theoretical study of lateral reaction mechanism of piles. *Geotechnique* , 27 (3), pp. 405-434.

Boeckmann, A. (2006). Load transfer in micropiles for slope stabilization from tests of large-scale physical models. *MSc thesis*, University of Missouri-Columbia.

Bosscher, P.J. and Gray, D.H. (1986). Soil arching in sandy soil. *Journal of Geotechnical Engineering* , 112 (6), pp. 625-645.

British Standard 1377 (1990). Methods of Test for Soils for Civil Engineering Purposes, British Standard Institution, London.

Broms, B. (1964). Lateral resistance of piles in cohesionless soils. *Journal of Soil Mechanics and Foundation Division* , 40 (1), pp. 73-84.

Cai, F. and Ugai, K. (2000). Numerical analysis of the stability of a slope reinforced with piles. *Soils and Foundations* , 40 (1), pp. 73-84.

Carder, D.R. and Easton, M.R. (2001). Analysis of performance of spaced piles to stabilise embankment and cutting slopes. *Transport Research Laboratory*, TRL Report 493.

Carder, D.R. and Temporal, J. (2002). A review of the use of spaced piles to stabilise embankment and cutting slopes. *Transport Research Laboratory*, TRL Report 466.

Chen, C.Y. and Martin, G.R. (2002). Soil-structure interaction for landslide stabilizing piles. *Computers and Geotechnics* , 29, pp. 363-386.

Chen, L.T. and Poulos, H.G. (1997). Piles subjected to lateral soil movements. *Journal of Geotechnical and Geoenvironmental Engineering* , 123 (9), pp. 820-811.

Chen, L.T., Poulos, H.G., and Hull, T.S. (1997). Model tests on pile group subjected to lateral soil movement. *Soils and Foundations* , 37 (1), pp. 1-12.

Cox, C. (2006). Personal communications.

Craig, W. (1984). Installation studies for model piles. *Proceeding of a symposium on the application of centrifuge modelling to geotechnical design*, W. Craig (Ed.), Balkema, Rotterdam, pp. 440-455.

Davies, J.P., Loveridge, F.A., Patterson, D., Carder, D.R. and Perry, J. (2003). Stabilization of a landslide on the M25 Highway London's Main Artery. *12th Pan-American Conference of Soil and Mechanics and Geotechnical Engineering*. Massachusetts Institute of Technology, Boston.

De Beer, E., and Carpentier, R. (1976). Discussion of “method to estimate lateral force acting on stabilising piles” by Ito and Matsui, *Soils and Foundations*, 17 (1), pp. 68-82.

Durrani, I. (. (2007). *Numerical modelling of discrete pile rows to stabilise slopes*. PhD thesis, University of Nottingham.

Durrani, I.K., Ellis, E.A. and Reddish, D.J. (2006). Modelling lateral pile-soil interaction for a row of piles in a frictional soil. *4th International FLAC Symposium on Numerical Modelling in Geomechanics 2006* ISBN 0-9767577-0-2, pp. 231-238.

Durrani, I.K. (2007). Numerical modelling of discrete pil rows to stabilise slopes. *PhD thesis*, the University of Nottingham.

Dyson, G.J. and Randolph, M.F. (1998). Installation effects on lateral load-transfer curves in calcareous sands. *Centrifuge 98*. Balkema, Rotterdam.

Ellis, E.A., Cox, C., Yu, H.S., Ainsworth, A. and Baker, N. (2006). A new geotechnical centrifuge at the University of Nottingham, UK. *6th International Conference of Physical Modelling in Geotechnics: ICPMG'06*. Taylor & Francis Group, London, pp. 129-133.

Fleming, W.G.K., Weltman, A.J., Randolph, M.F. and Elson, W.K. (1994). Piling engineering. *Taylor & Francis Books Ltd*.

Foray, P., Balachowski, L. and Rault, G. (1998). Scale effect in shaft friction due to the localisation of deformations. *Centrifuge'98*. Balkema, Rotterdam.

Garnier, J. and Konig, D. (1998). Scale effects in piles and nails loading tests in sand. *Centrifuge'98*. Balkema, Rotterdam.

Gui, M.W. and Bolton, M.D. (1998). Geometry and scale effect in CPT and pile design. *Geotechnical Site Characterization*. Balkema, Rotterdam.

Hassiotis, S., Chameau, J.L. and Gunaratne, M. (1997). Design method for stabiliziation of slopes with piles. *Journal of Geotechnical and Geoenvironmental Engineering* , 123 (4), pp. 314-323.

Hayward, T., Lees, A., Powrie, W., Richards, D.J. and Smethurst, J. (2000). Centrifuge modelling of a cutting slope stabilised by discrete piles. *Transport Research Laboratory*, TRL Report 471.

Ito, T. and Matsui, T. (1975). Methods to estimate lateral force acting on stabilising piles. *Soils and Foundations* , 15 (4), pp. 43-59.

Jeong, S., Kim, B., Won, J. and Lee, J. (2003). Uncoupled analysis of stabilising piles in weathered slopes. *Computers and Geotechnics* , 30, pp. 671-682.

Kulhawy, F.H. (1991). Drilled shaft foundations. *Foundation engineering book*, 2nd eds. Chap. 14. H.Y. Fang (Ed)., Van Nostrand Reinhold, New York.

Lee, C.Y., Hull, T.S. and Poulos, H.G. (1995). Simplified pile-soil stability analysis. *Computers and Geotechnics* , 17, pp. 1-16.

Liang, R. and Zeng, S. (2002). Numerical study of soil arching mechanism in drilled shafts for slope stabilisation. *Soils and Foundations* , 42 (2), pp. 83-92.

Lyndon, A. and Pearson, R.A. (1988). Skin friction effects on laterally loaded large diameter piles in sand. *Centrifuge 88*. Balkema, Rotterdam, pp. 363-370.

Perry, J., Pedley, M. and Brady, K. (2003a). Infrastructure cuttings - condition appraisal and remedial treatment. CIRIA Report C591.

Perry, J., Pedley, M., Reid, M. (2003b). Infrastructure embankments - condition appraisal and remedial treatment. CIRIA Report C592.

Poulos, H. (1999). Design of slope stabilising piles. Research Report. University of Sydney, Department of Civil Engineering.

Poulos, H.G., Chen, L.T. and Hull, T.S. (1995). Model tests on single piles subjected to lateral soil movement. *Soils and Foundations* , 35 (4), pp. 85-92.

Schofield, A. (1980). Cambridge geotechnical centrifuge operations: 20th Rankine lecture. *Geotechnique* , 30 (2), pp. 129-170.

Smethurst, J.A. and Powrie, W. (2007). Monitoring and analysis of the bending behaviour of discrete piles used to stabilise a railway embankment. *Geotechnique* , 57 (8), pp. 663-677.

Takemura, J. (1998). In K. a. Kimura (Ed.), *Centrifuge 98*, Balkema, Rotterdam. pp. 1087-1123.

Taylor, R. (1995). *Geotechnical Centrifuge Technology*. Blackie Academic & Professional.

Thompson, M.J. and White, D.J. (2006). Design of slope reinforcement with small diameter piles. In J. Y. Han (Ed.), *Proceedings of sessions of GeoShanghai 2006: Advances in Earth Structure: Research to Practice*. ASCE, GSP151. pp. 67-73

Viggiani, C. (1981). Ultimate lateral load on piles used to stabilize landslids. *Proceeding of 10th European Conference on Soil Mechanics and Foundation Engineering*, 3, pp. 555-560.

Wang, W.L. and Yen, B.C. (1974). Soil arching in slopes. *Journal of Geotechnical Engineering Division* , 100, pp. 61-78.

White, D.J., Take, W.A. and Bolton, M.D. (2003). Soil deformation measurement using particle image velocimetry (PIV) and photogrammetry. *Geotechnique* , 53 (7), pp. 619-631.

Won, J., You, K., Jeong, S., and Kim, S. (2005). Coupled effects in stability analysis of pile-slope systems. *Computers and Geotechnics* , 32, pp. 304-315.